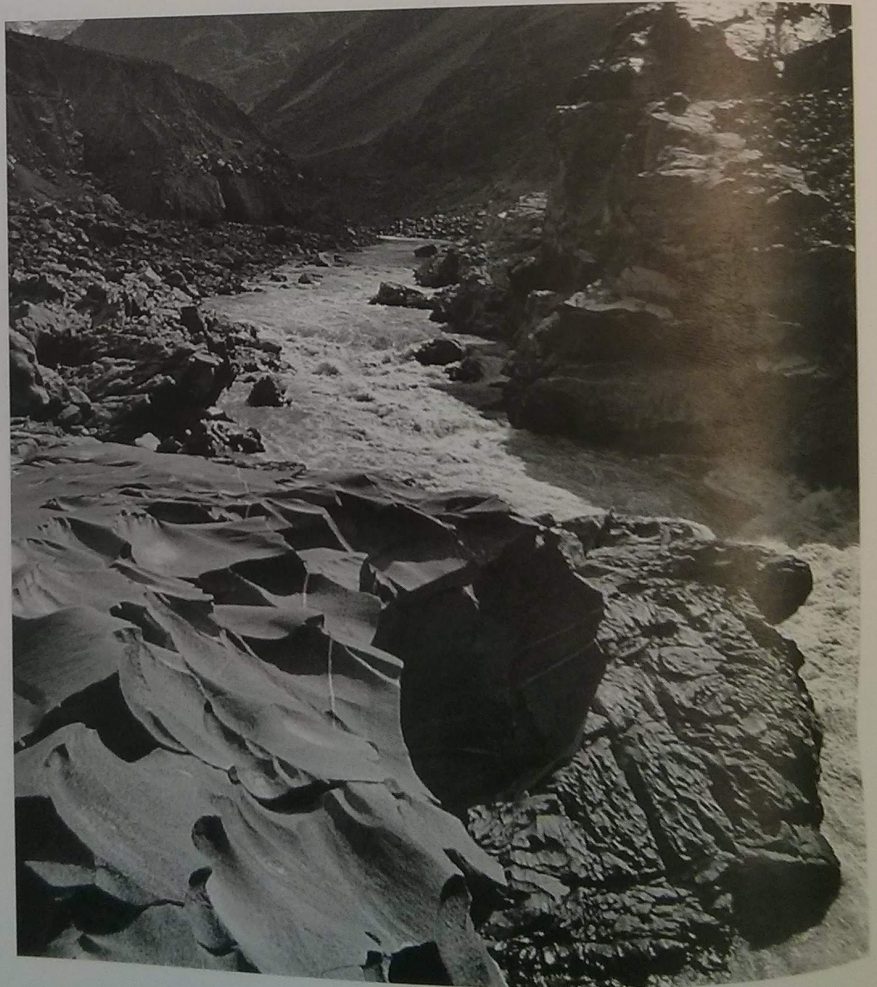



## CHAPTER 13

# Bedrock channels

Every river appears to consist of a main trunk, fed from a variety of branches, each running in a valley proportioned to its size, and all of them together forming a system of valleys, communicating with one another, and having such a nice adjustment of their declivities that none of them join the principal valley, either on too high or too low a level; a circumstance which would be infinitely improbable, if each of these valleys were not the work of the stream that flows in it.

Playfair, 1802, *Illustrations of the Huttonian Theory of the Earth*, p. 102

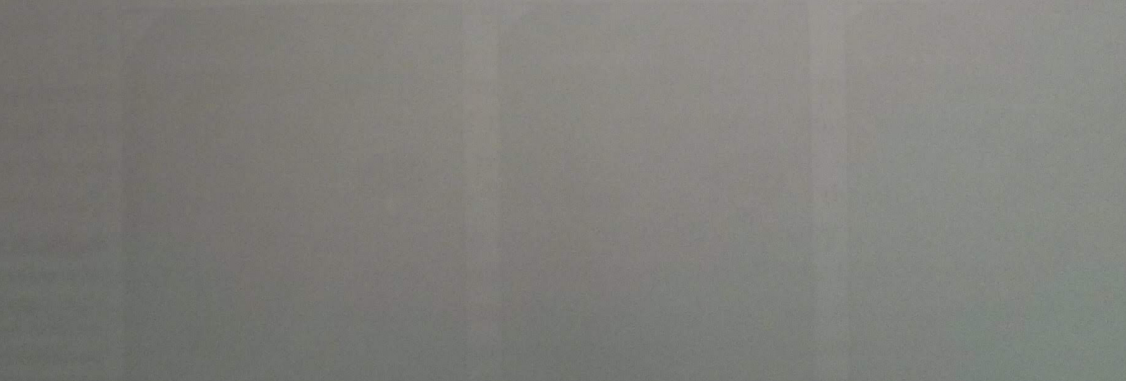




## In this chapter

---

In some of the earliest writing on geology, Hutton and Playfair noted the tendency of rivers and their tributaries to join smoothly together. Playfair, by far the better writer of the two, stated it most elegantly in the quote with which we begin the chapter. Rivers appear to adjust themselves such that the tributaries meet their trunk streams at grade, as sketched in Figure 13.1. This simple observation has become known as Playfair's law. Note that this contrasts with glacial valleys, in which tributaries often reach the trunk stream well above grade, and hence are said to "hang." Indeed, in the glacial hanging valley cases, rivers did not do the work of forming the valleys; glaciers did. In this chapter we address how rivers erode their channels when they encounter bedrock.



View looking up-river in the Indus River middle gorge. Scalloped bedrock 15 m above mid-April low flow demonstrates the large annual swing of river stage. Note human figure crouched beside flow in middle distance (photograph by R. S. Anderson).

Uplift of rock by tectonic processes sets in motion a series of geomorphic events that are led by the action of rivers. First, the slopes of rivers draining the uplifted region are steepened, promoting river incision into bedrock. River incision subsequently promotes hillslope erosion. The pace of the response of a landscape to uplift or to tectonics in general is therefore set

by the response of its rivers. Because bedrock channel incision controls landscape response, we consider this aspect of the geomorphology of rivers separately. In this chapter we will survey modern understanding of river incision into bedrock. We describe how we measure bedrock incision rates at several timescales, followed by a summary of the specific processes responsible for bedrock erosion. In this survey we introduce the concept of stream power, which is heavily utilized in the literature on river incision into bedrock. We then address the nature of the long valley profiles of bedrock rivers, meaning how they should look in simple (steady uplift, uniform rock) conditions, and in more complex (transient uplift, variable rock) conditions. In the end we will summarize the outstanding issues, as this topic remains a very active line of inquiry within the geomorphic community.

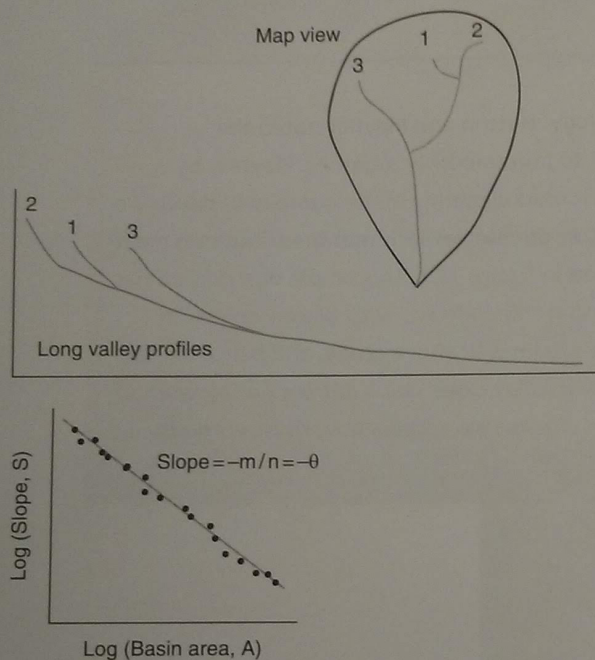


**Figure 13.1** Top: map view of channel pattern in a drainage basin, and profiles of main stem and tributaries. Bottom: profile shown in log-log space. Straight line implies a power-law relationship.

### Measurement techniques

River incision into bedrock is measured over several timescales using a wide range of techniques. In general, one studies this process best by choosing either very weak bedrock (clay badlands, for example), or a large river with a lot of power. Over long times, rivers leave behind markers of their former positions in the landscape. These include abandoned channel beds cut into bedrock, called strath terraces; lava flows that filled former channels, essentially fossilizing them; and certain kinds of cave passages, shown in Figure 13.2. The age of these features,  $T$ , and their height above the present channel,  $dz$ , yields the long-term incision rate,  $e = dz/T$ .

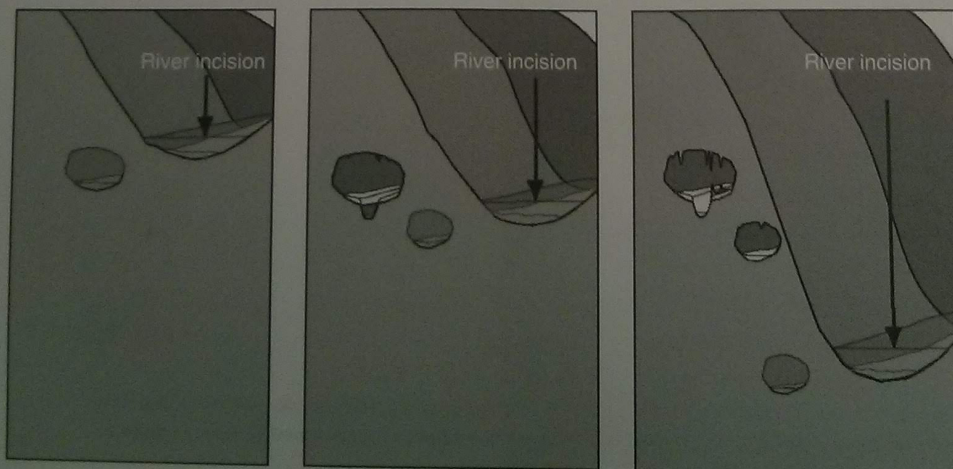


**Figure 13.2** Use of caves abandoned in the walls of river canyons to deduce river incision histories. Abandoned passages can contain quartz-rich sediment that can be dated using concentrations of cosmogenic radionuclides (figure courtesy of Greg Stock).

### Straths

Strath terraces are formed when a river cuts laterally into bedrock. They are abandoned when the river incises downward, leaving behind a bedrock bench that is often mantled with a thin cover of sediment (Hancock and Anderson, 2002). In some instances, especially in hard rock, the bedrock of these benches can be beautifully ornamented with potholes and flutes that clearly reflect that the bench was once the channel bed. In weaker bedrock, the bedrock morphology is less spectacular, and can be nearly planar. The mantling sediment can be coarse to fine alluvium, and up to many meters thick. They should not be confused with alluvial or fill terraces, in which the entire feature is composed of sediment.

### Lava flows

Because it is a fluid, lava flows down channels. When this happens, the lava instantly buries any sediments on the channel bed. If the cooled lava flow is less erodible than the local bedrock, subsequent fluvial erosion will favor the local rock, causing the channel to migrate to the side of the lava top. The abandoned lava flow is a cast, fossilizing the river channel. One example of this is the tablelands of the western Sierra Nevada foothills, in which sinuous basalt-capped ridges stand high in the present landscape. In this case, the landscape is said to have been "inverted": what was once the channel floor is now under a volcanic veneer at the ridge top. If the lava flows can be dated, for example by Ar/Ar methods, a minimum rate of incision can be estimated by dividing the height of the base of the lava flow above the modern river channel by its age.

### Caves

Some types of roughly horizontal cave passages can be identified as having been formed at or very near the baselevel imposed by the nearby surface stream (Palmer, 1991). These "phreatic" (meaning relating to underground water below the water table) passages are then abandoned as the stream incises further, sometimes developing a characteristic keyhole cross section illustrated in Figure 13.2. When sediment mantling the floors of these passages, or tucked in alcoves in them, can be identified as bedload from the adjacent river, the possibility of dating this

material exists. For example, if the sediment is granitic, and the cave is formed in marble, the sediment is clearly allochthonous (meaning it came from elsewhere). The time since the sediment was deposited in the cave can be used to calculate an incision rate. In essence, such caves serve the same role as strath terraces. However, because they are internal to the rock, they are relatively immune to removal by landsliding, and can therefore record even longer-term incision histories. Of course, carbonate bedrock is required, meaning this method is restricted to specific geologic settings.

Methods for constraining the ages of caves include paleomagnetism, dating of basal ages of speleothems, and calculation of burial ages using the concentrations of cosmogenic radionuclides (see Stock *et al.*, 2005). All but this last method pose significant problems. Paleomagnetism is a coarse tool; the last full reversal of the field, the Bruhnes-Matuyama, was roughly 700 ka. It has also been shown that the basal ages of speleothems (calcite cave deposits – usually stalagmites) are not trustworthy, and always post-date the true age of the cave derived by other more reliable methods. This reflects the fact that speleothems form very slowly from seeping water, sometimes individual drips from the ceiling, the beginning of which can significantly post-date the opening of the passage. As discussed elsewhere (Chapter 6) any quartz-bearing sediment that is buried deeply enough to be out of range of new cosmogenic production can be dated using the ratio of  $^{26}\text{Al}/^{10}\text{Be}$ . The ratio of these cosmogenically produced nuclides decays at a rate dictated by the decay rates of the two nuclides:

$$R = \frac{[^{26}\text{Al}]}{[^{10}\text{Be}]} = \frac{[^{26}\text{Al}]_o e^{-t/\tau_{\text{Al}}}}{[^{10}\text{Be}]_o e^{-t/\tau_{\text{Be}}}} = R_o e^{-t(1/\tau_{\text{Al}} - 1/\tau_{\text{Be}})} \quad (13.1)$$

The timescale over which this method works is several times the characteristic time,  $\tau = 1/(1/\tau_{\text{Al}} - 1/\tau_{\text{Be}}) = \tau_{\text{Al}}/[1 - (\tau_{\text{Al}}/\tau_{\text{Be}})]$ , which is about 2.07 Ma for the  $^{10}\text{Be}$ – $^{26}\text{Al}$  pair. Caves may therefore be dated back to about 5 Ma, which is a very useful time span for river evolution. In the Kings Canyon example illustrated in Figure 13.3, you can see that this long time span and the presence of numerous caves in the walls of the canyon provides unique control on the history of incision, revealing in this case a tenfold decline in incision rate.

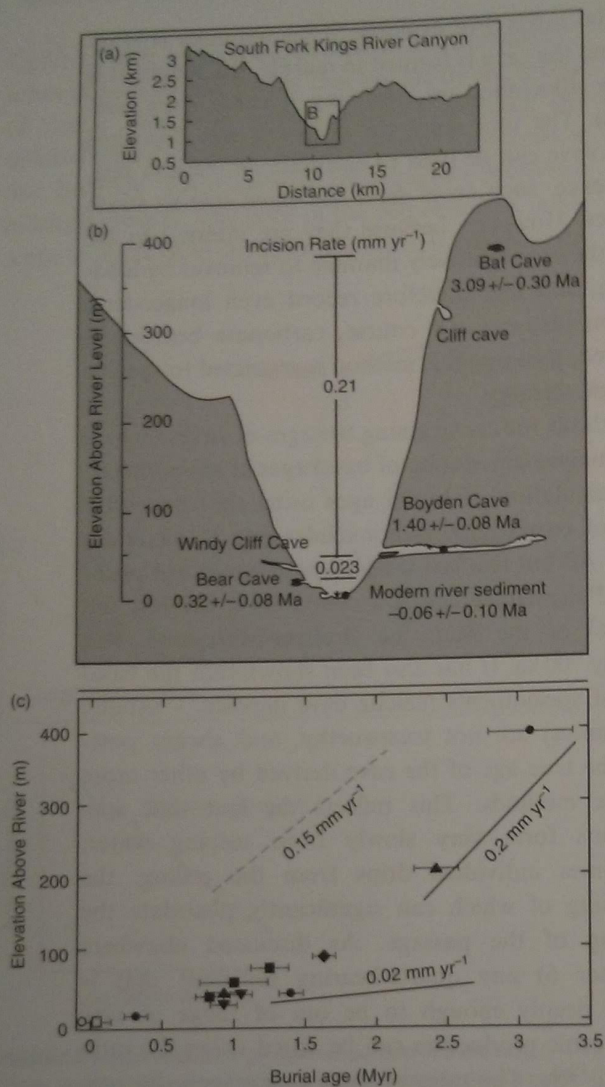


**Figure 13.3** Erosion history of Kings River Canyon based upon multiple cave ages derived from  $^{26}\text{Al}/^{10}\text{Be}$  in cave sediments. Rapid incision from 3 Ma to  $\sim 1$  Ma appears to have been followed by much lower rates since then (after Stock *et al.*, 2004, Figures 2 and 3).

### Cosmogenic radionuclides on the channel floor

In yet another application of cosmogenic radionuclides, erosion rates of the bedrock floor of a channel can be measured over millennial timescales. Consider sampling a piece of bedrock from the channel floor at low flow conditions. Just as for measurement of bedrock lowering rates at points on hillslopes or summits, the concentration of radionuclides will reflect the time a rock has spent within the nuclide

production zone. Ignoring decay (appropriate for rapid erosion rates), the concentration is

$$C = P_{\text{eff}}T = P_{\text{eff}}z^*/E \quad (13.2)$$

where  $z^*$  is the production length scale (roughly 60 cm in rock),  $T$  the time the rock took to be eroded the last  $z^*$ , and  $E$  the rate of erosion. The only trick lies in calculating the effective production rate,  $P_{\text{eff}}$ . This must be adjusted not only for latitude and altitude, as we have discussed in Chapter 6, but for the shielding by water at stages above the level of the sampling site (Hancock *et al.*, 1998). This can be done with the aid of a probability distribution of flow depths, and the density of water. The instantaneous shielding due to the water column will be

$$F = e^{-((H-z)/z_{*w})} \quad (13.3)$$

where  $(H-z)$  is the thickness of the water above the sampling elevation,  $z$ , and  $z_{*w}$  is the length scale for attenuation of cosmogenic radionuclide production in water (about 1.6 m). The results are average rates over a specific timescale, set by the time it took for the rock to come the last  $z^*$  to the surface. This time is  $T = z^*/E$ . For example, the Indus River erodes at rates of at least 1 mm/yr, making the averaging timescale roughly 600 years. This nicely fills a gap between rates deduced from real time monitoring (from one to a few years) and those deduced from dating terraces or caves.

### Short-term monitoring

Short-term incision rates can be measured using erosion pins or holes sketched in Figure 13.4(a). Holes can be either hand or machine-drilled into bedrock surfaces of the bed of the channel, measured carefully with a micrometer, and then re-measured a season or a year later. A variant of this method involves drilling holes that are used to set up a monument bar, from which erosion can be measured at many places along a profile. These methods avoid the dependence on the accidents of nature needed to form a strath, or a cave, but are limited to channels with relatively high erosion rates. Repeated measurements of this sort can resolve small fractions of 1 mm of erosion. They can also be used to address more fine-scale issues relevant to the specific processes accomplishing the erosion.

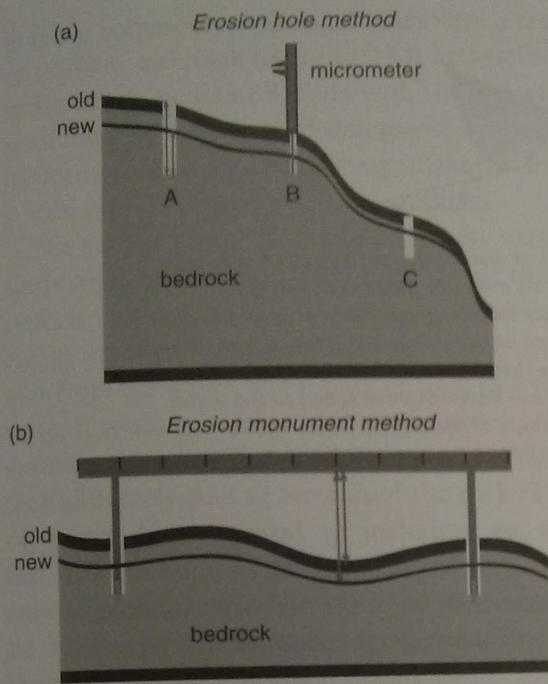


**Figure 13.4** Methods for measuring short-term erosion rates in bedrock channels. (a) Erosion holes whose depths are measured with a micrometer, which is repeated to determine the change in depth of the hole. (b) Monument method in which monument mounts are drilled into bedrock of channel floor, to which a rigid bar is mounted. The latter method allows measurement at many locations (ticks on bar) between the holes.

We illustrate these methods with two examples. Hancock *et al.* (1998) report results from the middle gorge of the Indus River in which the river crosses a band of various rock types in an area known to be exhuming at rapid rates from fission track analysis. The depth of the Indus River in this region swings by 10–15 m annually, reflecting snowmelt in the 100,000 km<sup>2</sup> drainage area above it. This allowed access to portions of the bed in April that would surely be covered by >10 m of sediment-laden water for a couple of summer months, and would be exposed again when the stage falls in the winter months. Hancock used erosion holes of the sort sketched in Figure 13.4(a) to document up to 12 mm of erosion in a single year, with strong dependence on rock type and on small-scale flow dynamics. As seen in the photograph of Figure 13.5, some of the pencil-thin holes had nucleated small erosion scour flutes in the downstream direction.

Employing a variant of the erosion hole monument method, Hartshorn *et al.* (2002) documented erosion caused by the huge super-typhoon Bilis as it hammered



**Figure 13.5** Fluted bedrock in channel of middle gorge, Indus River, Pakistan, as it passes through the Himalayas. Flow is from left to right, pencil for scale. Lowering of the gneissic bedrock occurs by upstream propagation of small-scale flutes, which ornament larger scale bed undulations. At this and similar sites, bedrock lowering rates of several mm/yr have been documented by repeated measurement of erosion holes (photograph by R. S. Anderson).

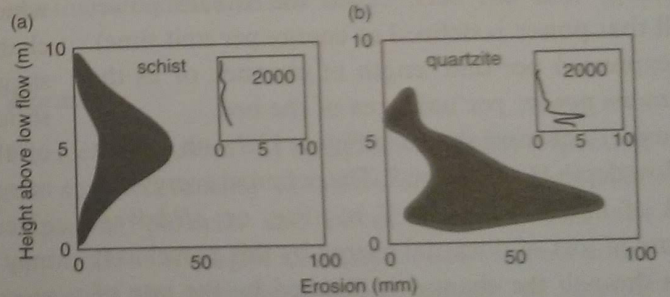
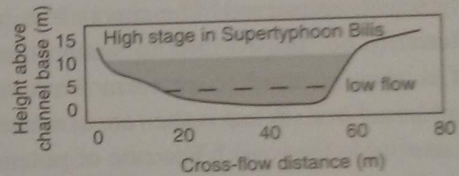


**Figure 13.6** Documentation of channel erosion in a bedrock gorge in Taiwan during Typhoon Bilis. Erosion patterns in both schist (left) and quartzite (right) show maxima well above the low-flow stage, and decline smoothly to zero at the maximum stage recorded (redrawn from Hartshorn *et al.*, 2002, Figure 3, reprinted with permission from the American Association for the Advancement of Science).

the highlands of Taiwan in 2000. Their results reproduced in Figure 13.6 reveal that the schist bedrock channel floor was lowered by up to 100 mm in this single event, more than an order of magnitude more than the erosion in an entire year of more normal hydrologic conditions. Interestingly, they report a pattern of

erosion that displays a maximum at about 5 m above the low flow stage, falling to zero at the high-water mark (10 m). This is yet another example of the importance of large events in geomorphology, and must be captured in any theory of fluvial bedrock erosion.

## Erosion processes

We now review the processes that are important in driving the erosion of bedrock in channels. We begin with a short introduction to the approach taken most commonly in modeling fluvial profile evolution, the stream power approach, as it sets the context for more specific physics.

### The stream power approach

A river is water falling down a sloping channel. The water uses gravitational potential energy as it moves down. Conservation of energy demands that the total energy of the system is conserved. The energy loss in falling must therefore be transformed to some other form. Some of it may be used to perform work of erosion on the channel bed. What is the rate at which energy is made available for work? The rate of potential energy loss has been called the stream power (recall that power is defined as energy per unit time). It is expressed per unit length of channel, or as the *unit stream power*, per unit area of the bed.

Consider a channel shown in Figure 13.7 with a width  $W$ , a flow depth  $H$ , and slope  $S$ . The potential energy of a parcel of fluid of volume  $V$  is  $\rho Vzg$ , or  $\rho HdxWzg$ . The rate of loss of potential energy by this parcel as it moves through the channel is dictated by the rate of loss of elevation, set by the flow speed and the channel slope,  $US$ . We may now formulate the rate of potential energy loss per unit length of channel,  $dx$ , as

$$\Omega = \rho g HWUS \quad (13.4)$$

where the  $dx$  has cancelled out, and we have defined  $S = \tan \theta$ . Noting that the quantity  $HWU$  is equal to the water discharge,  $Q$ , this reduces to

$$\Omega = \rho g QS \quad (13.5)$$

Finally, if we formulate this as a rate of power loss per unit area of bed by dividing the stream power per unit length of channel by the width,  $W$ , the result is the *unit stream power*,

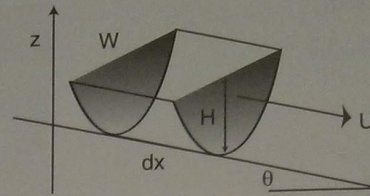


**Figure 13.7** A mass of water  $\rho Hdx$  has potential energy  $mgz$ . Since neither its mass nor gravity change as it moves, the water parcel loses potential energy at a rate dictated by the slope of the channel and the rate at which it loses elevation. The rate of loss of elevation,  $dz/dt$ , is in turn governed by the mean down-channel speed of the water parcel,  $U$ , and the slope of the bed. In other words,  $dz/dt = U \tan(\theta) = U \sin(\theta)$  for small angles.

$$\omega = \rho g QS/W \quad (13.6)$$

Noting that the shear stress at the bed of the channel is  $\tau_b = \rho g HS$ , an equivalent expression for unit stream power is

$$\omega = \tau_b U \quad (13.7)$$

and channel width is only slowly changing, then one can see the appeal of the stream power formulation and write

$$dz/dt = k\omega = k\rho g QS/W \quad (13.8)$$

where the constant  $k$  reflects the erodibility of the channel, among other things. This formulation suggests that the first-order control on river incision should be the local discharge of water, the local slope of the channel, and the channel width. One chief attraction of this approach is that two of these variables can be derived from maps. The channel slope may be derived from crossings of contours (or more recently from analysis of DEMs, for example using Rivertools (Peckham, 1998)). Recall the results of Seidl and Dietrich (1992), in which they deduced that erosion rates were proportional to the area–slope product,  $AS$ . If the water discharge is proportional to drainage area, then  $AS \sim QS$ , the proportionality constant reflecting the effective precipitation. The river discharge can at least crudely be associated with the local drainage area, which again can be assessed from maps using either a planimeter or analysis of DEMs if simplifying assumptions about the effective runoff can be justified. We note that this latter assumption breaks down if precipitation or effective runoff is highly non-uniform (see below about orographic effects). In addition, channel width cannot be derived from either

maps or commonly available DEMs with a resolution of 10–30 m, although recent LiDAR and stereo-photo methods can generate DEMs with the necessary 1 m resolution. In addition, specific processes may result in formulations that differ significantly from the stream power approach we have outlined.

The stream power formulation, or its variant, the shear stress formulation, does not identify the specific process responsible for incision. It relies upon an energy argument. A certain amount of energy is available from the water, and it may be used in a variety of ways. It could be used to heat up the water, to pick up sediment from the bed, or to generate cracks in rock that ultimately lead to erosion of the rock. The value of  $k$  may be conceived as including an efficiency factor, reflecting what fraction of this available energy goes into eroding the rock. We seek here to be more specific about the processes accomplishing the erosion. There is much debate about the efficacy of each of these processes. Their relative importance depends strongly upon the lithology (hardness, fissibility, pre-existing planes of weakness, and so on), the sediment load, and the fine-scale flow mechanics.

We can approach the problem as follows. Say lowering of the bedrock occurs in layers of thickness  $\delta$ , which are connected to one another by bonds of strength  $E$  (energy required to break a bond), and of density  $B$  bonds/unit area. The energy needed to detach the slab is therefore  $BE$ . This combination is akin to what is called the work of fracture, and has units of energy per area. The mean lowering rate, averaged over many detachments, is

$$\frac{dz}{dt} = -\frac{\delta}{T} \quad (13.9)$$

where  $z$  is the bed elevation,  $t$  is time, and  $T$  is the specific time needed to accumulate enough energy to break all these bonds. The time  $T$  may be simply calculated from

$$T = \frac{BE}{\alpha\omega} \quad (13.10)$$

where  $\omega$  is the rate of delivery of energy per unit area of bed [=  $E/L^2T$ ], or the unit stream power, and  $\alpha$  is the fraction of this power converted into breaking of bonds. Recall that unit stream power is the energy made available by dropping a parcel of water down the potential gradient per unit time and unit area of bed. It has units of  $M/T^3$ , or  $kg/s^3$  in SI units.

Substituting the expression for the timescale  $T$  into the general erosion equation (Equation 13.9), yields

$$\frac{dz}{dt} = -\frac{\alpha\delta}{BE}\omega \quad (13.11)$$

From this we can see the ingredients of  $k$ , the constant typically seen in the stream power formulation (Equation 13.8). Note that  $k$  has units of  $LT^2/M$ , or  $m^2 s^2/kg$  in SI units. But the way to think of it is as the product of an efficiency factor (and a pretty small one) with a slab thickness divided by the energy needed to break a unit area of such a slab free from the slab beneath it. The bigger the slabs, and the more efficiently the energy is delivered to the bed, the faster the erosion. The weaker the bonds (lower  $E$ ), and the fewer bonds there are per unit area (lower  $B$ ), the more rapid the erosion.

One can also accommodate a threshold in such a formulation if we acknowledge that the delivery of energy to the bed comes as packets and that the packets come in a variety of sizes (impacts of turbulent eddies, impacts of particles embedded in them). One can imagine that some of these are insufficient to break any bonds, meaning that this portion of the distribution of power does not participate in lowering the bed.

We now address those specific erosional processes that have been identified as being responsible for erosion in bedrock channels.

### Abrasion

Rock can be worn away by particles directly impacting the surface, causing abrasion of the surface. The impacting particles can be of all sizes, and can approach at all angles and speeds. Each impact either promotes the growth of a micro-crack, or extends existing cracks sufficiently to separate a small piece of the impacted rock. The erosion rate depends upon the properties of the flow, the amount and caliber of the sediment, and the susceptibility of the rock to abrasion. While there is no full theory of the physics of abrasional wear, we can appeal to what has been learned in the study of ventifaction, or abrasion by particles entrained in air (see Chapter 15 on sediment transport by wind). The basic physics are parallel.

We can make much progress with two facts: (1) The particles must hit the surface, and (2) when a particle does impact, the mass of rock ejected from the impacted surface is proportional to the kinetic energy of the impacting particle. These statements can be



combined by noting that the erosion or lowering rate of a rock surface is proportional to the flux of kinetic energy to that surface,  $q_{ke}$ . This may be written as

$$q_{ke} = C m_p U^3 \quad (13.12)$$

where  $C$  is the near-bed volumetric concentration of particles in the flow,  $m_p$  is the mass of an individual particle, and  $U$  the mean near-bed flow speed (which sets the speeds of the particles). The third power of the speed comes from the product of the kinetic energy of a particle, which goes as  $U^2$ , and the flux of particles to the surface, which goes as  $U$ . If in addition the particle concentration,  $C$ , depends upon the flow speed, then the dependence on flow speed will be even stronger. For example, in eolian systems,  $C \sim U^2$ , implying a fifth-power dependence on wind speed. The point is that the abrasion rate ought to depend very strongly on flow speeds. The nonlinearity in  $q_{ke}$  amplifies greatly the importance of high flow events, and indeed the peak flows in a given year.

But where and when do particles impact a surface? This depends strongly upon the details of the flow field at the bed. Clearly, if the bedrock is mantled by sediment, particles entrained in the flow cannot impact the bedrock. But if the bedrock is exposed, the impacts of particles can be highly non-uniform. The trajectories of water parcels become tangent to the non-porous bedrock surface as they approach it. Hence, in order to impact the surface, the suspended sediment particles must decouple from the flow. This decoupling is more likely over highly curved surfaces: the stronger the curvature, the more likely a particle will get flung against the surface, decoupling from the fluid due to its own momentum. The more massive the particle, the greater its momentum, and the lower the curvature necessary to cause decoupling. Consider a bump in the bedrock bed, or an immobile boulder on the bed shown in Figure 13.8. The flow responds to this obstacle to the flow well ahead of the bump, and the flow lines begin to deflect in response to the pressure field set up by it. On the rear of the bump, the flow lines reconverge. Under many natural conditions of flow speed and bump size, the flow "separates" in the lee of the obstacle, creating a zone occupied by tightly wound eddies. The flow curvature on the front of the obstacle is small, while the separation eddies display strong curvature. The result is the stronger decoupling of particles from the flow in the rear of obstacles, generating what has been called the "attack from the back."

Which grain sizes do the work? Is it particles participating in bedload or suspended load that accomplish the abrasion of the bed? While suspended particles are traveling at nearly the speed of the water, and therefore possess significant kinetic energy, bedload particles re-encounter the bed periodically and travel at only small fractions of the near-bed flow speed. In addition, bedload particles will impact neither the rear of an obstacle, nor the base of overhangs. Yet ornamentation of the river channel is commonly observed at these sites. Very fine sediment, on the other hand, what we call wash load, is so small that it is very tightly coupled to the flow, and will not diverge from it even when the flow displays strong curvature. The above observations suggest that it should be the medium-size fraction, the coarse fraction of the suspended load, that accomplishes the majority of the abrasion.

This is not to say that we may ignore bedload. Indeed, laboratory experiments performed by Sklar and Dietrich (2001) in rotating abrasion mills allow us to explore the role of bedload in abrasion. These experiments, the results of which are illustrated in Figure 13.9, have suggested that the abrasion rate is strongly dependent upon the strength of the bedrock being eroded; the erosion rate goes as the inverse square of the tensile strength, and is higher when the abrading sediment is stronger. More intriguing is the relationship between sediment load and erosion rate, shown in Figure 13.10. The dependence of erosion on the tensile strength suggests a means of collapsing many experiments onto one plot by normalizing the erosion rate with the square of the tensile strength of the bed. The results imply that erosion should be most efficient under some optimum sediment load. Below this load, the number of impacting particles limits bedrock erosion, while above it, the great number of particles near the bed prevents particle impact with the bed, and effectively shields it from erosion. These experiments have greatly influenced subsequent research on bedrock river incision. Some maintain that one can craft an incision rule in which the erosion rate depends upon the local transport rate through appeal to these experiments. Others maintain that access to the bed requires that the thickness of the alluvial fill on the bed must be explicitly accounted for, and that whenever that thickness is greater than the ability of the river to scour through it in a meaningful flood, bedrock incision by whatever process is prevented. In either case, attention is focused on

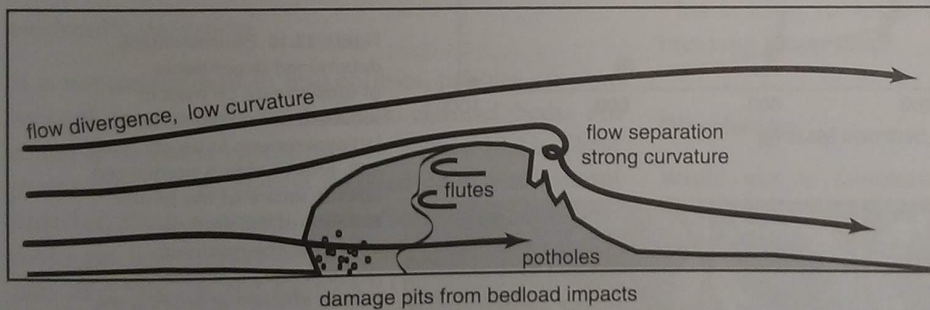


**Figure 13.8** The attack from the back. Top: boulder in the channel of the middle gorge of the Indus River, Pakistan. Flow is from left to right. Person kneeling beside river in distance (photograph by R. S. Anderson). Bottom: sketch of flow separation in the lee of obstacles in the flow generates very strong curvature of the flow, efficiently decoupling suspended particles from the flow (after Hancock *et al.*, 1998, Figure 6, with permission from the American Geophysical Union).

the complexity of bedrock river incision when we acknowledge that at most times and most places bedrock beds are observed to be mantled with sediment.

### Quarrying

Just as in subglacial erosion, quarrying of rock in chunks larger than single grains can be an efficient means of lowering the channel bed. There are two

steps to the process. First, a crack or fracture must be generated to isolate a block of channel bedrock, and then the block must be removed. The fracturing can be accomplished by impacts of large blocks with the bed, by hydraulic wedging (see below), by frost-cracking subaerial exposure during low stages, by cavitation, and so on (e.g., Whipple *et al.*, 2000). It may also be the case that the rock arrives at the river bed already highly fractured and jointed, simply due

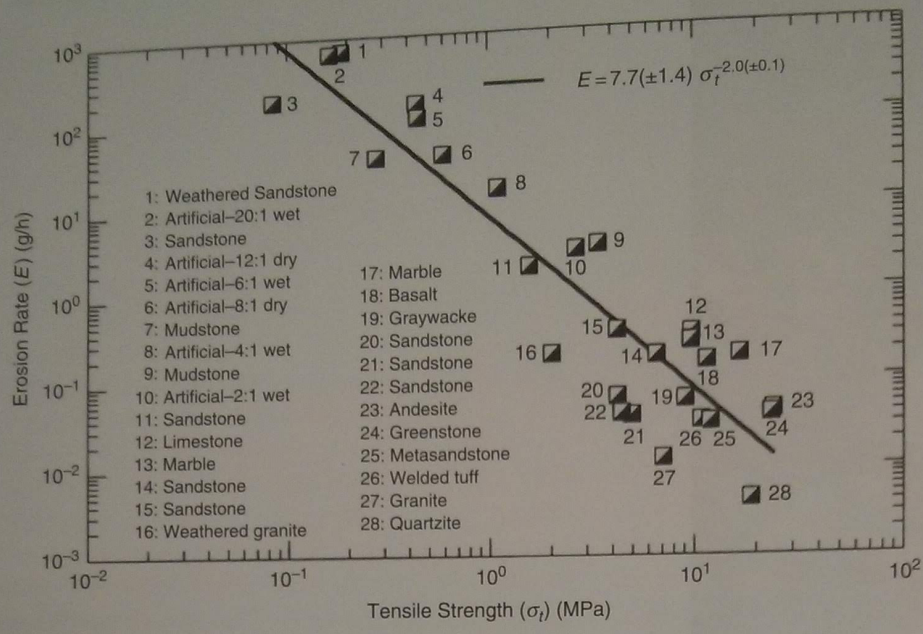


Figure 13.9 Dependence of erosion rate (in grams/hr) on the tensile strength of the rock being eroded, as determined by experiments in an abrasion mill. The power-law fit on this log-log graph suggests an inverse square relationship (after Sklar and Dietrich, 2001, Figure 2).

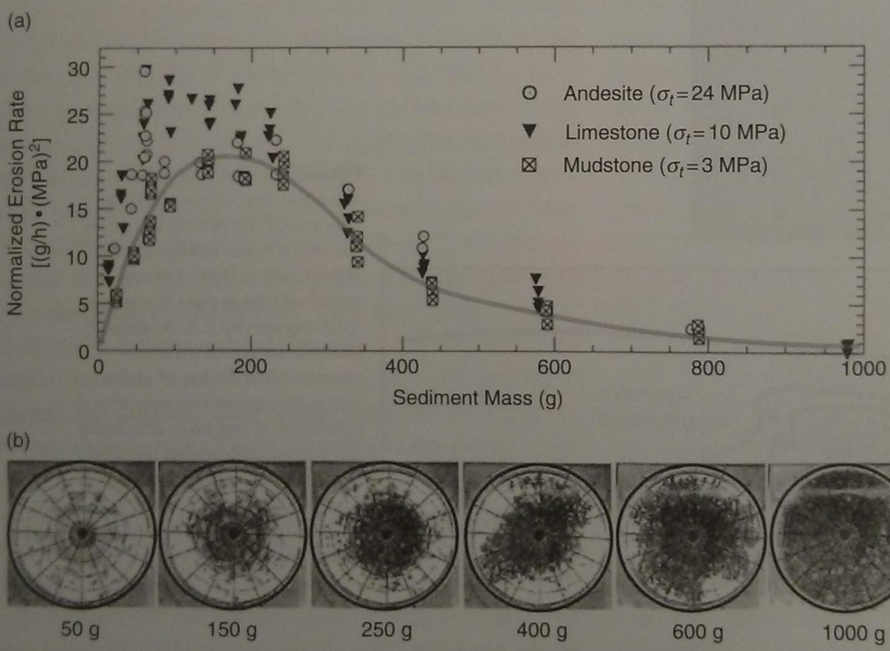
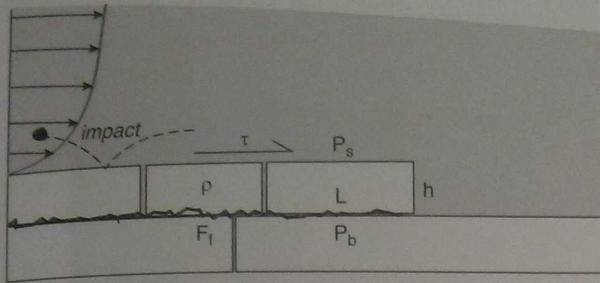


Figure 13.10 Experimentally determined dependence of erosion rate on mass of sediment in transport. Results of lab experiments in an abrasion mill. Erosion rate is normalized against square of the tensile strength of the eroding substrate. The maximum suggests a sediment loading that is most efficient at eroding the bed, above which sediment load damps erosion (after Sklar and Dietrich, 2001, Figure 4).

to the stress field associated with its position in a valley bottom (e.g., Miller and Dunne, 1996; Molnar, 2004), or the strain history to which the rock mass was subjected during faulting in the orogeny (Molnar *et al.*, 2007).

Taken most simply, the removal of bedrock chunks takes place by shoving a block across a planar surface

after it has been detached from its adjoining rock mass. We sketch the situation in Figure 13.11. The force provided by the shear of the flow over the top of the block must exceed the frictional resistance against the underlying rock. The forces include the mean pressure on the top of the block, the mean stress on the base of the block, and the friction on the



**Figure 13.11** Quarrying of bedrock blocks from a river bed. Stresses imposed by the flow, and by impacting particles, must overcome the resistance to entrainment arising from frictional contact with adjacent blocks, and with the weight of the block itself. Geometry matters: a block enclosed by others on all sides is far less likely to be entrained than one at the edge of the step in the bed.

base and sides of the block. In general, the likelihood of extraction of a block can be cast as a shear stress that must exceed a threshold or critical stress; the erosion rate should therefore scale as the excess shear stress:  $E \sim (\tau_b - \tau_c)$ . But it should also be clear that edges matter. While a block in the interior of a planar bed will experience the same fluid stresses on its top, it is geometrically constrained by adjacent downstream blocks. It is therefore to be expected that bedrock beds unravel headward, essentially as a set of micro-knickpoints.

### Hydraulic wedging

It is not uncommon to find cobbles, pebbles, or sand wedged into cracks in bedrock channel beds. An example of this is reproduced in Figure 13.12. These grains can be so tightly wedged that you cannot dislodge them without a crowbar. How did these rocks get into the cracks, and what role might they play in erosion of the bedrock? The obvious answers to the first question are (1) the rocks were forcefully injected into the crack, or (2) they were passively accepted into a crack that was momentarily widened while sediment was nearby. Given the specific sites, it is most likely the latter. But this merely raises the question of how cracks in the bed widen. While there exist no data to prove this, nor experiments targeting this phenomenon, the bed likely flexes due to the rapid and large pressure variations it experiences in the complex turbulence at high flows (akin to the shuddering of coastal cliffs associated with wave attack). This flexing needn't be large, as one can easily



**Figure 13.12** Pebbles perfectly wedged into a crack of Indus river bedrock. Lip balm for scale. Smooth surface of the outcrop reflects abrasion during immersion in moderate to high flows. Pebbles cannot be removed without breaking the pebble. Clasts are likely wedged into the crack when it is temporarily widened during pressure fluctuations associated with high flows. The phenomenon is discussed briefly by Hancock *et al.*, 1998 (photograph by R. S. Anderson).

imagine a small crack accepting a small grain, then not being able to close; some later flex allows a yet larger grain to enter, propping it open yet further, and so on. In this fashion an existing crack in the bedrock may grow. Beds with wider or more numerous initial cracks would be most susceptible. Note also that bed-load sediment is required for this process to operate. This is akin to some engineering applications for breaking down solids.

### Dissolution

While not a dominant player in most settings, dissolution of a channel bed can be important in highly soluble rock types and in cave settings. The greatest testimony to this is the formation of caves in carbonate rocks. Because dissolution is generally not considered in analyses of surface channel incision, we will turn to work on cave formation to characterize the controls on channel growth by dissolution (Palmer, 1991).

The rate of wall retreat,  $S$ , in a channel due to dissolution is given by

$$S = \frac{Q}{p\rho_r} \frac{dC}{dL} \quad (13.13)$$

where  $Q$  is the water discharge,  $p$  is the wetted perimeter,  $\rho_r$  is the rock density, and  $dC/dL$  gives the change in relevant solute concentration with

distance downstream. The downstream change in solute concentration is controlled by the dissolution rate of the rock, but also depends on the ratio of mineral surface area to water volume, the degree of chemical under-saturation, and the time it takes a water parcel to move through a reach. These dependences are expressed in a rate equation, which yields the rate of concentration change. In a later step, we will relate  $dC/dL$  to this rate equation:

$$\frac{dC}{dt} = \frac{A'k}{V} \left(1 - \frac{C}{C_s}\right)^n \quad (13.14)$$

where  $A'$  is the surface area of rock exposed to water,  $V$  is the volume of water,  $C/C_s$  is the saturation ratio,  $k$  is the reaction coefficient, and  $n$  is the reaction order. We rewrite the left-hand side as being given by the change in solute concentration divided by the water residence time, or

$$\frac{dC}{dt} = \frac{\Delta C}{V/Q} \quad (13.15)$$

where  $V/Q$  is the residence time for water within a stream reach. Using the approximation  $\Delta C/L = dC/dt$  in Equation 13.15, and combining Equations 13.13–13.15, we see that the rate of wall retreat is given by

$$S = \frac{k}{\rho_r} \left(1 - \frac{C}{C_s}\right)^n \quad (13.16)$$

Interestingly, the mineral surface area,  $A'$ , in the rate equation is equivalent to the wetted perimeter and reach length,  $pL$ , in Equation 13.13 and divides out of the expression. Experimental data show that the reaction order increases as the saturation ratio approaches 1.0, which has the effect of significantly slowing dissolution rates.

### Knickpoint migration

In some instances, lowering of the channel bedrock is accomplished by upriver migration of discrete steps, or knickpoints, in the profile. Here a knickpoint is defined as a steep reach sandwiched between two low-gradient reaches, as illustrated in Figure 13.13. The result is a lowering history at a point that is held at a very low rate for long periods, punctuated by rapid incision as the knickpoint migrates past. These steps occur at many scales. As a small-scale example, channels in the Blue Hills badlands of Utah, cut in the soft Cretaceous seaway shales, have profiles punctuated

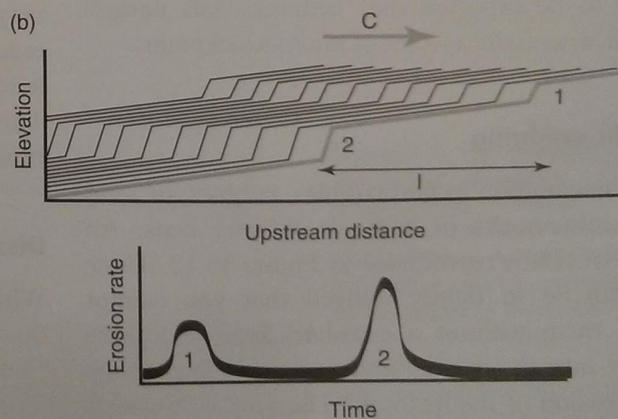
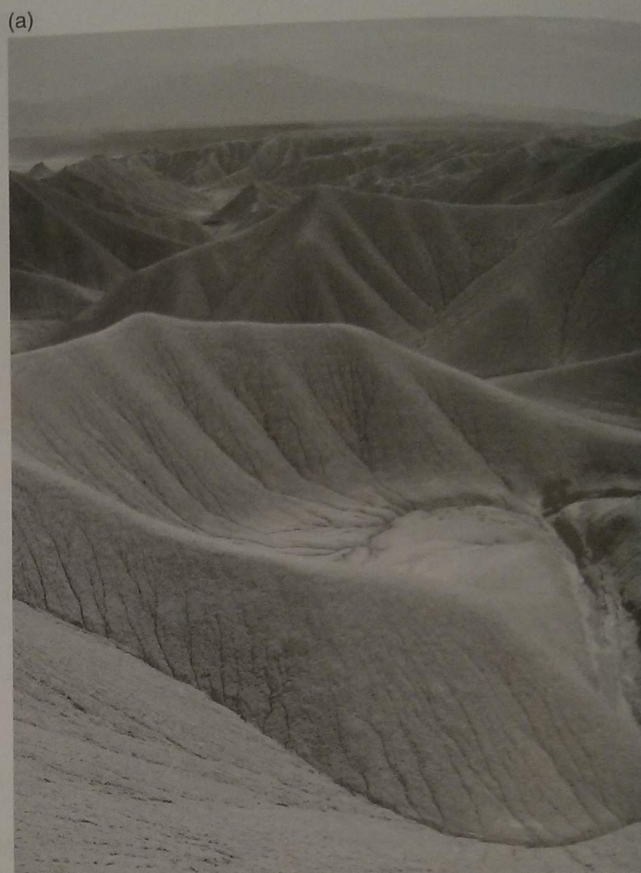


**Figure 13.13** Knickpoint migration. (a) Bluehills badlands near Fremont River, Utah, with Henry Mountains in distance. The major channels in these badlands incise largely by passage of discrete knickpoints 10–50 cm tall (overview photograph by R. S. Anderson). (b) The speed, or celerity,  $C$ , of the knickpoint up the system, depends upon rock type and water discharge. Lowering of the channel bed is accomplished largely by the migration of knickpoints past a site, which occurs over a small fraction of the total time.

by knickpoints 10–30 cm tall (Figure 13.13(a)). Over the course of a single season, in which the channels were dry except during flash floods that lasted 15–30 minutes, the knickpoints migrated up-channel by about a meter. The channel floor did not experience net erosion anywhere else. The mean lowering rate of the channel may be quantified as

$$e = CH/\lambda \quad (13.17)$$

where  $C$  is the celerity or speed of migration of the knickpoint,  $H$  its height, and  $\lambda$  the spacing between knickpoints. In order to estimate the long-term mean erosion rate, we must therefore know not only the characteristics of the steps, their height and spacing, but what governs their rates of migration.

At the other extreme lie some of the world's largest waterfalls, such as Victoria Falls on the Zambezi (described first by the great British explorer Livingstone), or Niagara Falls, where the river plummets many tens of meters before reaching the plunge pool at the base of the falls. The specific processes driving the lowering at the knickpoint, or headward erosion of the waterfall, are numerous. While Gilbert (1907) argued for the undermining of the head of the waterfall by backwearing induced by plunge-pool erosion, others have appealed to the weathering of the rock, groundwater sapping focused at the base of the step, stress relief of the headwall, and focusing of stress by the step in the profile itself. It is in the plunge pools at the base of waterfalls and major rapids in rivers that rivers are capable of overdeepening their bedrock floors. The topography, for example, beneath the Maid of the Mist plunge pool at the base of the present Niagara Falls is overdeepened by more than 30 m. Other similar steps in the bedrock occur further downstream, and have been interpreted as recording past locations where the rate of retreat of the falls was slow (see Figure 13.14; Philbrick, 1970).

### Summary of processes

It is some combination of the processes we have described above that do the work of lowering bedrock channels. As rivers cross from one rock type to another, the dominant process may change. Clear examples of this include the tributaries to the Grand Canyon in Arizona, in which the profiles cross massive sandstone reaches bounded by shales. Erosion by quarrying of the highly fissile shale is efficient, while

erosion in the massive sandstones is restricted to abrasion, which is much less efficient. The profiles reflect this: they are steep in the sandstones, and lay back in the shales. The local channel features change in accord with the dominant process. Where the rock is sufficiently fissile to allow quarrying, the bed tends to be ragged. In contrast, where the rock is massive, disallowing quarrying, abrasion dominates, and the resulting morphology is fluted, polished and/or potholed. The latter phenomenon is illustrated in Figure 13.15, in which massive Sierran granite is being eroded by potholing along the Stanislaus River.

More commonly, rivers cross complex structures that are not well bedded, and encounter three-dimensional bodies of rock with differing characteristics. These hard places may stall or steepen the profile for some time, and then let it flatten as the erosion proceeds below the hard rock. We now turn to the long-term evolution of river profiles in bedrock channels.

## Stream profiles in bedrock channels

We may now ask what the longitudinal profile of a bedrock river should look like. How does it differ from that of an alluvial river? How should it reflect changes in the lithology across which the river flows? How should it reflect the uplift rate of the rock, or the pattern of uplift? How long should a bedrock river take to respond to changes in uplift, or in climate? As usual, we start with the simplest cases. Here the simplest is the steady-state case in which constant climate drives fluvial incision into a uniformly rising rock mass of uniform erodibility.

### Steady uniform case

For the sake of conformity with the existing literature, we will generalize the stream power rule to acknowledge the possibility that specific processes can yield different dependences on slope and on water discharge than the pure stream power case. Starting with the unit stream power equation, we generalize to

$$E = k_1 A^m S^n \quad (13.18)$$

where  $k_1$  now absorbs the density of water, the acceleration due to gravity, the susceptibility of rock to erosion, the effective precipitation relating area to discharge, and the scale for the width of the channel.

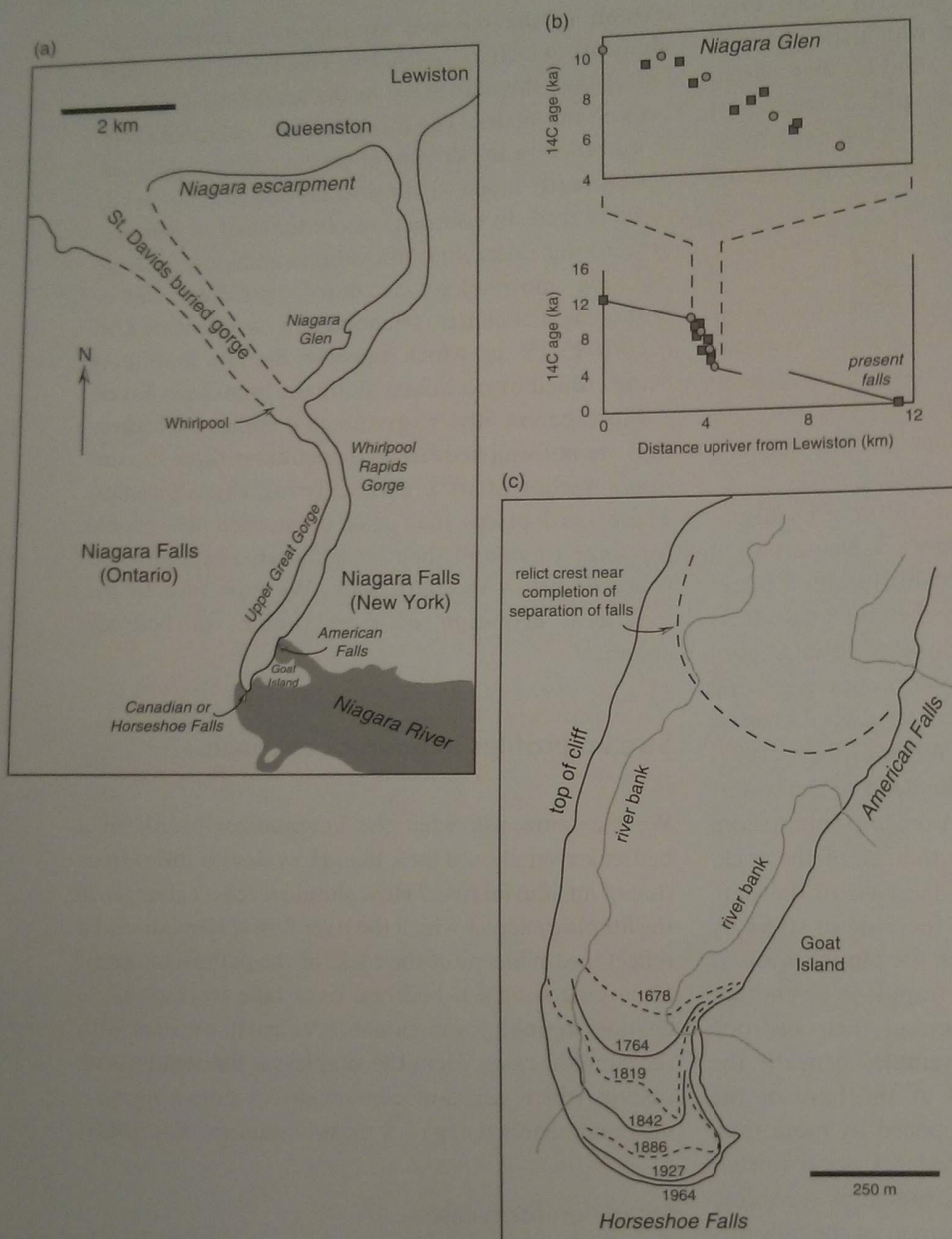


**Figure 13.14** Niagara Falls and its retreat history. (a) Map of Niagara River through the falls showing two major waterfalls and several prominent narrows en route to Lewiston (after Pengelly *et al.*, 1997, Figure 2). (b) Retreat history documented using  $^{14}\text{C}$  dating of molluscs in riverbank (squares) and Wilson terrace deposits (circles). The retreat rate was much higher through the Niagara Glen area, leaving a narrow gorge segment. Average retreat rate has been 1 m/yr over the Holocene (after Tinkler *et al.*, 1994, Figure 5, with permission from Elsevier). (c) Historical retreat history documented by repeated surveys of the cliff top reveals continued retreat at roughly 1 m/yr (after Philbrick, 1970, Figure 1).

We return to this width problem later in the chapter. In steady state, the erosion rate,  $E$ , must balance exactly the uplift rate of the rock,  $U$ , which for simplicity we assume to be spatially uniform. This leads to

$$S = (U/k)^{1/n} A^{(-m/n)} \quad (13.19)$$

In other words, we expect (predict) an inverse relationship between slope and drainage area that is very

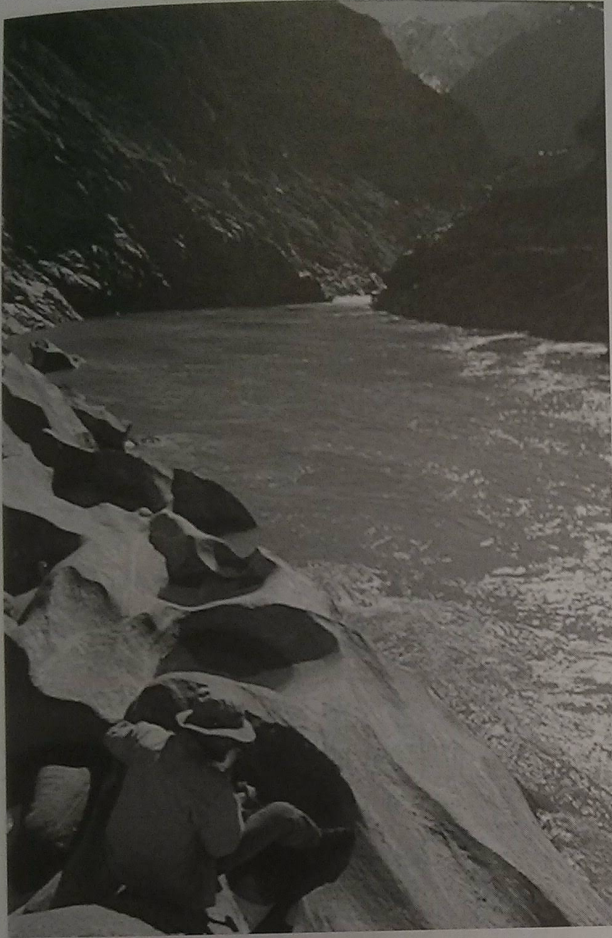


**Figure 13.15** Potholes beside the Indus River in its middle gorge below the Skardu basin. Here massive migmatitic granitoid rock disallows plucking of blocks, forcing the river to abrade its channel floor, resulting in ornamentation of the bed by potholes. Photo taken at April low flow conditions; high flows are roughly 14 m above this (photograph by R. S. Anderson, 1996).

specific, as is shown in Figure 13.1. The ratio  $m/n$  has been called the concavity index,  $\theta = m/n$ , as it dictates the rapidity with which the slope changes as area increases (and hence with distance downstream), while the collection of constants  $(U/k)^{1/n}$  is called the channel steepness. Tucker and Whipple (2002) have reviewed the predictions of various stream erosion models. Below we summarize the expected profiles in several specific cases.

#### Steady case, but non-uniform bedrock

We can easily see from Equation 13.19 that we should expect an inverse relationship between the channel slope,  $S$ , and the erodibility of the rock,  $k$ . In fact,

over a small reach in which neither the rock uplift nor the discharge changes, the slope is a measure of the erodibility. The ratio of erodibility of adjacent reaches can be measured by the ratio of the channel slopes:  $k_1/k_2 = S_2/S_1$ . Note that in such cases the steep reaches of the profiles should not be interpreted to reflect a transient response to baselevel fall, as we discuss below. These sites should remain steep, and the steep section will not migrate up or downstream. This is exemplified in Figure 13.16, in which we show the profile of the Wind River as it crosses the Owl Creek Mountains. This is a granite-cored Laramide range. The basins on either side are composed of easily eroded Tertiary sedimentary rock; the river is significantly less steep as it incises through these basins.

#### Steady uplift, non-uniform precipitation: the orographic effect

This treatment presented so far has utilized the simplifying assumption that precipitation is uniform. This assumption allows the straightforward transformation of basin area into discharge. In general, this is not the case. In fact, a better assumption is that precipitation increases with elevation due to the orographic effect. This problem of orographic precipitation was reviewed comprehensively by Smith (1979); we have introduced this phenomenon in the Atmosphere Chapter 5. Recently, Roe *et al.* (2002) have addressed the expected changes in the steady-state stream profiles when the interaction of precipitation field with the topography (the orographic effect) is incorporated formally. In general, this requires incorporation of a function that describes the pattern of precipitation with distance from the divide,  $P(x)$ , so that we can assess the expected river discharge:

$$Q(x) = \int_0^x P(x') \frac{dA(x')}{dx'} dx' \quad (13.20)$$

where the prime indicates a dummy variable of integration,  $A(x)$  is the distribution of drainage area as a function of distance from the drainage divide. Note that for the uniform rainfall distribution case,  $P(x) = P_0$ , Equation 13.20 reduces to  $Q(x) = P_0 A(x)$ , and the drainage area may be taken as a perfect proxy for river discharge.



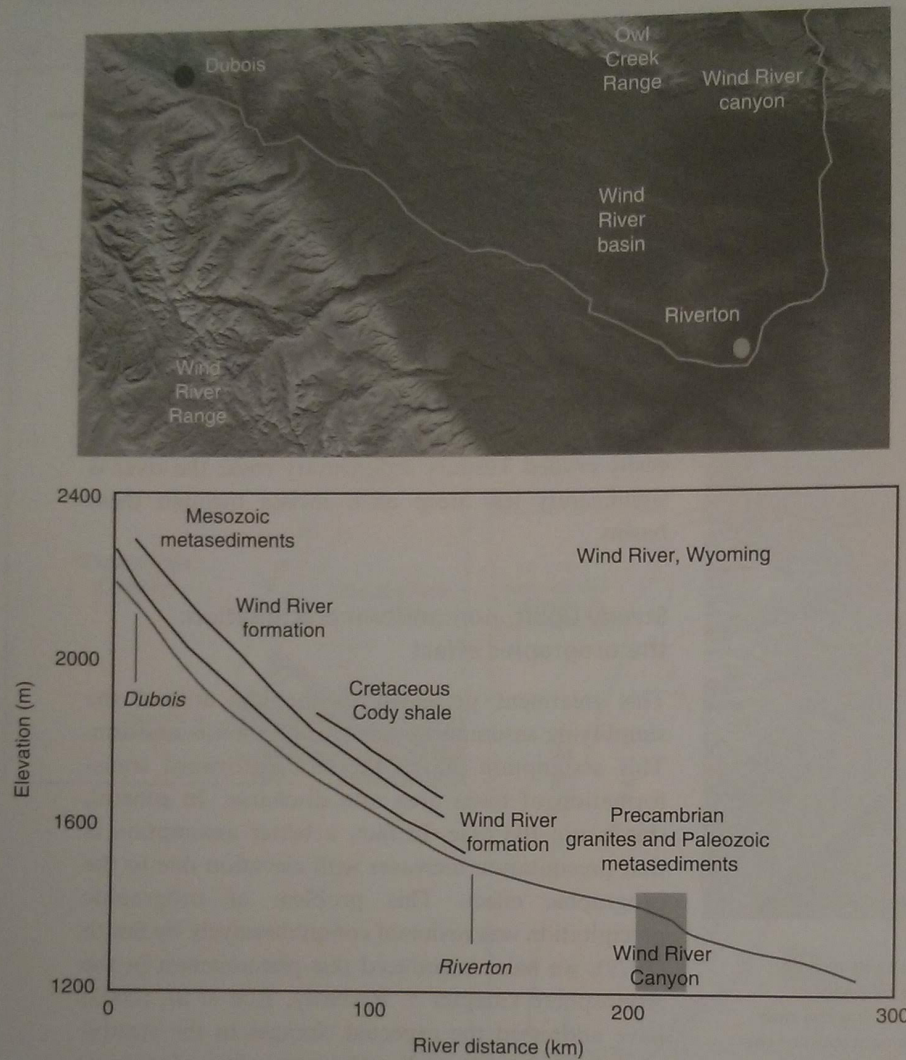


**Figure 13.16** Top: DEM of the Wind River region, northern Wyoming. Bottom: profiles of Wind River and associated terraces through Wind River valley and Owl Creek Mountains (Wind River Canyon). Note the strong steepening of the river through the gorge, in which the river encounters Precambrian crystalline rocks, in contrast to the Mesozoic and Cenozoic sediments through which the river is incising up- and downstream of the gorge (after Hancock *et al.*, 1999, Figure 2, with permission from Elsevier).

But is this simple form of  $P(x)$  appropriate for realistic landscapes? We have introduced the roles of topography in altering the pattern of precipitation in Chapter 5. Here assume for simplicity that the wind is steady in both speed and direction, approaching a mountain front at speed  $V$  (Figure 13.17). There are three effects (at least) that must be captured. First, droplets of water must grow from the airmass through condensation to sizes large enough to fall at rates that exceed the rate of rise of the airmass. The formation of droplets depends upon the degree of saturation of the airmass. This in turn depends upon the temperature of the air,  $T$ , and upon the rate of lifting of the air,  $w$  ( $=VS$ ). Second, once droplets

begin to fall (at which time they are dubbed by the atmospheric science community to be hydrometeors), they will drift further downwind before they reach the ground. The effects of temperature and rate of lift have opposing influences (Figure 13.17). As discussed in Chapter 5, the result is a pattern in which the maximum precipitation is shifted downwind from the maximum upwind-facing slope of the topography. For short hills, this can yield a maximum in precipitation downwind of the crest, but more commonly, at the mountain range scale, this results in a precipitation maximum upwind of the crest of the range. Roe *et al.* (2002, 2003) have explored the role of orographically induced non-uniform precipitation on the

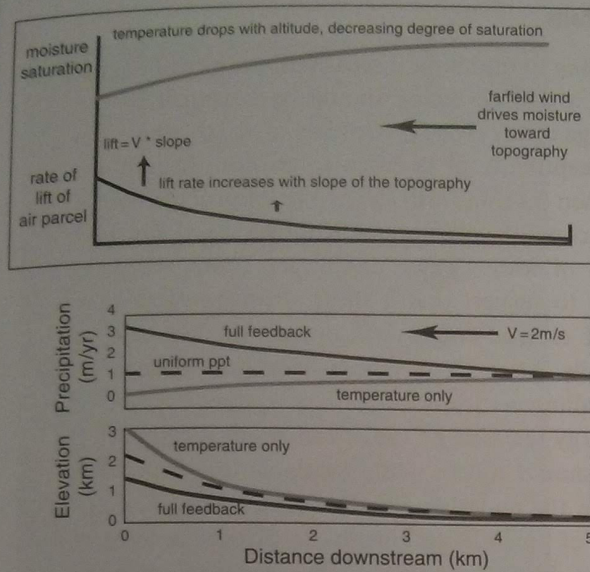


**Figure 13.17** Changes in bedrock steady stream profiles caused by orographic feedbacks. Top: competing effects of slope and elevation on precipitation. The slope of the topography forces the airmass to rise, promoting precipitation. The temperature drop with elevation reduces the degree of moisture saturation. Middle: resulting change in precipitation pattern from the far-field rate for temperature effect only, and for both effects. The slope effect dominates. Uniform precipitation case shown for comparison (dashed). Bottom: resulting steady-state profiles for temperature-only and full models. The local channel slope needed to accomplish incision of rising rock mass is everywhere lower in the full model, resulting in a shallower profile and lower total relief in the channel network (redrafted from Roe *et al.*, 2002, Figure 1).

profile of a bedrock river. As sketched in Figure 13.17, holding the tectonic forcing of the landscape constant (and uniform), the expected steady river profile developed in the face of more realistic orographic precipitation has a lower overall slope, resulting in a lower maximum topography (range crest) than the counterpart expected from uniform precipitation. This is a direct consequence of the enhanced precipitation in the headwaters, which results in more discharge everywhere downstream. Given that the stream power goes as the product of the slope and the discharge, less channel slope is required to drive the incision necessary to counter rock uplift.

### The transient case

In reality, tectonic and climatic forces vary through time on many timescales. An important question is

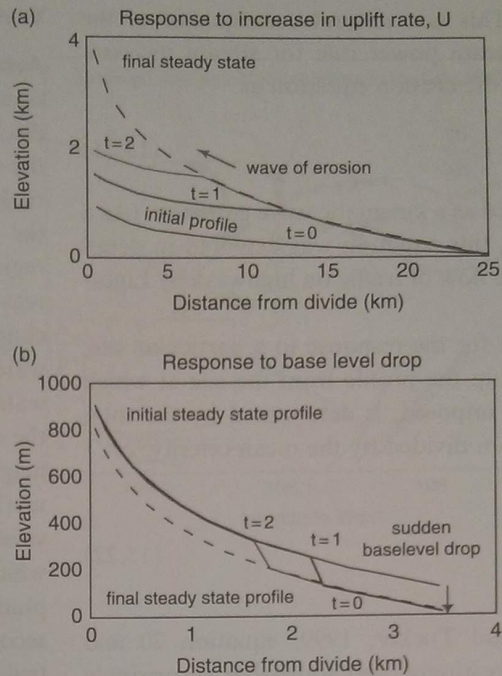


**Figure 13.18** Response of bedrock river profiles to (a) an increase in rock uplift rate, and (b) a baselevel drop (from Whipple and Tucker, 1999, Figures 4 and 6, with permission from the American Geophysical Union).

how rapidly a profile responds to a step change in either forcing. What is the characteristic timescale over which the change from one to the other steady-state profile occurs? And what form does the response take? Does the response occur first in the headwaters and propagate down-channel, or vice versa?

Although not definitive, one of the hallmarks of a river system in a transient state is a convexity or knickpoint in the longitudinal profile. (This is not diagnostic of transience, as a steep section of river may instead be localized by a reach of resistant bedrock, as discussed above.) As can be seen from the schematic profiles in Figure 13.18, the response to both baselevel drop and to a change in uplift rate occurs first at the mouth of the system. The information about the baselevel drop is transmitted up the river profile at a rate that is dictated by the stream discharge and the erodibility of the channel, as we saw in the discussion of knickpoints. The same occurs for a change in uplift rate. The rate of propagation of the knick, or replacement of one profile with the other, is set by the "celerity," or wave speed,  $C$ , of

the response. This is a natural consequence of the form of the stream power rule for stream incision. One may write the erosion equation as

$$\frac{\partial z}{\partial t} = \frac{k\rho g Q}{W} \frac{\partial z}{\partial x} = C \frac{\partial z}{\partial x} \quad (13.21)$$

which is classified as a kinematic wave equation. (As a historical aside, this equation was explored in detail in describing the flow of traffic on highways by Light-hill, 1978).

The timescale for the response to a particular site, at a distance  $L$  up the profile from the site at which the baselevel is imposed, is determined by the total distance upstream divided by the mean celerity, or

$$T = \int_0^L \frac{dx}{C(x)} \quad (13.22)$$

(see Whipple and Tucker, 1999, equation 20 and following). Interestingly, and somewhat surprisingly at first glance, the response time is not very sensitive to drainage basin size. This is because large drainages often have high discharges, which means the response rapidly propagates up the network (because  $C \sim Q$ ). As the discharge declines, the rate of progress of the response, be it a knickpoint or simply a break in slope, declines. This is particularly the case at tributary junctions, where the drainage area declines by a step dictated by the size of the tributary. The expected location of knickpoints in a real basin with several tributaries at some significant time after a baselevel drop is illustrated in Figure 13.19. In this instance the Colorado River serves as the local baselevel for all of the tributaries shown. The knickpoints, which here are all major dry falls on small streams exiting the thinly laminated oilshale of the Eocene Piceance Creek formation, are found at locations that differ in terms of their distance from the river. Undoubtedly these all were cast off the Colorado when this major river began incising in the late Cenozoic. That they all have experienced the same baselevel history, and are all located in uniform bedrock, makes this a fruitful natural experiment that allows one to explore the degree to which the rules we have been discussing work in a natural setting. This has indeed been done, and the predictions from the simple celerity model discussed here fit the observed locations of the knickpoints remarkably well (Berlin and Anderson, 2007; Figure 13.19).

## Waterfalls

According to the above discussions, the rate of migration of a discrete knick should be governed by the discharge of the river,  $Q$ . Crudely,  $C = kQ$ , where  $k$  is the susceptibility of bedrock to erosion. In uniform rock, then (i.e., uniform  $k$ ), the rate of propagation of the knickpoint will slow as it moves upstream into regions of lower water discharge. There are good reasons to suspect that a shear stress-based rule for channel erosion might not operate in the case of waterfalls. After all, the shear stress goes to zero for water falling vertically. Nonetheless, some fraction of the energy released by the fall of water through that height should still be made available for performing work on the underlying and adjacent bedrock. Conversion of potential to kinetic energy occurs, most of which is locally dissipated (the water exiting the plunge pool reach is not going tens of meters per second!). That the discharge of water still exerts control on the rate of recession is suggested by work on Niagara Falls.

Along the Niagara River (Figures 13.14 and 13.20), which connects Lake Erie to Lake Ontario through an 11 km channel, the rate of retreat of Niagara Falls appears to have experienced a period from roughly 10 500 to 5500 yr BP during which the recession was greatly diminished below that either prior to or after this period (Tinkler *et al.*, 1994). The story of Niagara Falls is therefore tangled intimately with the history of the Great Lakes, whose drainage has been greatly affected by the post-glacial rebound of the region as the Laurentide ice sheet vanished (e.g., Pengelly *et al.*, 1997). Tinkler *et al.* (1994) hypothesize that this 5 ka period was one in which a major fraction of the flow from the upper Great Lakes was diverted to the Ottawa River, bypassing both Lake Erie and Lake Ontario (Figure 13.14). The diminished flow resulted in a slowing of the recession of the Falls by a factor of five, accomplishing 1 km of retreat in 5 ka, compared to the roughly 1 km retreat in 1 ka, or 1m/yr rate over the last 5–6 ka. Interestingly, the fivefold reduction of the regression rate corresponds to an estimated sevenfold diminution of the discharge. More detailed study of the recession rate in historical time shows that the retreat process is complex. The historical retreat rate of Horseshoe Falls of roughly 0.3 m/yr is accomplished by non-uniform retreat of the falls (Philbrick, 1970). It appears that generation of a deep notch in

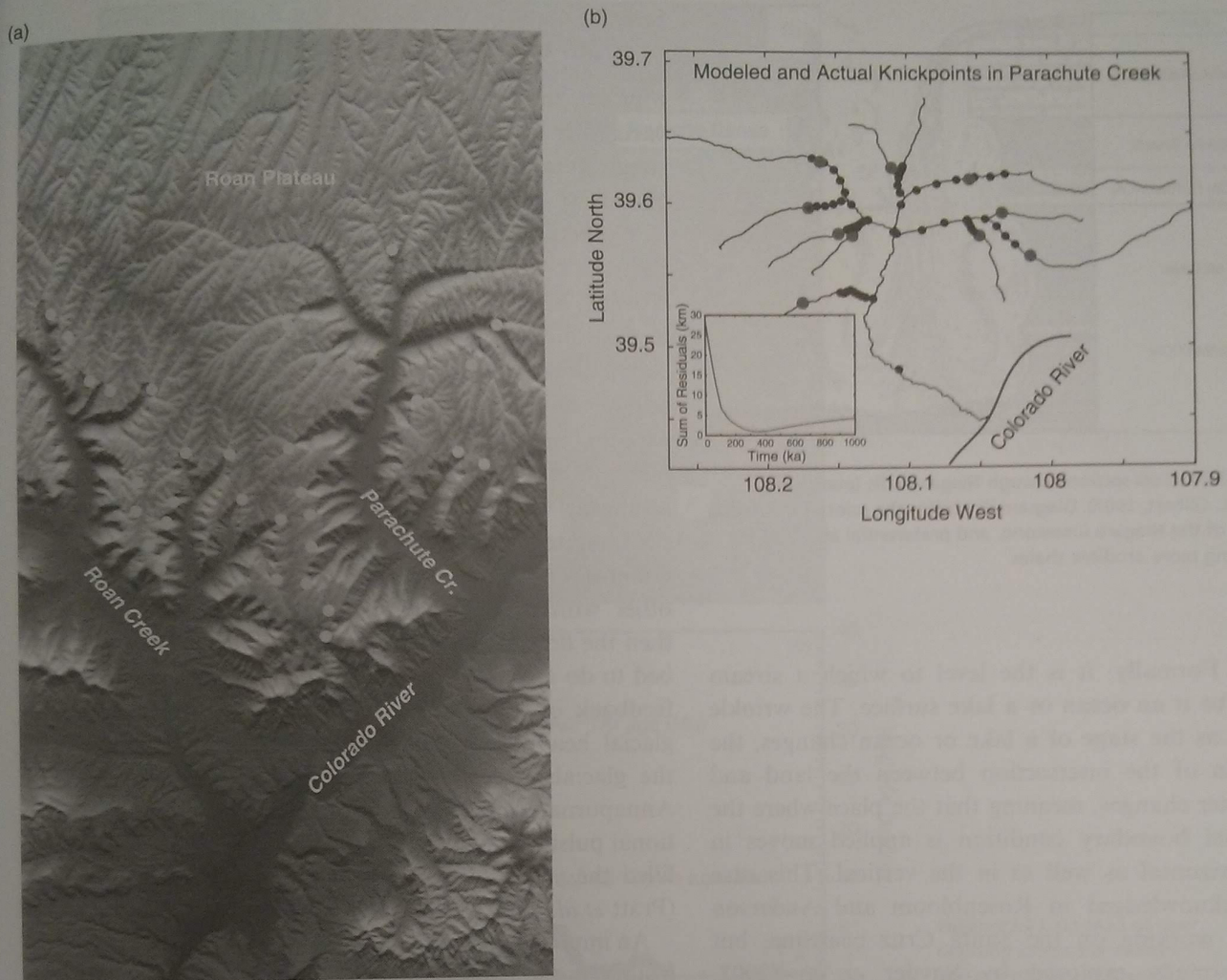


**Figure 13.19** (a) Map of Parachute and Roan Creeks, Roan Plateau, Colorado, showing modern locations of knickpoints. (b) Results of 350 ka celerity model of knickpoint migration in Parachute Creek. Open circles: present positions of knickpoints. Dots: locations of model knickpoints at 20 time increments. Most knickpoints fit well with this simple model. Inset: goodness of fit measured by sum of misfits of knickpoint locations, as a function of simulation time. Best fit 350 ka for the given choice of  $k = 5 \times 10^{-10} \text{ (m yr)}$ , and a critical area of  $0.5 \text{ km}^2$  (after Berlin and Anderson, 2007, Figure 8, with permission from the American Geophysical Union).

plan view occurs first, followed by broadening into a new horseshoe shape.

While less information is available on the yet taller Victoria Falls on the Zambezi River, the late Pleistocene retreat rate is of the same magnitude, a fraction of a meter per year (Derricourt, 1974). The details of the processes occurring are still not clear; this issue of the mechanics of waterfall retreat remains a target for future research.

Another example of a transient profile is that of the river draining the Nameche Barwa syntaxis on the eastern end of the Himalayan orogen. Finnegan

*et al.* (2008) have shown that the present profile of the river displays a prominent knickzone as the river punches across a zone of presumably high rock uplift rate at the western syntaxis of the Himalayas (Figure 13.21). Both the stream power and the long-term erosion rate, as revealed by cooling ages of at least two thermochronometers, peak in the knickzone.

#### Response to baselevel lowering

One must be careful in thinking about the role of baselevel as a boundary condition for bedrock

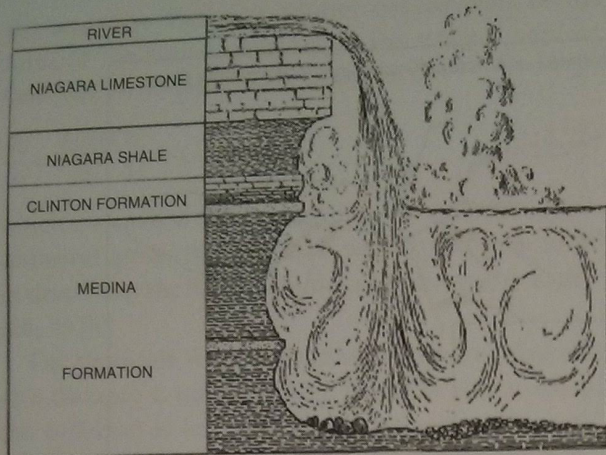


**Figure 13.20** Cross section through Niagara Falls (plate VIII from G.K. Gilbert, 1907). Diagram illustrates the roles of the strong caprock of the Niagara limestone, and preferential attack of the underlying more erodible shales.

rivers. Formally, it is the level to which a stream tends, be it an ocean or a lake surface. The wrinkle is that as the stage of a lake or ocean changes, the position of the intersection between the land and the water changes, meaning that the place where the baselevel boundary condition is applied moves in the horizontal as well as in the vertical. This case was acknowledged in Rosenbloom and Anderson (1994), working on the Santa Cruz coastline, but was formally explored by Snyder *et al.* (2002, 2003a), working near the Mendocino triple junction along the northern California coast. As illustrated in Figure 13.18, rapid lowering of the baselevel (sea level fall) initiates a wave of incision that travels up the stream. Rapid sea level rise transforms the mouth to an aggrading system, disallowing further erosion of bedrock until the next sea level fall. This problem set-up has been nicely employed in the treatment of the problem of how the large circum-Mediterranean rivers responded to the dramatic drying out of the Mediterranean that has been called the Messinian salinity crisis (Hsu, 1972, 1983; Loget and Van Den Driessche, 2009).

The response to tilting of a basin due to some large-scale tectonic process can be assessed by imposing a change in slope to the entire stream profile. Once again, the response begins at the mouth of the stream, for the reason that the proportional change in slope there is much larger than in the headwaters.

### Role of climatic variability: the origin of strath terraces

Finally, one must acknowledge the role of climatic variability in carving the alpine channels we see. If the stream power rule discussed above pertains, then any climate swing that yields more effective precipitation (for effective precipitation read effective discharge of the river) should result in greater rates of bedrock erosion. In fact, if we were just to consider abrasion as the dominant process, one might argue that greater water discharge should result in higher flow speeds, and hence in greater erosion rates. Couple this to the expected increase in sediment discharge that this flow increase may incite, and the effects become highly nonlinear. This argument breaks down, however, if the climate swing produces sediment in such great quantities that it clogs the channel with sediment. In other words, if the channel aggrades significantly, then the flow is unable to gain access to the bedrock bed to do any work on it. This will act as a negative feedback or a brake on the system. In rivers with glacial headwaters, this was likely the case during the glacials. Recent work on a river draining the Annapurna Himalayas has shown that the aggradational pulse associated with the last glacial maximum filled the valley to a height of many tens of meters (Pratt *et al.*, 2002).

An important consequence of this sediment loading history is the formation of strath terraces in rivers with glacial headwaters (Hancock and Anderson, 2002). These are especially well developed (broad) surfaces if the river crosses easily eroded sedimentary rock, as is the case for the Wind River as it crosses the Wind River Basin of Wyoming (Figure 13.22; see also Figure 13.16). The numerical model of strath formation is based upon the following simple reasoning, shown schematically in Figure 13.23. If the alluvial thickness is greater than a river typically scours over the course of the dominant floods, the bedrock channel floor beneath the alluvium is no longer eroded. However, the bedrock channel banks are susceptible to erosion if the river channel swings against the bedrock wall. During times of aggradation, then, the river bevels laterally, widening a braidplain or channel meander belt. Upon decline of the sediment input from the glaciers, the balance of sediment input to sediment output from the downstream reaches changes sign, and the alluvium is thinned, eventually

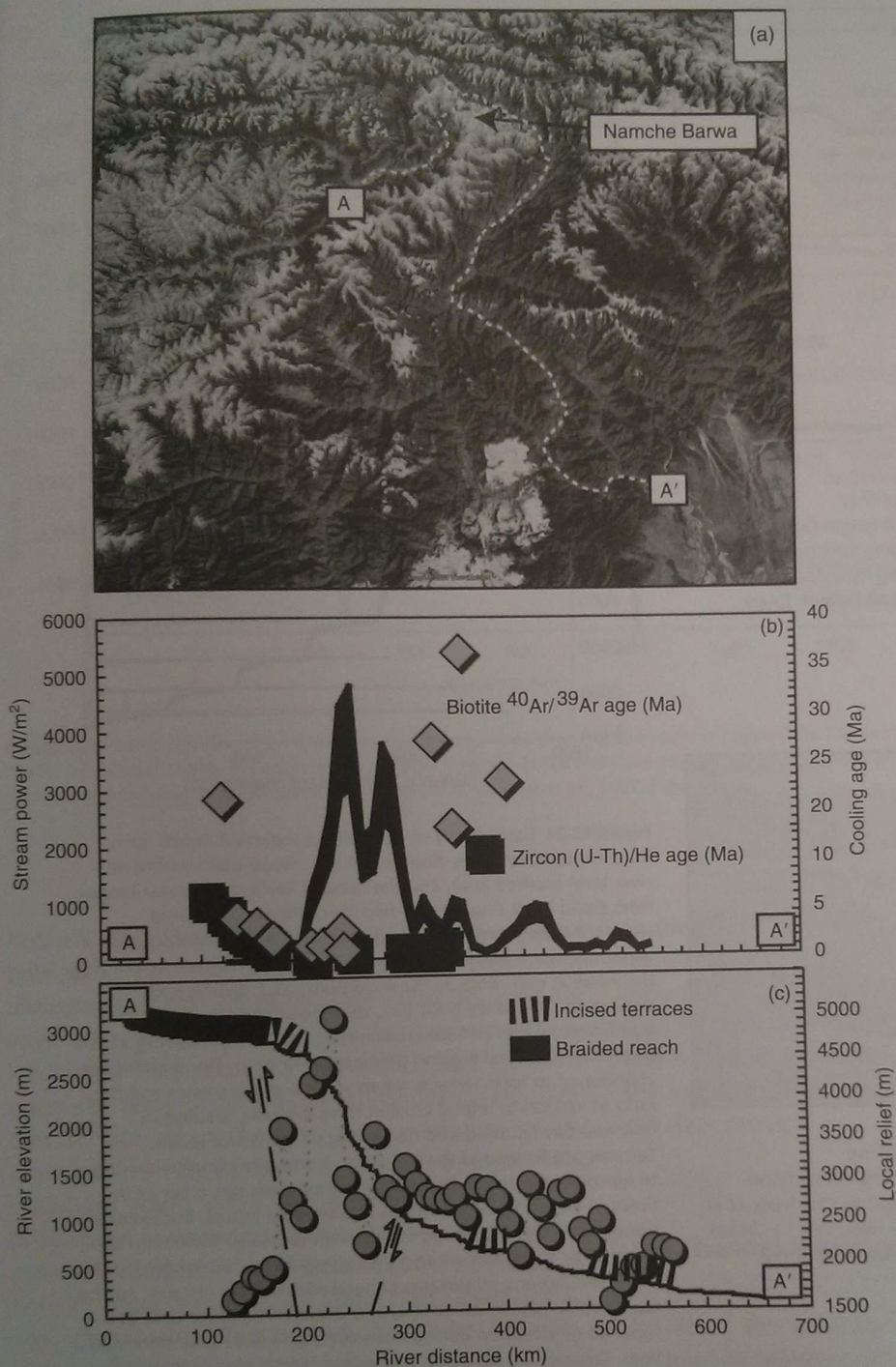
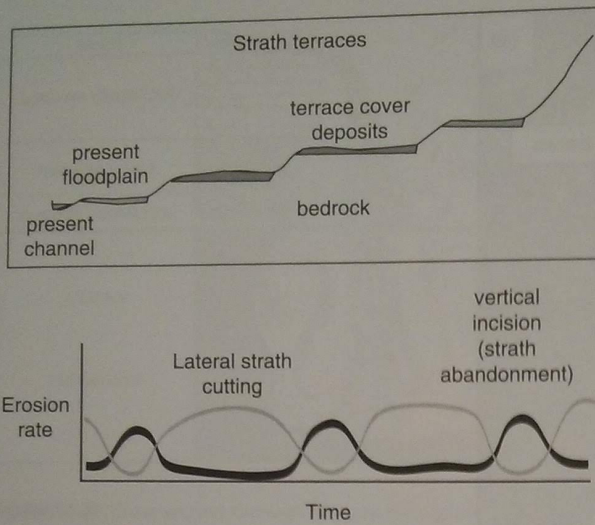


Figure 13.21 (a) Map of river draining across the eastern syntaxis of the Himalayas, anchored by Namche Barwa. (b) Stream power profile (bold line) from A–A' down the 700 km reach of the river depicted in the map. (c) Channel profile and adjacent local relief (circles) of the landscape. The steep knickzone in the channel is associated with high local relief of almost 5 km, and a peak in stream power. Cooling ages based upon biotite <sup>40</sup>Ar/<sup>39</sup>Ar and zircon (U-Th)/He reach their minima within the knickzone (after Finnegan *et al.*, 2008, Figure 11).

allowing the river access to the bedrock floor. The river then resumes erosion into bedrock where it happens to be lowered onto the bedrock floor, and the remainder of the widened bedrock platform

is abandoned as a terrace once flood flows can no longer access the surface. As shown in Figure 13.24, climate swings can therefore generate stacks of strath terraces, gravel-mantled bedrock surfaces whose



**Figure 13.22** Geometry (top) and proposed origin (bottom) of strath terraces. Lateral strath cutting (grey line) occurs when the channel is blocked from vertical erosion by a thick alluvial cover. A strath is then abandoned by vertical incision (black line) when the alluvial cover thins.

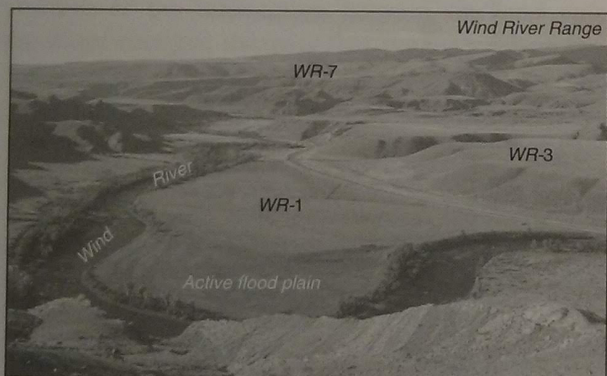


**Figure 13.23** Wind River terraces as seen looking downstream near Dubois, Wyoming. Above the active flood plain, three prominent strath terraces mapped by Chadwick *et al.* (1997) are cut into the valley wall above the river: WR-1 (~20 ka); WR-3 (~120 ka); WR-7 (~600 ka) (after Hancock *et al.*, 1999, Figure 1, with permission from Elsevier).

abandonment times should correspond to the terminations of glacials.

### The roles of landslide dams

Many bedrock rivers punch through steep mountainous terrain. It is in fact the incision of the rivers into

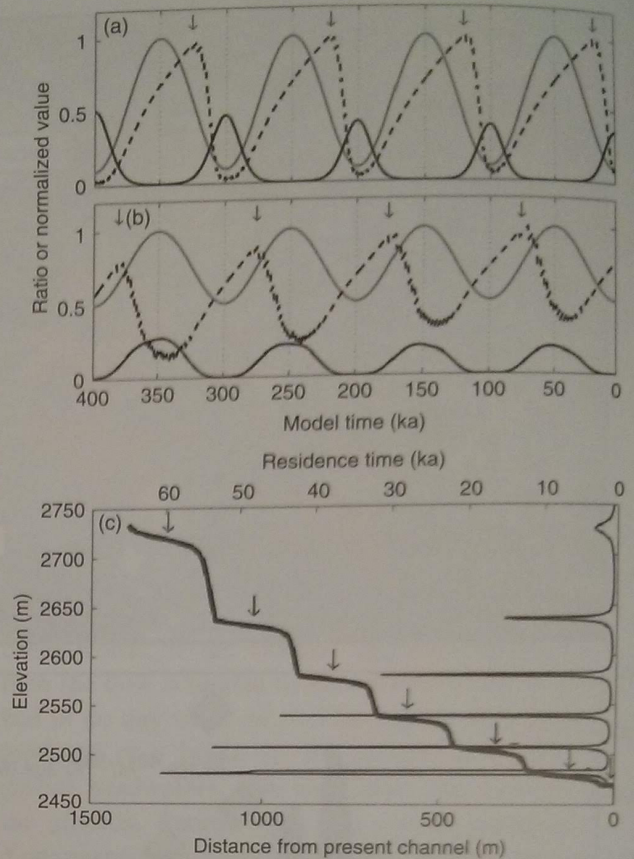


**Figure 13.24** Top: history of normalized sediment inputs (gray line), normalized valley-floor width (i.e., flood-plain width) at river level (dashed line), and the ratio of vertical to lateral erosion rates (solid black line) during two simulations: (a) tenfold sediment-supply variation and (b) twofold dominant-discharge variation. Inputs and valley-floor widths are normalized by dividing the value at each time by the maximum value during each simulation. The valley floor (i.e., the "flood plain") widens most significantly when vertical erosion rates are low, producing a ratio of vertical to lateral erosion that is small or zero. Flood plains are abandoned to form terraces when vertical erosion rates and the ratio of vertical to lateral erosion rates increase, leading to renewed downcutting and narrowing of the active valley. Terraces are formed at the transition from valley-floor widening to narrowing (arrows). Terrace formation does not occur at the times of either maximum inputs or minimum inputs, but instead significantly lags the timing of the maximum (e.g., sediment-supply maxima) or the minimum (e.g., water-discharge minimum) inputs. In the simulations, all terraces generated are strath terraces. (c) The topographic profile (thick line) and channel-residence time as a function of elevation during downcutting in this simulation (thin line). Terraces are related to periods of lateral planation during long channel residence within a narrow elevation range. Residence time at individual terrace levels reaches up to many tens of thousands of years, indicating that the river spent most of the simulation forming terraces (after Hancock and Anderson, 2002, Figures 5 and 7).

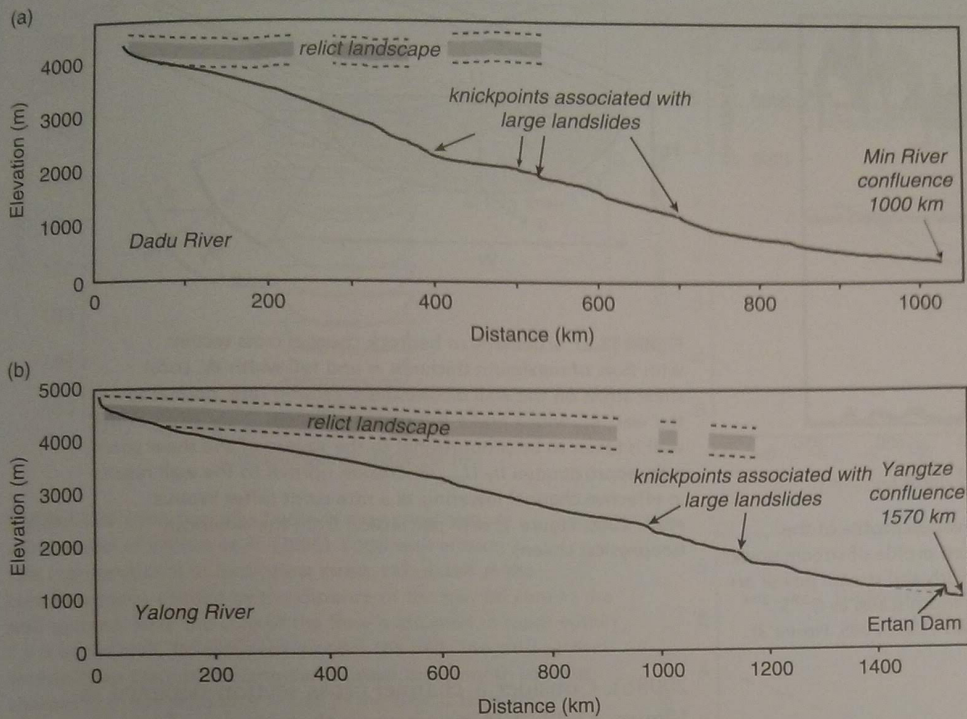


**Figure 13.25** Long profiles of (a) Dadu and (b) Yalong Rivers draining the eastern edge of the Tibetan Plateau. "Relict landscape" marks the edge of the plateau into which the rivers are incising. Knickpoints or convex channel segments associated with large landslide dams are noted (after Ouimet *et al.*, 2007, Figure 4).

bedrock that lowers the baselevel for the adjacent hillslopes, which in turn steepens them. In many instances this can result in slopes that are near the angle of repose, and therefore fail occasionally as landslides. This process is inevitable, and therefore raises the issue of how such landslides create dams that should affect the long-term evolution of the river profile. There are two likely options. The landslides could serve to stall bedrock erosion by promoting sedimentation behind the dam, which prevents erosion of the bedrock by mantling it. On the other hand, if the dams fail catastrophically, the erosion downstream might be enhanced above that one would expect from non-flood discharges.

Working on the rivers draining the eastern margin of the Tibetan Plateau, Ouimet *et al.* (2007) have documented many landslides and their legacy in the channel profile. We reproduce their chief result in Figure 13.25. Clearly, the greater the number of large landslide dams that deliver large caliber sediment

to the river, the more they will slow the long-term incision of the river into rock. They argue that the longer it takes a river channel to remove a landslide dam by incision through the landslide debris, and to remove all landslide-related sediment, the stronger the influence these events have on the evolution of the river profile.

### The channel width problem

In all of the analyses we have described there is an implicit assumption about channel width. Either it is held constant, or it is assumed to have some simple distribution down-valley. Investigation of this problem is one of the present frontiers in fluvial geomorphology. In reality the channel of a bedrock river can be eroded at any and all points on the channel perimeter. The rate of erosion is dictated by the erosion process, the protection of the bed by any



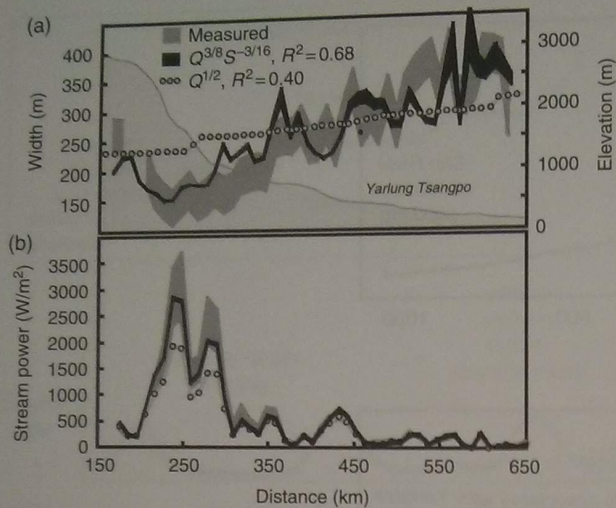


**Figure 13.26** (a) Channel width and elevation profile of the Yarlung Tsangpo River, and (b) associated profile of stream power per unit area. Spatial distributions of width and stream power are far better approximated assuming that width scales as  $Q^{3/8}S^{-3/16}$  rather than simply as  $Q^{1/2}$  (after Finnegan *et al.*, 2005, Figure 3).

sediment mantle, the availability of tools to perform the erosion, and so on – really the same issues faced in our treatment of channel lowering. But it should be clear from the first formula for stream power that a feedback exists between width evolution and channel lowering rate: the wider the channel, the lower the thickness of the flow, the lower the shear stress, and the lower the vertical erosion rate.

### Empirical constraints

Data on bedrock channel width is rarely collected. Where it has been documented (e.g., Finnegan *et al.*, 2005; see also Finnegan *et al.*, 2007; see Figure 13.26), bedrock channel width appears to increase with flow discharge as  $W \sim Q^{0.4}$ , and to decrease with channel slope as  $W \sim S^{-0.2}$ . Such data also hint that a bedrock channel responds to rapid incision by narrowing (e.g., Duval *et al.*, 2004; Whittaker *et al.*, 2007a,b). Channels have been shown to narrow, for example, as they cross active folds in the Himalayan foreland (Lave and Avouac, 2000, 2001).

### Theory

We summarize here recent theoretical work aimed at explaining these observations (Wobus *et al.*, 2006,

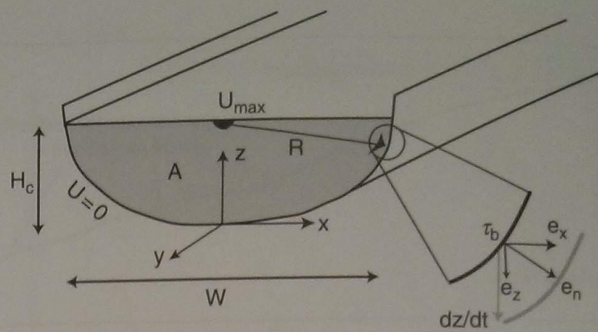


**Figure 13.27** Schematic of bedrock channel cross section with flow of maximum thickness  $H$  and full width  $W$ . Local shear stress on the wall dictates local erosion rate, normal to the wall,  $e_n$ , with  $x$  and  $z$  components shown. Shear stress at the wall is taken to be proportional to the square of the shear strain rate, approximated by  $U_{\max}/R$ . Erosion normal to the wall results in effective channel lowering at a rate  $dz/dt$  (after Wobus *et al.*, 2006, Figure 1, with permission from the American Geophysical Union).

2008b). Consider a channel cross section depicted in Figure 13.27. Let us assume that the erosion rate anywhere along the periphery of the channel is set by the local shear stress (this assumption can be relaxed or replaced as we learn more about the dependence of erosion rate on flow properties). This shear stress is not set solely by the local flow depth, as there is shear within the flow in the other dimension; the flow speed goes to zero along the entire perimeter, and there must be both  $\partial u/\partial z$  and  $\partial u/\partial x$  shear. As a first approximation, consider the shear stress to be proportional to the square of the shear strain rate ( $\partial u/\partial r$ ) evaluated at the wall. The erosion rate is then cast as

$$e_n = -k \left( \frac{U_{\max}}{R} \right)^2 \quad (13.23)$$

where  $U_{\max}$  is the flow speed in the middle of the channel, and  $R$  is the local distance from this core to the position on the wall. Again, this is only an approximation, as the flow field is no doubt more complex than this would imply. Indeed, slight alteration of this simplest model of the flow field can yield a very realistic map of the basal shear stress (Wobus *et al.*, 2006). The erosion rate may be decomposed into  $e_x$  and  $e_z$  components, and the location of the wall can be updated. One must also demand that a force balance on the fluid cross section exist, meaning

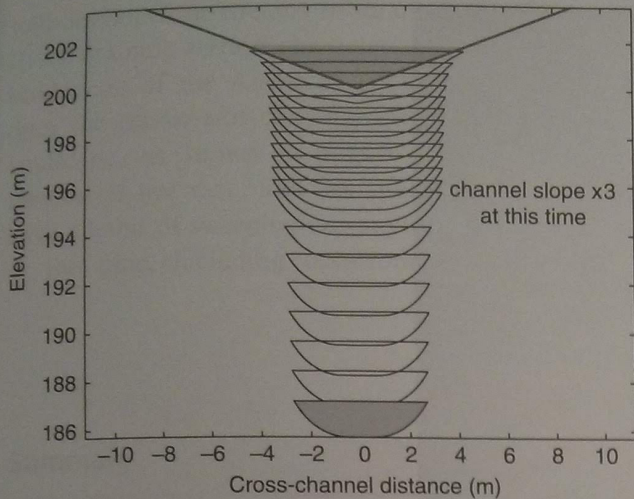


**Figure 13.28** Evolution of a bedrock river cross section using model of Wobus et al. (2006). Local wall erosion rate is proportional to local shear stress, calculated as the core flow speed divided by the distance of the nearest core to the wall squared. Here the core of the flow is assumed to reach within  $1.5 H$  of the wall. No sediment mantles the bed. The cross section evolves from the initial triangular channel to a smooth concave channel with the ratio  $W/H = 3.68$  in the time it takes for channel lowering by roughly one channel depth, i.e., by  $T = H/(dz/dt)$ . Tripling of the channel slope results in much faster erosion, and a narrowing of the channel.

that the shear stress integrated along the wall must balance the down-valley weight of the fluid.

Starting with an arbitrary cross section, Figure 13.28 shows how such a channel cross section should evolve in the face of these physics. Independent of the initial shape of the channel, the channel evolves toward a smooth concave shape that eventually achieves a geometry that lowers uniformly. In other words, the channel form self-organizes. Interestingly, under these assumptions, the steady-state geometry achieves a definite width to depth ratio of  $W/H = 2.9$ . The detailed shape may be predicted from the demand that the channel lowers uniformly at steady state. The dependence of width on discharge and on channel slope matches well that observed in the field. Experiments may then be performed in which we link many channel cross sections to explore the interchange between channel cross-sectional shape and channel long profile.

While this is certainly not the final word on the topic, we are encouraged by the recent progress. With this theoretical edifice in place, in which channel wall elements are explicitly treated and allowed to evolve,

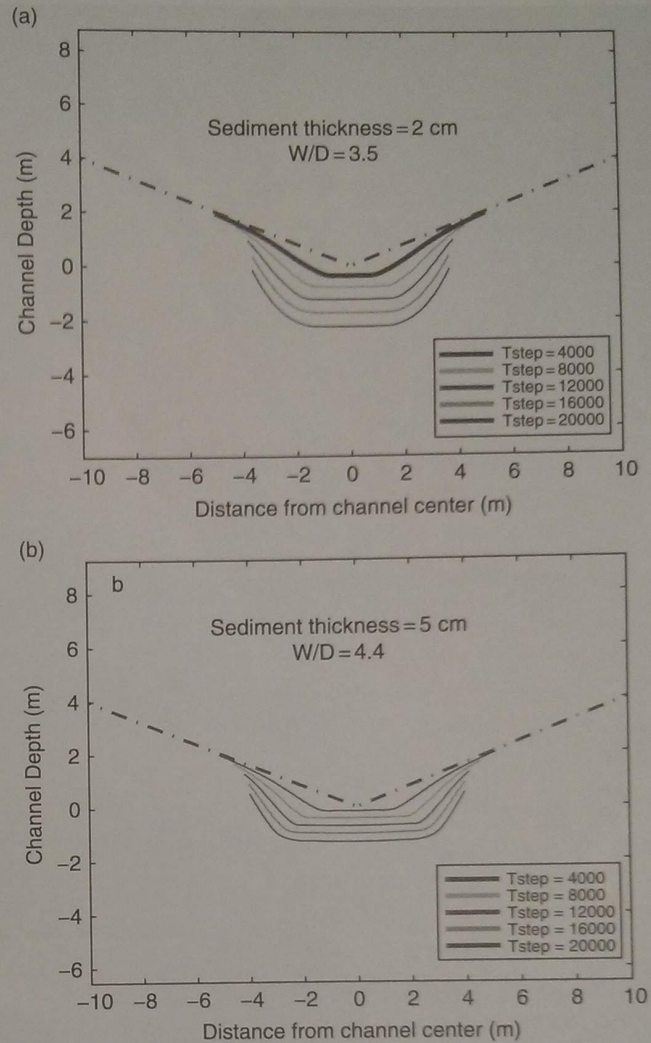


**Figure 13.29** Effect of sediment cover on channel width. The greater the sediment cover (a: 2 cm; b: 5 cm), the more the erosion is focused on the channel walls rather than the channel floor.

we can now explore the roles of specific erosional processes and how they will depend upon location in the channel cross section, the role of sediment mantle on the bed, the role of discharge variations, and so on. As a hint of things to come, consider the numerical experiment shown in Figure 13.29. We have dictated the presence of a finite alluvial mantle, and dictate that the rate of erosion depends upon the thickness of this mantle in an exponential manner. In other words, the erosion rate falls off exponentially with sediment thickness, with a length scale set by the expected distribution of scour depths. Sediment many times this thickness will prevent entirely any

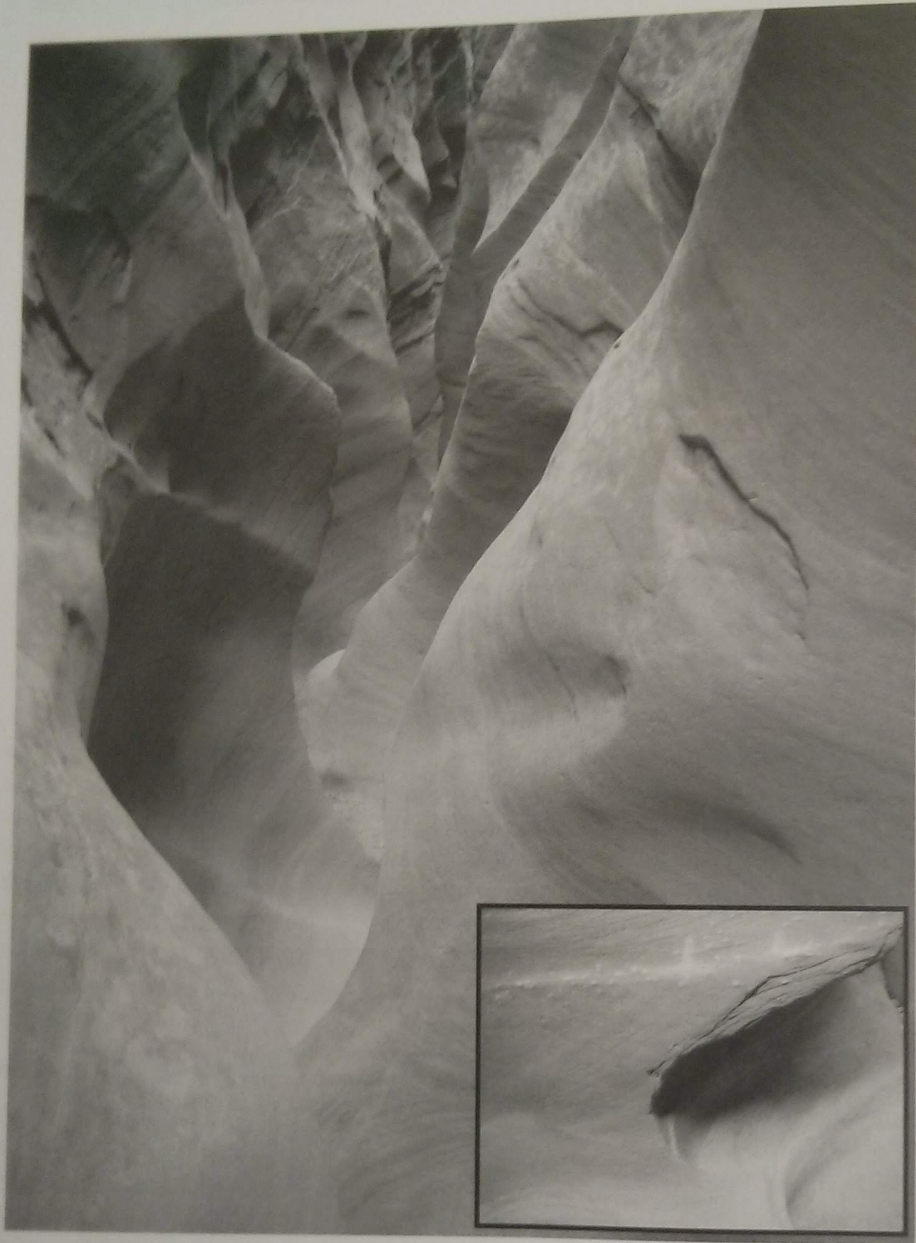


**Figure 13.30** Little Wildhorse slot canyon, Utah. Smooth channel walls attest to the role of suspended sand in abrading the walls. Flow is away from observer. Inset: the bases of delicate flanges separating the smooth wall undulations are occasionally cracked, strongly suggesting a role for the larger clasts embedded in the flash floods that carve these channels. Flow is from left to right (photographs by R. S. Anderson).

erosion of the bed. The effect is to widen the channel significantly, as channel walls can be eroded while the channel floor is prevented from eroding. This effect will help to explain the significantly larger  $W/H$  ratios seen in real bedrock rivers. Indeed, as we have discussed above, this effect is the root of the generation of strath terraces, which are therefore essentially a corollary to the effect of sediment on the river bed.

### Slot canyons

One cannot close a discussion of bedrock incision by rivers without at least advertising some of the most spectacular forms attributed to these processes. Slot canyons are extremely narrow canyons carved by rivers that leave as their legacy intricately carved walls reaching well above any reasonable flow depth (see Wohl and Merritts, 2001). These are especially

well developed in streams tributary to the Colorado River draining terrain characterized by the massive sandstones of the American southwest. These produce the classic slot canyons that characterize this landscape, as shown in Figure 13.30. The flows themselves are rare, and are often flashfloods that have a habit of sweeping out anything in the canyon at the time, including occasionally humans. The

undulations of the walls of these canyons display evidence of discrete impacts of both small and large clasts embedded in the flows. Abrasion of all sides of the channel walls smacks of the role of suspended sands. Yet, cracks in delicate flanges and flutes between wall forms near the channel floor suggest a role for the larger clasts involved as bedload (see the inset in Figure 13.30).

## Summary

The dominant process of erosion by streams into bedrock varies with lithology. Highly jointed rock can be efficiently eroded by quarrying, while massive bedrock requires abrasion. As abrasion is generally less efficient than quarrying, massive bedrock reaches are typically steeper. Incision of bedrock requires that bedrock be exposed in the channel. For this reason, spatial and temporal variation of the alluvial cover of the bed, driven by sediment supply conditions on hillslopes and in the headwaters, can greatly influence the long-term rate of incision. In fact, we cannot explain the presence of strath terraces in bedrock river systems without appeal to the climate-driven variations in sediment supply.

Steady-state longitudinal bedrock river channel profiles should display concave up profiles. This reflects the inevitable increase in discharge with distance downstream; the greater the discharge, the lower the required slope to accomplish the work of erosion. For the same reason, Playfair's law holds; if small tributaries indeed join the trunk stream at grade, they must be steeper because they discharge less water.

The pattern and rate of response of a fluvial system to changes in its boundary conditions, or to changes in the climate, depends upon the size of the drainage, the lithology (loosely captured in  $k$ ), and the discharge. Most changes in boundary conditions drive an upstream-propagating response, the rate of which declines with upstream distance, reflecting the decline in both drainage area and water discharge with distance upstream.

The channel cross section self-organizes into a smooth concave up form under steady conditions. It translates downward uniformly, and has a  $W/H$  ratio of roughly 3 in pure bedrock channels. The channel narrows as valley slope increases, and widens as water discharge increases. The time for accommodation of changes in these factors is scaled by the channel depth divided by the incision rate, and can be quite small for some

channels. It is therefore significantly easier for a channel to adjust its width than to adjust its slope.

## Appendix: Future work and research needs

While much has been accomplished in the last 15 years of research on this important geomorphic problem, there remains much to do in the field of bedrock river incision. While the community has begun to employ methods capable of documenting annual erosion rates, and has begun to exploit the available geomorphic markers to deduce erosion rates over thousand- to million-year timescales, no method of real-time (hourly to daily or weekly) measurement of bedrock erosion exists. Such a method would allow us to determine the detailed conditions of river discharge and sediment load under which erosion is most efficient.

Further exploration of the channel width issue is warranted. While a theoretical edifice is in place, we need more detailed field observations of channel width and its dependence on water discharge, rock properties, and sediment supply. Just as in the long valley profile, we also need more explicit treatment of specific erosional processes, moving beyond the simple stream power approaches. As an extreme example, the stream power rule used so heavily in this field breaks entirely on a vertical waterfall, at which the stream power should be infinite.

Models of river evolution have tended to be simplified, and lack acknowledgment of the full complexity of real systems. These include incorporation of realistic orographic effects, variation in drainage area and channel width, variation in lithology (and hence in process type), and non-uniform rock uplift patterns in both time and space. Full linkage of bedrock channel response to the history of sediment and water delivery from the headwaters of the channel system has not been accomplished.

## Problems

- Graph the expected history of retreat of a river knickpoint in which the distribution of basin area is  $A = 5(L - x)^{1/2}$ , where  $L$  is the length of the full channel and  $x$  is the distance upstream from the mouth of the basin. The speed of the knickpoint as it is cast off from the basin exit is  $U = 10$  mm/yr. Plot the dimensionless knickpoint speed  $u/U$  as a function of the non-dimensional distance upstream  $x/L$ . (Note: you will find it useful to stop your plot at say  $x/L = 0.9$ .)
- At the historical rate of retreat of Niagara Falls, how long will it take for the falls to reach Lake Erie?
- Consider a strath terrace along a river etching into bedrock. We have determined its age to be 130 ka using  $^{10}\text{Be}$  concentrations in the sediment capping the terrace. It is presently 55 m above the river. Calculate the mean rate of river incision in the time since the surface was abandoned.
- In using the stream power formulation in bedrock incision problems, we are assuming that some fraction of the potential energy released by dropping the parcel of water in elevation is used to work on the bedrock. Here instead assume that all of that potential energy is converted to heat. Estimate how much a parcel of water will warm up as it drops from its source area in the Himalayas to the ocean. Assume that the elevation of the parcel is 6500 m when it is released by melt from a glacier. The specific heat capacity of water,  $c$ , is  $4.19 \times 10^3$  J/kg-K. (Hint: the problem is to convert the water's initial potential energy into heat. Ignore the contribution from passage into a warmer climate; we are interested in isolating the effect of energy conversion.)
- Calculate the mean rate of lowering of the channel floor in shale badlands in which the lowering is accomplished entirely through passage of small knickpoints. You measure the step heights to be 20 cm tall, the spacing between them to be 75 m, and repeated visits to the field reveal that the rate of propagation of the knickpoints is 40 cm/year.
- Figure 13.3 illustrates the incision history of Kings River as deduced by dating of caves embedded in the valley walls. For the sample from Bats Cave, which is shown as having been abandoned at 3.09 Ma, calculate the ratio of  $^{26}\text{Al}$  to  $^{10}\text{Be}$  that must have been documented in the cave sediment.
- Figure 13.16 shows how the Wind River in Wyoming steepens as it passes through Wind River Canyon. If we assume that the gradient of the stream changes fivefold and that the river has achieved a steady profile, meaning that it is incising at the same rates above, within, and below the canyon, how much less susceptible is the crystalline rock in the canyon to erosion than the sedimentary rocks outside the canyon? Discuss your assumptions.
- Thought question.* If the stream power formulation captures the essence of the bedrock river incision problem, will the effect of ponding of water behind a landslide dam, and then suddenly releasing it in a catastrophic flood, alter the expected long-term rate of incision of the river downstream of the dam?
- Thought question.* Again referring to Figure 13.3, discuss how different the interpretation of Kings Canyon evolution can be given that we have dated several caves rather than simply Bat Cave, or Boyden Cave.
- Thought question.* Can we use the stream power formulation for bedrock erosion in a vertical waterfall? Why/why not? (Hint: think about what the slope of the waterfall is, and calculate the expected lowering rate of the bed upstream, at, and downstream of the waterfall.)

11. *Thought question.* The river erosion rate estimates obtained from strath terraces are averages over the time since the terrace was abandoned by the river. If the erosion of the river downward into rock occurs only when the sediment supply from the headwaters is low, and this occurs during interglacials, explain why there is an apparent acceleration rate in river incision reported from dating several strath terraces on a single river. (*Hint:* you will need to acknowledge the climate history through the last several glacial–interglacial oscillations (recall the  $\delta^{18}\text{O}$  record from deep sea cores).)
12. *Thought question.* Consider a simple semicircular channel in bedrock. If we assume that the erosion rate of the bedrock floor is governed by the local shear stress exerted by the flow on the bed, and we further assume that the local shear stress is simply  $\tau_b = \rho gHS$ , where  $S$  is the down-valley slope of the channel and  $H$  is the local depth of the water, graphically depict how the channel cross section ought to evolve through time. (It is this problem that inspired the work of Wobus *et al.* (2006, 2008b) in which they are forced to abandon this simplistic formulation for the boundary shear stress.)
13. *Thought question.* Consider a bedrock river with a longitudinal profile that displays a strong convexity well upstream of its mouth. How would you discriminate between the possibilities that this convexity is due to (i) a change in rock type, and (ii) a transient response to a baselevel drop at some time in the past?
14. *Thought question.* Discuss how a bedrock river should respond to glacial–interglacial fluctuations in baselevel of the order of 120 m. What legacy of the glacial sea level low stand might be seen in the present profile or subsurface stratigraphy, and what might govern the magnitude of these effects?

## Further reading

Tinkler, K. and E. Wohl (eds.), 1998, *Rivers Over Rock*, Geophysical Monograph 107, American Geophysical Union.

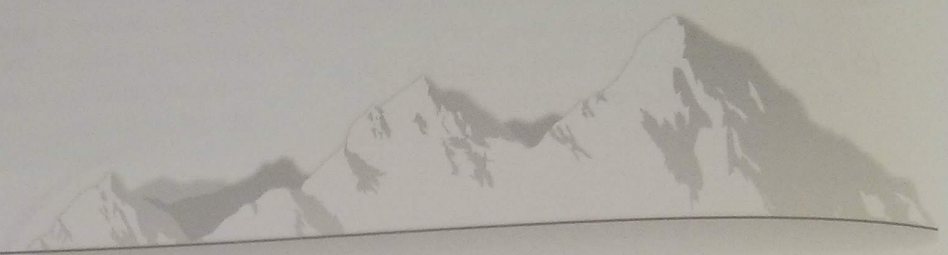
*This edited volume represents the state of our knowledge of bedrock rivers as of the late 1990s. It grew out of a Chapman Conference on the topic, and contains contributions from sites around the world.*

Whipple, K. X., 2004, Bedrock rivers and the geomorphology of active orogens, *Annual Reviews of Earth and Planetary Science* **32**: 151–185.

*An excellent review from a scientist immersed in this topic, this paper provides a convenient entrance into the theory of bedrock channel evolution as applied to rivers draining growing mountains.*

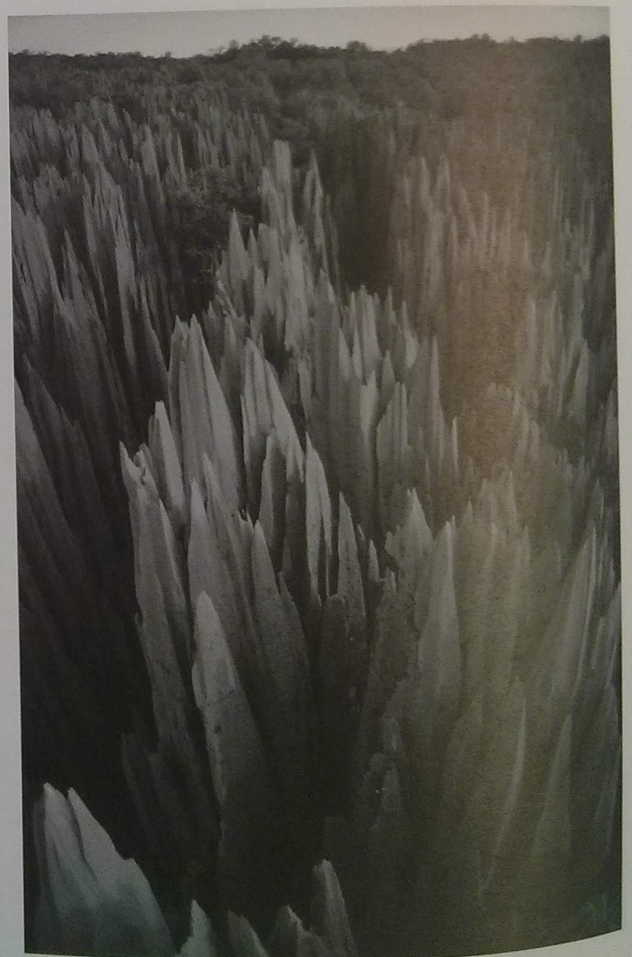
CHAPTER 10

# Hillslopes



The Hills erect their Purple Heads  
The Rivers lean to see  
Yet Man has not of all the Throng  
A Curiosity.

Emily Dickinson, *The Hills erect their Purple Heads*



## In this chapter

Every place in the terrestrial world that is not a channel or a beach is a hillslope of one or another stripe. The hillslope forms, the processes that shape them, and the rates at which these processes act vary radically in both space and time. How can we organize our thoughts about these fundamental elements in the geomorphic system? What is in common among hillslopes? And how can we impose some conceptual order on how they vary from one climate to another?

(a) Jack Schmitt and LRV on the Apollo 17 mission, at the edge of Shorty Crater. The Moon's surface is all hillslopes (image #AS17-137-21010, from [http://www.apolloarchive.com/apollo\\_gallery.html](http://www.apolloarchive.com/apollo_gallery.html)).

(b) Pinnacled limestone landscape of Tsingy de Beuaraha National Park, Madagascar. This is as far from a diffusive landscape as one can get (copyright 2009 Frans Lanting, [www.lanting.com](http://www.lanting.com), photograph 006446-01).



Consider the Moon for a moment. As shown in frontispiece figure(a), the entire surface of the Moon is composed of hillslopes. There are no channels. That lunar hills look as familiar as they do, with convex hilltops and concave footslopes, indicates that despite the lack of an atmosphere and of precipitation, and of vegetation or any other biological processes, the form of the landscape is not significantly different. In contrast, consider a terrestrial landscape like that in the limestone terrain called the Tsingy in Madagascar, shown in frontispiece figure(b). Here the landscape looks very unfamiliar. Tsingy means pointed hills, referring to the 100 m-tall fins in the photograph. The rarity of this kind of landscape tells us the processes dominating here are special, out of the ordinary. Indeed, this entire landscape is formed by the dissolution of soluble rock. We hope that by the end of this chapter you will be aware of the processes acting in more common terrestrial landscapes, which can serve as a means of highlighting the differences between these and other end-member landscapes, either rare terrestrial forms, or forms in other planetary surfaces.

One way to classify hillslopes is by whether they are soil-mantled or are bare bedrock. The shapes of these two types of slopes will be quite different: soil-mantled slopes tend to be smooth and rounded, while rocky slopes are generally steeper and more jagged. The processes dominating in each case differ too. We must address both the production of mobile material (which we attempt to do in Chapter 7), and the movement of this material. We will begin by examining soil-mantled slopes, where mass balance principles can be applied. In later sections we will address the force balance issues that are important in the evolution of rock slopes.

As always, we will begin by enforcing the conservation of some quantity, this time the mass of regolith. Regolith is generated by the weathering of bedrock (Chapter 7), and can move from one place to another by a variety of processes. In general, therefore, we must know something about the processes involved in the transportation of regolith. We must decipher to what extent the process depends upon the local slope of the land surface, whether it depends upon the position on the slope – the distance from the hillcrest. We must also address what happens at the foot of a slope: whether the material moved downhill accumulates at the foot, or is taken away by the conveyor belt of the local stream channel.

Hillslopes, in other words, do not exist in isolation, but are linked to their bounding channels. To put it mathematically, channels serve as the bottom boundary conditions for the hillslopes.

One may break many hillslope processes into those that result from some single “continuous” process, for instance the slow viscous creep of material down a slope; or the integrated or summed effects of discrete small-scale events – even slow creep is often the result of a sum of smaller motion events. For instance, both the higgledy-piggledy motion of individual sand grains blasted from a soil surface by the impacts of raindrops, and the helter-skelter motion of material driven by the digging of animals, can result in the net downslope motion of material. In such instances, we must know something about both the geomorphic result of an individual “event,” and the intensity or areal density of such events: how many events occur in a unit area of surface per unit of time. Some parts of the problem may be deterministic, meaning that the outcome of an event is knowable once we know the initial conditions (e.g., the trajectory of a grain is calculable once we specify the angle and speed at which it is launched), while others are likely stochastic, meaning they can be treated only in a statistical way (e.g., the size distribution of raindrops). We will see that the resulting downslope transport often results from the asymmetry of such events; it is slightly more likely that rainsplashed grains will be ejected downhill than uphill (and those ejected downhill travel longer paths), and it is more likely that gophers place their diggings downhill of their hole than uphill. In all cases, we wish to parse the problem into pieces that represent the several factors involved: the meteorology, the susceptibility of the landscape to the particular process, and the geomorphic “reaction” or response to the meteorological process.

In general these hillslope processes are not constant in time, but respond significantly to the variable forcing of the weather. This introduces yet another “stochastic” aspect to hillslopes that must be understood and quantified before the long-term behavior of hillslopes can be understood. We must know what questions to ask of the meteorology, what statistical measures of the weather must be documented. And given that the timescale over which hillslopes evolve is typically very long relative to the time over which climate remains steady, a reasonable (although

difficult) goal of this research would be to quantify how specific processes depend upon different climates. While most hillslope processes are dominated by the forces imposed by the action of gravity, we will see that in several instances biology plays an important role in the operation of hillslopes. For example, rodents and insects burrow into hillslopes and move material about. Tree roots act in several ways: they pry apart rock, they dilate soil, and they provide cohesion to the soil, strengthening it against the tendency to fail in landslides, and so on. When the trees fall down, the soil bound up in these same roots can be transported in the direction of the fall. We must learn to ask the proper questions of the biological system, just as we must learn to ask the proper questions of the meteorological system.

### Convexity of hilltops

Most hilltops are convex upward. The slope increases monotonically with distance from the divide. They are rounded, not pointed; they look like hills on the Moon, not the fins in Tsingy, Madagascar. G. K. Gilbert was the first to treat this convexity of hilltops in a formal way. In a wonderful paper in which he describes in words the process of hillslope diffusion, he forces us to think in an orderly way about the controls on rates of soil creep (Gilbert, 1909). He described in words the conservation of mass at several points along what he called a "mature" hillslope shown schematically in Figure 10.1. We use the term "steady state" today to describe Gilbert's mature hillslope, meaning a slope that is not changing in form through time – the entire hilltop is migrating downward steadily, but the shape of the landscape is unchanging. Gilbert noted if the shape of the hillslope and depth of regolith is unchanging, the quantity of regolith passing each point must increase downslope. Because slopes commonly have a uniform thickness of regolith, the average velocity of creep must increase downslope. He then reasoned that because gravity provides a greater downslope impelling force on a steeper slope, that the slope at any point is adjusted to provide just the increased transportation of regolith required by the mass balance. Gilbert shows that creep rates depend directly on hillslope gradient, and that this understanding can explain an important part of the landscape, the hillcrest.

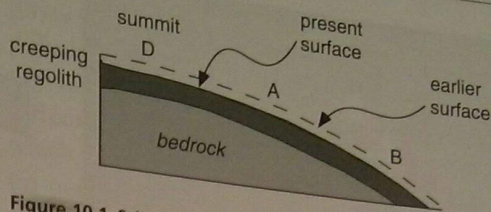


**Figure 10.1** Schematic cross section of a steady-state convex hilltop. Summit at D and two equally spaced points A and B are shown. The hill surface is shown at two times – early (dashed) and present. The entire hilltop has been lowered by the same amount. Bedrock weathers to mobile regolith at the bedrock–regolith interface. Regolith produced between the summit, D, and the point A must be transported past A by creep, while all regolith produced between D and B must be transported past B. If the transport process is slope-dependent, the slope at B must be twice that at A. This is the essence of convex hilltops (after Gilbert, 1909, Figure 1).

Gilbert's analysis pertains to a precise set of conditions. He considers only places where creep occurs, and specifically does not consider places being eroded by running water. You know from experience that erosion by running water, exemplified by gullies and river channels, produces concave-upward profiles. Gilbert's discussion of only steady-state forms was primarily for convenience – we will see how to relax this assumption shortly. He also assumed that the regolith thickness remains uniform with distance downslope. This assumption, supported by field observation, is the one that allows him to make the inference that creep rate depends on slope.

Although Gilbert called upon creep of the regolith, one of the goals of this chapter is to show that his result is more universal than this. Note what happens if we assume that the downslope flux of regolith is linearly dependent upon the local slope of the hill. Since the amount of regolith that must be passed increases linearly with distance from the hillcrest, the slope must also increase linearly with distance. This is fundamentally why hilltops are convex. In fact, steady-state hilltops are not only convex, which is a loose term, but they are parabolic (the slope does not just increase, but they increase *linearly* with distance from the divide) whenever the process moving regolith from place to place depends linearly upon the local slope. Figure 10.2 shows an example of a parabolic hillcrest, the shape made visible by the shadow of a straight-edge. While the one depicted is developed in the clay badlands of Utah, similar parabolic forms are found developed in



Figure 10.2 Hilltop profile in Blue Hills badlands in central Utah revealed by shadow cast by straight-edge. Bedrock is Tropic Shale of the Cretaceous interior seaway. Note the convex crest, with very high curvature (photograph by R. S. Anderson; Jon Stock and Melissa Swartz for scale).

Precambrian granites and other rock types – although the curvature is significantly less. We discuss these examples further later in the chapter.

### Mass balance

Let us recast the problem in its most general form, a little more formally. Making no assumptions about process or that the system is in steady state, we can still conserve mass. Consider the mass of regolith within a box on the hillslope, sketched in Figure 10.3. The word statement is

$$\text{rate of change of regolith mass [M/T]} = \text{rate of regolith inputs [M/T]} - \text{rate of regolith outputs [M/T]}$$

Treating all sides of the box (except the top, through which, in the absence of very strong winds, we may safely assume no regolith is lost or gained), this becomes

$$\frac{\partial(\rho_b R dx dy)}{\partial t} = \rho_r \dot{W} dx dy + Q_x(x) dy - Q_x(x + dx) dy + Q_y(y) dx - Q_y(y + dy) dx \quad (10.1)$$

where  $R$  is the regolith thickness,  $\dot{W}$  is the weathering rate [L/T], or the rate of production of regolith,  $\rho_r$  is the density of rock, and  $\rho_b$  is the bulk density of the

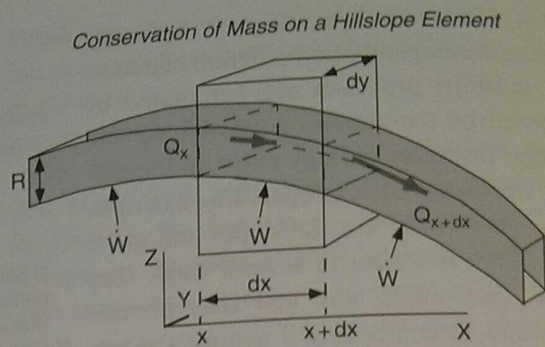


Figure 10.3 Conservation of mass on a hillslope element of size  $dx$  by  $dy$ , capturing the essence of Gilbert's (1909) argument for convex hilltops. Spatially uniform weathering supplies new regolith to each hillslope element. For a steady hillslope form, in which a uniform regolith thickness,  $R$ , is maintained, there must be a spatial gradient in the lateral transport of regolith,  $Q_x$ , increasing linearly with distance,  $x$ , from the hillcrest.

regolith. If we align the  $x$ -direction of our box with the local slope, it is safe to ignore mass fluxes across the sides of the box ( $Q_y$ ) and Equation 10.1 then becomes

$$\frac{\partial(\rho_b R dx dy)}{\partial t} = \rho_r \dot{W} dx dy + Q_x(x) dy - Q_x(x + dx) dy \quad (10.2)$$

Noting that we may hold the length of the sides of the box to be unchanging with time, we may remove them from the derivative on the left-hand side and divide through by  $dx dy$ . If we assume that the bulk density,  $\rho_b$ , also does not change, we may pull it out of the derivative as well, and the left-hand side then becomes simply the rate of change of regolith thickness with time. On the right-hand side the  $dy$  vanishes entirely. The equation can then be arranged to become

$$\frac{\partial R}{\partial t} = \frac{1}{\rho_b} \left[ \rho_r \dot{W} - \frac{Q_x(x + dx) - Q_x(x)}{dx} \right] \quad (10.3)$$

From our introduction to calculus, we recognize the term in brackets on the right-hand side to be the spatial derivative of the regolith discharge,  $\partial Q_x / \partial x$ :

$$\frac{\partial R}{\partial t} = \frac{\rho_r}{\rho_b} \dot{W} - \frac{1}{\rho_b} \frac{\partial Q_x}{\partial x} \quad (10.4)$$

We have, in Equation 10.4, a general statement of conservation of mass on a hillslope in one dimension. The steady-state case that Gilbert postulated is captured by taking the time derivative to be zero, producing

$$\rho_r \dot{W} = \frac{dQ_r}{dx} \quad (10.5)$$

In words, Equation 10.5 requires that the local production rate of regolith by weathering of the bedrock beneath (the left-hand side) must be exactly balanced by the spatial change in the discharge of regolith with distance down slope (the right-hand side). Otherwise, regolith will pile up in the box, or be slowly drained from the box.

One may simply integrate this equation to arrive at a prediction of the spatial pattern of regolith discharge on a slope:

$$Q_r = \rho_r \dot{W} x \quad (10.6)$$

Regolith discharge simply increases linearly with distance from the divide ( $x = 0$ ), at a rate governed by the regolith production rate.

The more general statement of the conservation of mass on a hillslope is the non-steady-state (or “transient”) case, Equation 10.4, or its two-dimensional analog. In order to solve this general case, or in order to understand the evolution of a particular hillslope, we need to know about the processes that give rise to the two terms on the right-hand side of Equation 10.4. First, what establishes the rate of regolith production (see Chapter 7)? And second, what process or suite of processes is involved in moving regolith downslope? In order to determine how this process might depend upon slope, or upon position on the hillslope, or upon climate, we need to explore the physics (and chemistry... and biology) of the specific hillslope processes involved.

## Diffusive processes

Geomorphologists often talk about diffusive landscapes, or diffusive processes. Diffusion, whether it be of ink in a glass of water, smoke in air, or heat in a solid, tends to smooth out spikes in the concentration of some property. Landscapes dominated by diffusive erosion processes have rounded edges, because diffusion

attacks sharp corners. Before turning to specific physical processes, let us consider briefly the general diffusive case. The goal is to develop the diffusion equation for a hillslope. The diffusion equation comes about by combining two concepts: conservation of mass, which we have just developed, and a rule for how flux variables. For many processes, we might expect the flux rule to be something like:

$$Q = -kx^m \frac{\partial z^n}{\partial x} \quad (10.7)$$

where  $m$  and  $n$  are constants setting the relative importance of distance from the divide,  $x$ , and of slope,  $\partial z/\partial x$ , respectively, and  $k$  sets the efficiency (scale) of the process. In the diffusive case,  $m = 0$  and  $n = 1$ , in other words the regolith discharge depends solely, and linearly, on the local slope,  $\partial z/\partial x$ . In this case, Equation 10.4 becomes

$$\frac{\partial R}{\partial t} = \frac{1}{\rho_b} \left[ \rho_r \dot{W} - \frac{\partial(-k(\partial z/\partial x))}{\partial x} \right] \quad (10.8)$$

If we make the simplifying assumption that the hillslope efficiency constant,  $k$ , is spatially uniform, i.e., does not depend on  $x$ , then we can remove the  $k$  from the derivative to obtain the diffusion equation:

$$\frac{\partial R}{\partial t} = \left( \frac{\rho_r}{\rho_b} \right) \dot{W} + \kappa \frac{\partial^2 z}{\partial x^2} \quad (10.9)$$

where  $\kappa = k/\rho_b$ , and is called the landscape diffusivity. The ratio in front of the weathering rate reflects the inflation or bulking of the material as it is transformed from rock to soil. As in any other diffusion equation, the diffusivity must have units of  $L^2/T$ , as this does.

Equation 10.9 is a diffusion equation for a hillslope. This or an analogous diffusion equation comes up frequently in physical systems. Diffusion equations always describe the variations of some quantity in time (here, that quantity is regolith thickness, but it could also be concentration of a solute or temperature). We have already seen its cousin as a diffusion equation for temperature when heat is transferred conductively. The connection is that the transport of the quantity of concern (here regolith, or heat) is proportional to a spatial gradient in a related quantity (topography, or temperature). When we combine this concept with the need to conserve regolith (or heat), we find that the variations of that quantity always depend upon the

second spatial derivative of something (here, that something is surface elevation). The second derivative describes the curvature of the surface, or the rate of change in slope. You can see from Equation 10.9 that regions with high curvatures will undergo the greatest changes in regolith thickness. This is the reason that diffusion tends to smooth topography: in regions of high curvature (dimples or bumps on the hillslope) the regolith will either be thickened or thinned fastest, leading to smooth slopes. We arrived at the diffusion equation when we chose a transport rule (Equation 10.7) in which the flux of sediment depended only on slope, and not on distance downslope. Had we chosen a transport rule with an  $x$  dependence ( $m \neq 0$  in Equation 10.7), we would not have arrived at a diffusion equation. Transport of sediment by flowing water is an example of a process that does not lead to diffusive behavior, as we shall see. See the random walk box (Box 10.1) below to see how one can also arrive at a diffusion equation by appeal to summation over many potential particle paths.

The diffusion equation is a partial differential equation. In general, these can be solved analytically only under very simple conditions. Because the diffusion equation is so common, solutions for many particular conditions are available. One useful compendium is Carslaw and Jaeger's *Conduction of Heat in Solids* (1967), which has much broader application than its title implies. We can easily find the solution for the steady case, in which we set the left-hand side to zero. This transforms the equation into an ordinary differential equation, one in which the dependent variable,  $z$ , depends upon only one variable,  $x$ . The curvature is then a constant, set by the regolith production rate and the diffusivity,  $\kappa$ :

$$\frac{d^2z}{dx^2} = -\frac{\rho_r \dot{W}}{\kappa \rho_b} \quad (10.10)$$

Note that the curvature is negative, meaning that the topography is convex up. Equation 10.10 can be integrated once to obtain the slope as a function of position:

$$\frac{dz}{dx} = -\left[\frac{\rho_r \dot{W}}{\kappa \rho_b}\right]x + c_1 \quad (10.11)$$

The constant of integration,  $c_1$ , is 0 because at  $x = 0$  (the hillcrest) the slope is zero. A second integration yields the topography,  $z(x)$ :

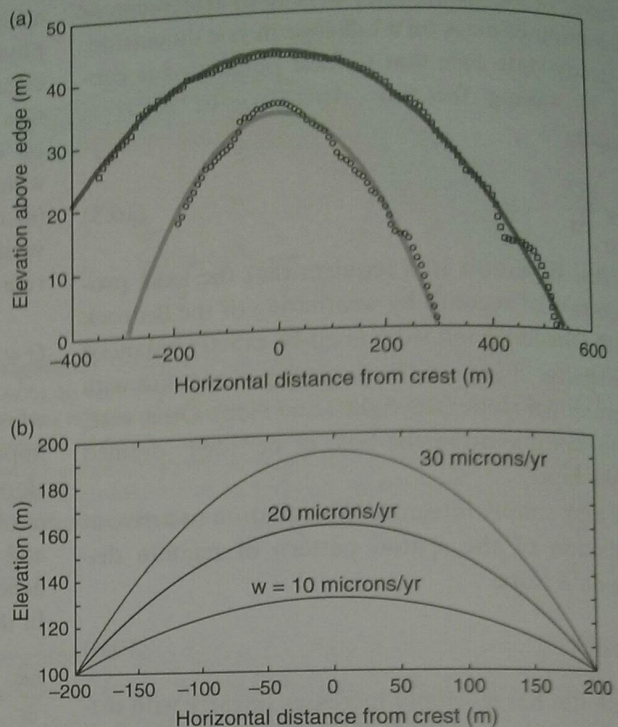


**Figure 10.4** (a) Profiles of summit of Goat Flat in the Wind River mountains. Dots are data from hand-leveling of the topography. Curves are best-fitting parabolas through the data. Other than anomalous knicks into the hillslopes, usually associated with bedrock ledges or nivation hollows, the parabolas fit well. The curvature in this landscape is essentially uniform (after Anderson, 2002, Figure 3, with permission from Elsevier). (b) Analytic solutions for profiles of steady-state hilltops for three prescribed regolith production rates. As the rate of production increases, the curvature must increase to accommodate the required increase in downslope regolith transport.

$$z = -\left[\frac{\rho_r \dot{W}}{2\kappa \rho_b}\right]x^2 + c_2 \quad (10.12)$$

where  $c_2$  is another constant of integration. Note that  $c_2$  is an elevation. We may choose it by specifying the elevation at some location. In this case, shown in Figure 10.4, the easiest location is the hillcrest, where  $x = 0$ . Then  $c_2 = z_{\max}$ . Then Equation 10.12 describes an inverted parabola, a simple geometrical shape with the characteristic that the slope is zero at the crest and increases linearly with distance from the crest. As G. K. Gilbert argued in 1909, this hillslope shape must arise if regolith is being produced everywhere at the same rate. In other words, if  $\dot{W}$  is not a function of  $x$  (is uniform in  $x$ ), and if the regolith discharge rule is simply

### Box 10.1 From random walk to diffusion

Here we illustrate how one can move from a description of a microscopic process to a differential equation that describes the evolution of a system at a macroscopic level. The following derivation is a shorthand summary of Einstein's theory of Brownian motion (Einstein, 1905) (pers. comm. Greg Tucker).

Assume we have an ensemble of particles moving randomly and independently from one another, and for now simply consider motion left and right, in the  $x$ -direction. Let  $p(\delta x, \tau)$  denote the probability of a particle (which could be a water molecule, a mosquito, a sediment grain, etc.) making a jump of distance  $\delta x$  in a time interval  $\tau$ . Let  $C(x, t)$  denote the concentration of particles at point  $x$  at time  $t$ . ( $C$  can be read as the number per unit length in this one-dimensional treatment.) Our goal is to write an equation for  $C(x, t)$  that captures the macroscopic outcome of zillions of moving particles without having to follow the dynamics of any particular particle.

If the concentration,  $C$ , of particles is a function of location and time, then the concentration at position  $x$  at some short time interval,  $\tau$ , in the future is equal to the concentration at time  $t$  at a distance  $-\delta x$  away times the probability of moving exactly  $\delta x$  during  $\tau$ , integrated over all possible hop distances. Mathematically, this may be summarized as

$$C(x, t + \tau) = \int_{-\infty}^{\infty} p(\delta x, \tau) C(x - \delta x, t) d(\delta x) \quad (10.13)$$

This equation would be far easier to handle if we could pull  $C(x - \delta x, t)$  out of the integral. It turns out we can do this by performing a Taylor expansion around  $C(x, t)$  (see Appendix B):

$$C(x - \delta x, t) \approx C(x, t) - \delta x \frac{\partial C(x, t)}{\partial x} + \frac{\delta x^2}{2} \frac{\partial^2 C(x, t)}{\partial x^2} - \frac{\delta x^3}{3!} \frac{\partial^3 C(x, t)}{\partial x^3} + \dots \quad (10.14)$$

Substituting this expression for  $C(x - \delta x, t)$  into the integral in Equation 10.13 yields

$$C(x, t + \tau) \approx \int_{-\infty}^{\infty} p(\delta x, \tau) \left( C(x, t) - \delta x \frac{\partial C(x, t)}{\partial x} + \frac{\delta x^2}{2} \frac{\partial^2 C(x, t)}{\partial x^2} - \frac{\delta x^3}{3!} \frac{\partial^3 C(x, t)}{\partial x^3} + \dots \right) d(\delta x) \quad (10.15)$$

This looks discouraging, but since  $C(x, t)$  is not a function of  $\delta x$ , we can remove it from the integral and rearrange to get

$$C(x, t + \tau) \approx C(x, t) \int_{-\infty}^{\infty} p(\delta x, \tau) d(\delta x) - \frac{\partial C(x, t)}{\partial x} \int_{-\infty}^{\infty} p(\delta x, \tau) \delta x d(\delta x) + \frac{\partial^2 C(x, t)}{\partial x^2} \int_{-\infty}^{\infty} p(\delta x, \tau) \frac{\delta x^2}{2} d(\delta x) - \frac{\partial^3 C(x, t)}{\partial x^3} \int_{-\infty}^{\infty} p(\delta x, \tau) \frac{\delta x^3}{3!} d(\delta x) + \dots \quad (10.16)$$

While again this looks more complex than where we began, we are poised to simplify it by appealing to some definitions of statistical moments (see Appendix B). First, note that it is a property of a probability density function that the integral over all possible probabilities must equal 1. The first term therefore becomes simply 1:

$$\int_{-\infty}^{\infty} p(\delta x, \tau) d(\delta x) = 1 \quad (10.17)$$

allowing us to rewrite Equation 10.15 as

$$C(x, t + \tau) = C(x, t) - \frac{\partial C(x, t)}{\partial x} \int_{-\infty}^{\infty} p(\delta x, \tau) \delta x d(\delta x) + \frac{1}{2} \frac{\partial^2 C(x, t)}{\partial x^2} \int_{-\infty}^{\infty} p(\delta x, \tau) \delta x^2 d(\delta x) - \frac{1}{3!} \frac{\partial^3 C(x, t)}{\partial x^3} \int_{-\infty}^{\infty} p(\delta x, \tau) \delta x^3 d(\delta x) + \dots \quad (10.18)$$

**Box 10.1 (cont.)**

The integral in the second term is the definition of the mean value of  $\delta x$ , or the first moment of the distribution  $p(\delta x)$ . Likewise, the integral in the second term looks almost like the variance. In fact, it is the second *raw moment*, which is equivalent to the variance but is calculated around zero rather than around the mean. In general, the  $n$ th raw moment of a probability distribution  $P(x)$  is defined as

$$\mu'_n = \langle x^n \rangle = \int_{-\infty}^{\infty} P(x)x^n dx \tag{10.19}$$

where the angle brackets denote an average. From this definition, you can see that each of the integral expressions in our Taylor series (Equation 10.17) corresponds to a raw moment of the distribution of hop-length distribution  $p(\delta x, \tau)$ . Equation 10.18 may now be rewritten:

$$C(x, t + \tau) - C(x, t) = -\frac{\partial C(x, t)}{\partial x} \langle \delta x \rangle + \frac{\partial^2 C(x, t)}{\partial x^2} \frac{\langle \delta x^2 \rangle}{2} - \frac{\partial^3 C(x, t)}{\partial x^3} \frac{\langle \delta x^3 \rangle}{3!} + \dots \tag{10.20}$$

If we divide all the terms by  $\tau$ , the left-hand side of the equation becomes the definition of a derivative in the limit that  $\tau$  goes to zero:

$$\lim_{\tau \rightarrow 0} \left( \frac{C(x, t + \tau) - C(x, t)}{\tau} \right) = \frac{\partial C(x, t)}{\partial t} = \lim_{\tau \rightarrow 0} \left( -\frac{\partial C(x, t)}{\partial x} \frac{\langle \delta x \rangle}{\tau} + \frac{\partial^2 C(x, t)}{\partial x^2} \frac{\langle \delta x^2 \rangle}{2\tau} - \frac{\partial^3 C(x, t)}{\partial x^3} \frac{\langle \delta x^3 \rangle}{3!\tau} + K \right) \tag{10.21}$$

If we neglect the higher-order terms that contain cubes, etc., of the small distances  $\delta x$ , which is something we can do because as we shrink  $\delta x$  these terms shrink yet faster, and define the constants

$$v \equiv \lim_{\tau \rightarrow 0} \frac{\langle \delta x \rangle}{\tau} \tag{10.22}$$

and

$$D \equiv \lim_{\tau \rightarrow 0} \frac{\langle \delta x^2 \rangle}{2\tau} \tag{10.23}$$

we are left with a partial differential equation for the evolution of the concentration of particles:

$$\frac{\partial C(x, t)}{\partial t} = -v \frac{\partial C(x, t)}{\partial x} + D \frac{\partial^2 C(x, t)}{\partial x^2} \tag{10.24}$$

The first term on the right-hand side represents advection (or “drift”), while the second represents diffusion. This advection–diffusion equation appears, for example, in groundwater contaminant transport problems. From this derivation, you can see that the advection coefficient,  $v$ , represents the mean speed of a particle (that is, the average hop length divided by hop duration). Also note that if the average hop length is zero (i.e., there is an equal probability of going left or right), then the advection term disappears and we are left with a standard diffusion equation that we saw first in Chapter 3 in dealing with heat conduction problems. We also see that the diffusivity coefficient,  $D$ , represents the mean-squared particle displacement divided by hop duration (Equation 10.23).

In Figure 10.5 we illustrate this phenomenon by simulating a random walk of 10 000 particles. Each particle is allowed to take a random step drawn from a normal distribution with a standard deviation of 0.2 units, and a mean step length of 0.01 units. We report the new histogram of the positions of the particles after every 1000 steps. Through time, you can see the mean drift of the population to the right, reflecting the first term in the equation, and a spreading of the population reflecting the diffusive behavior of the population captured in the second term.

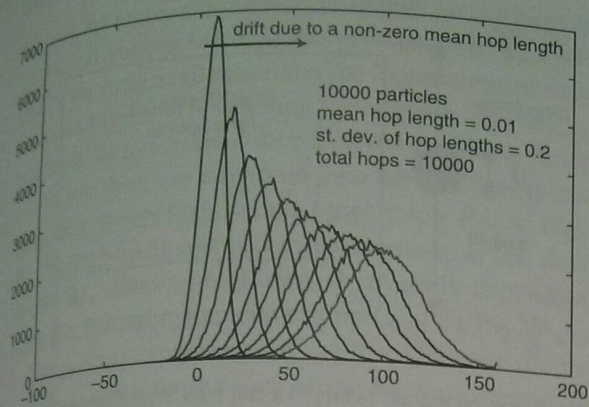


Figure 10.5 Random walk. Resulting migration and spread of a set of 10 000 particles whose behavior is governed by random hops. All particles originate at  $x = 0$  (not shown). Histograms of positions shown at 1000 hop intervals. The mean position drifts to the right at speed =  $0.01/\text{timestep}$ . The spread increases as the square root of time, while the magnitude of the peak in concentrations decays as the square root of time.

dependent on local slope. This is the essence of a diffusive landscape: hilltops are convex. Any sharp (high curvature) corners in the landscape are rapidly smoothed. One can see in Figure 10.4(a) that indeed some hilltops are not only convex, but are parabolic.

We now have a conceptual framework in which to explore both hillslope transport processes and hillslope forms. Convex slopes are likely to result from diffusive processes, in other words, regolith transport that is simply proportional to local slope. Other hillslope shapes, such as convexo-concave profiles, are likely to result from transport processes that depend upon something other than local slope, such as distance from the hillcrest. Let us now consider a few specific transport processes. Our goal in part will be to learn enough about the transport processes to allow us to construct models for  $Q$  that acknowledge its dependence on both climate and slope material properties.

### Hillslope processes

One may classify hillslope processes in many different ways. In our treatment, we break these processes down into grain-by-grain processes, and mass (or continuous) processes. One could also classify them as deterministic and stochastic, or in many other ways. We will start with the process of rainsplash,

an example of a grain-by-grain process. Although rainsplash is not a dominant process in many landscapes, the physics that drive it are clear, and are amenable to experimentation. Attention to the rainsplash problem will allow us to develop experience with parsing a process into its component pieces, which can be applied to other more common cases.

### Rainsplash

Bare soil surfaces are modified by the direct impact of raindrops, a process called *rainsplash*. Individual raindrops blast grains from the surface. On sloped surfaces, ejected grains travel longer trajectories downhill than uphill, resulting in a net downhill motion of material. Since the process may be cast as one in which the flux of material is proportional to the slope, this is a candidate for diffusive behavior. Note as well that it is a process that involves the summation over many individual particle motions, providing a linkage to the development of the diffusion equation through the random walk model described in the box above. Below we attempt to place the rainsplash process in a more formal setting, in order to assess the dependence of this process on the climate and the type of hillslope material. As hinted above, we will parse the problem into three parts:

- the number of ejected grains per impact and their velocities as a function of the impacting drop size;
- the resulting trajectories of the grains once ejected;
- the probability distribution of drop sizes and the total number of drops per unit area per unit time in a storm.

The first two are physics problems, while the third is a meteorological problem. In fact, these three pieces yield the transport associated with a particular storm. The long-term transport rate, averaged over even a year, and certainly over decades to millennia, requires averaging over a spectrum of storms. We must, however, start at the scale of a raindrop.

Studies have shown that the number and velocity of grains dislodged from soil surfaces by individual raindrops are roughly proportional to the kinetic energy of the impacting drop. While the response of the granular surface to raindrops is complex, having to do with the changes in the surface through the course of a storm, and to the specific grain size



distribution of the surface, and so on, we wish here to focus on the fundamental physics. The details of the surface response are treated extensively in the literature, much of it in the soil science literature.

The problem of the delivery of kinetic energy can be broken into the need to know the number of raindrops per unit area of the surface per unit time (the raindrop flux), and the kinetic energy of each drop at impact. From the expression for kinetic energy,

$$E_k = \frac{1}{2} Mv^2 \tag{10.25}$$

we see that the latter calculation reduces to knowing the mass,  $M$ , and the impact speed,  $v$ , of a drop. Calculating the mass of a raindrop is easy. Despite the illustration on the Morton salt containers, raindrops are approximately spherical (actually the large ones pancake a bit, presenting a broader cross section to the air), and their mass is therefore  $M = \rho_w \pi D^3 / 6$  for a drop of diameter  $D$  and water density  $\rho_w$ . We see already that the kinetic energy varies at least as the cube of the raindrop diameter.

What about their impact speeds? Like any object falling under the influence of gravity, a raindrop accelerates until the drag force opposing its motion is equal to the force pulling it downward, the weight of the particle. At this point, the vertical speed no longer increases, and the drop is said to be at its fall velocity (also called its terminal velocity or settling velocity). This balance is an example of Newton's law of motion, which states that the acceleration of an object is equal to the sum of the forces acting on it and is inversely proportional to the mass of the object. We have all memorized this as  $F = ma$ . By the time a raindrop hits the ground, it has achieved its fall velocity, which means that the acceleration in this familiar equation  $a = F/m$  is zero. This condition occurs when  $F = F_{\text{drag}} + F_w = 0$ , where  $F_{\text{drag}}$  is the drag force acting on the drop, and  $F_w$  is the weight of the drop. We note that this weight should be the buoyant weight, in general, but that in this case the weight of the displaced fluid (air) is trivial and may be neglected. Since  $F_w$  and  $F_{\text{drag}}$  act in opposite directions, they have opposing signs, and the fall velocity is reached when their magnitudes are equal.

The force balance on a raindrop is illustrated in Figure 10.6. The vertical coordinate is  $z$ , taken to be positive upward, and, as is common in fluid mechanics, we call the vertical velocity  $w$ . The only

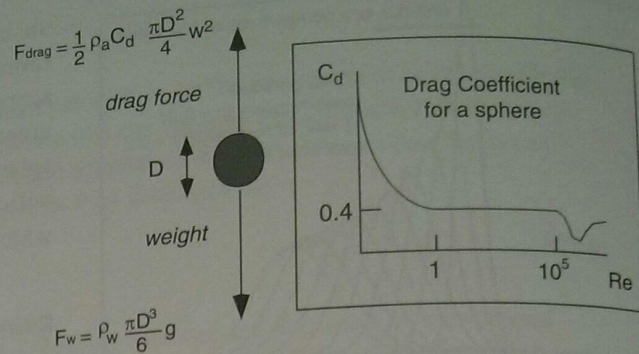


**Figure 10.6** Forces on a grain falling in a still fluid. At the settling speed, the drag force and weight are exactly balanced. The drag coefficient,  $C_d$ , is a function of the Reynolds number,  $Re$ , showing an inverse relationship for low  $Re$  and near-constant values around 0.4 for high  $Re$ . This is interrupted by the "drag crisis" near  $Re = 10^5$ , in which the drag coefficient diminishes twofold.

acceleration in this case is in the vertical, meaning that we can write the acceleration of the drop to be the rate of change of the vertical speed, or  $dw/dt$ . The weight acts downward, in the negative  $z$ -direction, and may be written as  $F_w = -Mg$ . The opposing force acting to retard the fall, the drag force, is a little more complicated, as it depends strongly upon the speed of the object relative to the fluid. One can write a general formula for the drag force on a sphere,

$$F_{\text{drag}} = \frac{1}{2} \rho_a C_d \frac{\pi D^2}{4} w^2 \tag{10.26}$$

where  $\rho_a$  is the density of the fluid through which the particle is moving (air in this case),  $C_d$  is a non-dimensional parameter called the *drag coefficient*, and  $\pi D^2 / 4$  is the cross-sectional area of a sphere presented to the flow. The drag coefficient is dependent upon the speed of the object relative to the fluid (and in general on the shape of the object – here we will assume a sphere). The value of the drag coefficient depends upon whether the flow around the object (our raindrop) is laminar or turbulent. In fluid mechanics, one relies upon a quantity called the Reynolds number,  $Re$ , to determine whether the flow field is laminar (low  $Re$ ) or turbulent (high  $Re$ ):

$$Re = \frac{\rho_w w D}{\mu} \tag{10.27}$$

where  $\mu$  is the dynamic viscosity of the fluid. This is only one of the many non-dimensional numbers one encounters in fluid mechanics problems. In this case,

the number represents the relative importance of inertial forces and viscous forces in the problem. The dependence of the drag coefficient upon the Reynolds number is shown in Figure 10.6. Ignoring the little dip out there at very high Re (a feature dubbed the drag crisis, at Re of  $10^5$  or so), there are essentially two asymptotic expressions, one at very high Re, the other at low Re. At high Re, the drag coefficient becomes a constant, at 0.4. And at low Re, the drag coefficient is inversely dependent upon Re, following the relationship  $C_d = 24/Re$ .

The general expression for the force balance on the particle is given by the sum of the buoyant weight of the particle (its weight less that of the fluid it displaces) and the drag force:

$$M \frac{dw}{dt} = -(\rho_w - \rho_a) \frac{\pi D^3}{6} g + \frac{1}{2} \rho_a C_d \frac{\pi D^2}{4} w^2 \quad (10.28)$$

To determine the settling velocity, which by definition occurs when the weight is exactly balanced by the drag force, we simply set the left-hand side of Equation 10.14 to zero, insert the relevant drag coefficient, and solve the equation. Breaking the relation  $C_d$  (Re) into two domains, reflecting low and high Re, results in two expressions for settling velocity, one for low and the other for high Reynolds numbers:

$$\text{for low Re: } w = \frac{gD^2\rho_w}{18\mu} \quad (10.29)$$

$$\text{for high Re: } w = \sqrt{\frac{gD\rho_w}{0.3\rho_a}} \quad (10.30)$$

Equation 10.29 demonstrates that the fluid viscosity,  $\mu$ , which relates the rate of shear strain in a material to the local shear stress on that material, plays a role in governing the settling speeds at low Re.

If you are doing such a calculation, you should check to make sure you have chosen the correct formulation of the drag coefficient, by assessing the Re associated with the calculated settling velocity. If you used the low Re formulation, and find  $Re > 1$  for the calculated settling velocity, or vice versa, you have used the wrong formulation. In Figure 10.7 we show the fall velocities for objects of several densities in both water and air, calculated using a fuller representation of the  $C_d(Re)$  function that spans the transition region between low and high Reynolds numbers (see Morsi and Alexander, 1972).

While the above discussion is general, let us return to the problem of raindrops. We are now in a position to assess the dependence of the kinetic

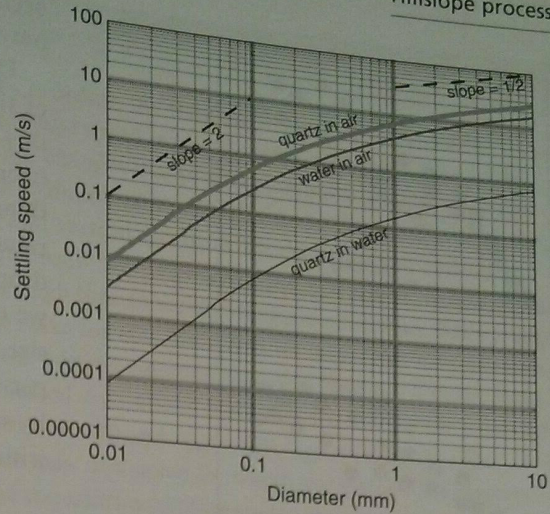
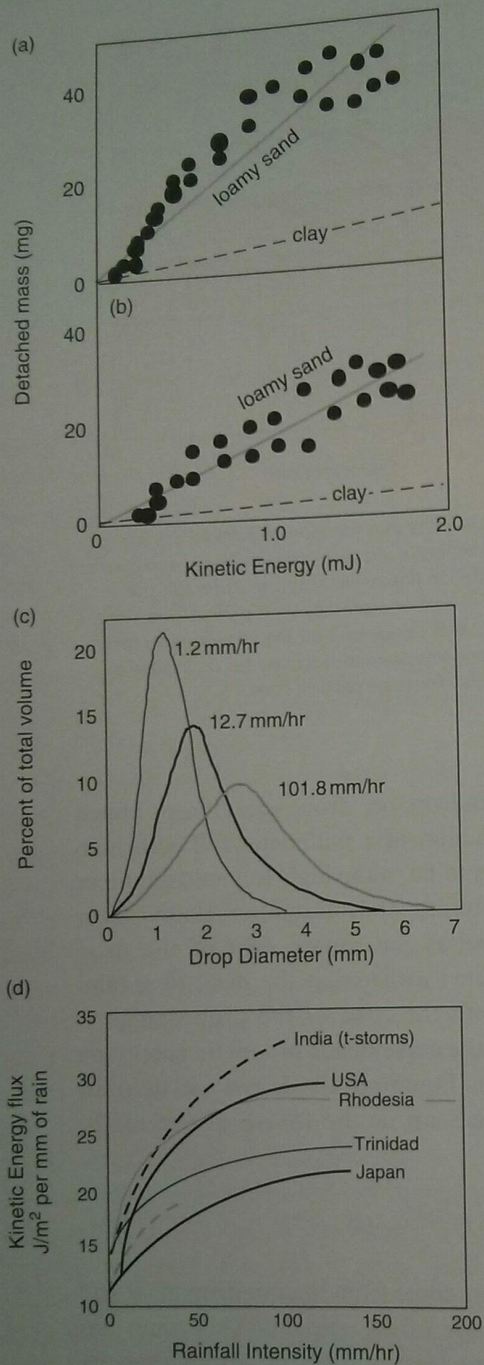


Figure 10.7 Settling velocity as a function of particle size for three cases: water droplets in air, quartz grains in air, and quartz grains in water, plotted in linear-linear space. Although the settling velocity increases monotonically with particle size, note the steeper increase (as  $D^2$ : slope of 2 on the log-log plot) for small particle sizes, and less dramatic increase (as  $D^{1/2}$ : slope of 1/2 on the log-log plot) for large particle sizes.

energy of a raindrop on drop size. Drops much larger than a fraction of a millimeter fall with high enough velocities to be in the high Reynolds number regime, and therefore obey Equation 10.30. Their velocities increase as the square root of the drop diameter. We noted earlier that the mass of a raindrop increases with the cube of the drop diameter. When we assess the dependence of kinetic energy on drop diameter in Equation 10.25, we see that the kinetic energy goes up as the fourth power of the drop diameter:

$$E_k = \frac{1}{2} Mv^2 \sim D^3 [D^{1/2}]^2 \sim D^4 \quad (10.31)$$

where three powers come from the raindrop mass and one from the square of the velocity. This result has strong implications for the types of storms that are important in driving rainsplash erosion: those capable of producing large drops ought to be many times more effective in transporting sediment. Empirically, high-intensity rainstorms have much larger drops (e.g., Laws and Parsons, 1943; Kneale, 1982), reflecting the fact that high-intensity storms are typically convective storms with high columns within which the raindrops are allowed to grow to very large sizes (see Figure 10.8). The rainsplash effects of the



**Figure 10.8** Raindrop sizes and their effects. (a and b) The mass ejected from a uniform surface for both a loamy sand and a clay surface as a function of kinetic energy of the raindrop size (after Sharma and Gupta, 1989). Data shown as filled circles are approximated as a linear function of kinetic energy. The difference between (a) and (b) is that the soil moisture in (b) is lower, meaning that grains are held more tightly by surface tension of the water in the pores. (c) Distribution of raindrop sizes for three different rainfall intensities (after Laws and Parsons, 1943). The dominant drop size increases by 1 mm for every order of magnitude increase in the rainfall intensity. (d) Distribution of kinetic energy flux as a

occasional summer cloudburst should therefore far outweigh the effects of many winter drizzles.

The flux of kinetic energy to the ground is the sum of the kinetic energy of all the drops. We can get at this impossible-sounding number if we know the distribution of drop sizes in a rainstorm, which is something that is measurable. The probability density of raindrop size,  $p(D)$ , describes the fraction of all the drops in a storm within each size category,  $dD$ . Since we can now calculate the kinetic energy of any drop size, the total kinetic energy delivered to the surface per unit time per unit area of the landscape is obtained by summing over the drop sizes. This is done formally with the integral

$$E_k = \sum_{i=1}^N E_{ki} = N \int_0^{\infty} E_k(D)p(D)dD \quad (10.32)$$

where  $N$  is the total number of drops landing on a unit surface area in a unit of time (say an hour), or the "raindrop flux," and  $p(D)$  is the probability density of raindrop size distribution (e.g., Figure 10.8(c)). The integral yields the mean kinetic energy of the raindrops. Note that if we replace the kinetic energy of the drop with the volume of the drop, the equation becomes one for the rainfall intensity (volume per unit area per unit time, which is a length per time, say mm/hr).

One could also think of this quantity as "rain power." Power has units of energy per time; for example, 1 watt = 1 joule/second. Rain power would be defined as  $P = N\bar{E}_k$ . We will see a similar quantity again when we explore the problem of stream incision into rock, in which case it is termed "stream power." In both cases we will be asking how efficiently this power is converted into geomorphic work.

But we are not yet done with the rainsplash problem. We have defined the meteorological forcing of the system, but have not yet assessed the response of the landscape. We must address the efficiency of the meteorological engine. We need to translate the ejection of grains from the surface to a transport distance, and we need to determine the circumstances in which

**Caption for Figure 10.8 (cont.)** function of rainfall intensity for several localities. Note the different curves for India, with and without thunderstorms (after Selby, 1982, Figure 5.22, with permission of Oxford University Press). For a recent review, see van Dijk et al., 2002, Figures 3–5.

**Box 10.2 The parabolic grain trajectory**

Assuming that the drag on the grain is negligible in this problem, the horizontal speed of the grain is unchanging between its launch and its landing. Its horizontal speed is  $u = V_0 \cos(\theta)$ , where  $V_0$  is the initial speed of the grain. The vertical speed, on the other hand, changes due to gravitational acceleration. Again ignoring drag, the vertical acceleration is simply  $-g$ . The evolution of its vertical speed is therefore  $w = w_0 - gt$ , where  $w_0 = V_0 \sin(\theta)$ . We may integrate the horizontal and vertical speeds to obtain horizontal and vertical positions,  $x$  and  $z$ , through time. These “parametric equations” for its position are:  $x = ut = V_0 \cos(\theta)t$ , and  $z = V_0 \sin(\theta)t - (1/2)gt^2$ . One may plot these positions through time to see that they are parabolas. But we may use a trick to discover the dependence of  $z$  on  $x$ , i.e., to solve for  $z(x)$ . Note that we may solve the  $x$ -position equation for time:  $t = x/V_0 \cos(\theta)$ , and replace the  $t$  in the vertical equation with this formula. The resulting equation for  $z(x)$  is  $z = x \tan(\theta) - \frac{g}{2V_0^2 \cos^2(\theta)} x^2$ , which is indeed a parabola. Note that we recover the expected trajectory length by solving for where  $z = 0$ . This occurs at  $x = 0$  and at  $x = (2V_0^2/g) \cos(\theta) \sin(\theta)$ . The advantage of casting the problem in this form is that we may now solve for where this parabola intersects a surface of prescribed slope. This treatment of ballistic trajectories (motion under gravity alone) and many more twists on the theme are elegantly presented in Neville DeMestre’s book, *The Mathematics of Projectiles in Sport* (1990).

this results in net downslope transport. What is the fate of the ejected grains? If we know the speeds and the angles at which particles are ejected from the surface, and the slope of the surface, we can calculate the distance the particles will travel before re-encountering the local surface, as shown in Figure 10.9. Ignoring the drag of the air, and any wind that might accompany the storm (we are aiming at a first-order understanding here), the trajectories of ejected grains are parabolas (see Box 10.2). On a flat surface, they would travel a distance

$$L = \frac{2V_0^2}{g} \cos \theta \sin \theta \tag{10.33}$$

where  $V_0$  is the initial speed of the ejection from the bed, and  $\theta$  is the launch angle with respect to the horizontal. As is sketched in Figure 10.9, on a tilted surface, the distance traveled is shorter on the uphill side and longer on the downhill side of the ejection site. It is the average of the uphill and downhill distances that scales the net rainsplash transport. To first order, the mismatch in up- and downslope distances is proportional to the local slope, in other words,  $L_{net} = aS$  where  $S$  is the local slope and  $a$  is a constant. We can determine crudely how big the discrepancy is between the hop length on a flat surface and the hop length on a canted surface by solving for the intersection of the grain trajectory (a parabola) with a

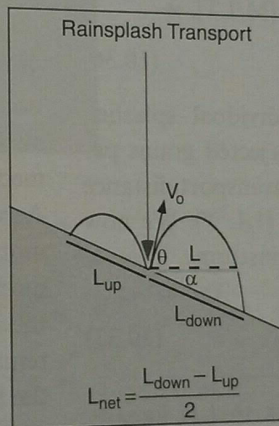


**Figure 10.9** Schematic of effects of a raindrop on ejection of sediment. The length of the downslope trajectory,  $L_{down}$ , is greater than that upslope,  $L_{up}$ , leading to net downslope transport,  $L_{net}$ , associated with each drop impact.

sloping surface (a straight line). The discrepancy, or  $dL = L_{down} - L$ , is roughly

$$dL = \frac{2V_0^2 \cos^2 \theta}{g} \tan \alpha \tag{10.34}$$

where  $\alpha$  is the slope of the surface. The sum of the discrepancy from upslope truncation and downslope extension of the trajectories is roughly twice this. Noting that  $\tan(\alpha)$  is approximately the negative of

the local slope,  $dz/dx$ , we obtain the following expression for the net transport length:

$$L_{\text{net}} = -\frac{4V_o^2 \cos^2 \theta}{g} \frac{dz}{dx} \quad (10.35)$$

Note that for a flat surface,  $dz/dx = 0$ , Equation 10.35 predicts a net transport of zero, as expected. For a given launch angle, the net distance increases essentially linearly with hillslope angle, and depends strongly upon the launch speed.

We have now determined that the transport rate ought to increase as the slope increases. This hints that the process may be diffusive. In a diffusion problem, however, we need to know how to weld together information about the mean transport rate of an ejected grain with information about the process intensity. In this case the intensity is set by the number of drops landing on a surface per unit area per unit time, the raindrop flux. The net transport rate of mass per unit width of the hillslope, also called the specific discharge with units of  $[M/LT]$ , is

$$Q = m_p n L_{\text{net}} N \quad (10.36)$$

where  $m_p$  is the mass of an individual splashed particle,  $n$  is the mean number of ejected grains per raindrop impact,  $L_{\text{net}}$  [L] is the net transport distance length, and  $N$  is the raindrop flux  $[1/L^2T]$ . We now have a transport rule for a given rainstorm:

$$Q_x = -m_p n N \frac{4V_o^2 \cos^2 \theta}{g} \frac{dz}{dx} \quad (10.37)$$

Note that this boils down to a flux that is linearly related to the local slope, the transport constant in front of the slope being related to the meteorologically important variables in the problem. We therefore expect diffusion from rainsplash! To summarize, in models of landscape evolution a hillslope process is often invoked in which the flux of regolith is simply cast as  $Q = -k(dz/dx)$ .

We may break Equation 10.37 down into

$$Q = P\beta L_{\text{net}} \quad (10.38)$$

where  $P$  is rain power and captures the meteorological forcing,  $\beta$  is the mass ejection efficiency (e.g., Sharma's data) which describes the susceptibility of the landscape to rainsplash transport, and  $L_{\text{net}}$  reflects the asymmetry of the trajectories. It is this latter effect that dictates the slope dependence of the transport

process (i.e., sets the roughly linear increase in transport with slope angle).

Recent experimental work on raindrop impacts has illuminated the details of the process. Using very high-speed video, Furbish *et al.* (2007) recorded the impact of raindrops of various sizes on sandy substrates at various inclinations. Several examples are shown in the photographs in Figure 10.10. They found that the asymmetry of the distribution of splashed grains was largely due to the asymmetry of the ejecta, rather than by the asymmetric truncation of parabolic trajectories described above. In other words, upon impact with an inclined surface, the redirection of the momentum of the water in the raindrop entrains more grains at higher speeds in the downslope direction than upslope direction. The net effect is similar, in that a mean downslope transport of grains occurs, but the physics behind the asymmetry of the resulting splash, leading to a non-zero  $L_{\text{net}}$ , differs.

The bottom line is therefore that one should expect a downslope drift of particles due to the summation of the effects of many raindrop impacts. The realization that this process is akin to a random walk has allowed the treatment of rainsplash in the statistical mechanical framework we have abbreviated in Box 10.1. A commonly observed phenomenon in the desert has motivated Furbish *et al.* (2009) to take the statistical mechanical approach to the next level. Most bushes in the desert sit on small mounds of sediment that are remarkably similar in their footprint to the canopy of the bush. These researchers suggest that the bush serves as something of an umbrella, reducing the number and intensity of raindrops beneath the canopy; in other words, as illustrated in Figure 10.11, the bushes generate non-uniform raindrop activity. The random walks of sediment driven by raindrop impacts will lead to a net accumulation of grains beneath the bush; while many raindrops in a ring outside the bush canopy drive sediment inward, the lower number of raindrop impacts beneath the canopy fail to drive sediment outward at the same rate. The net flux is therefore established simply by the gradient in the raindrop activity. But as the mound grows in height, the outward slope of the topography begins to take effect, creating an outward drift of particles. The mound reaches a steady configuration when the inward flux of particles due to the activity gradient in raindrops is balanced by the outward drift of particles due to the slope of the mound.

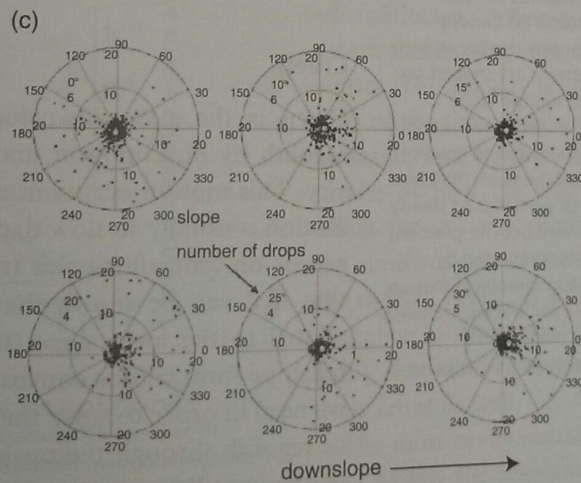
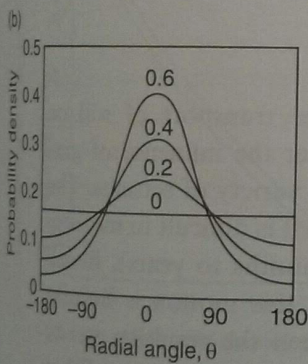
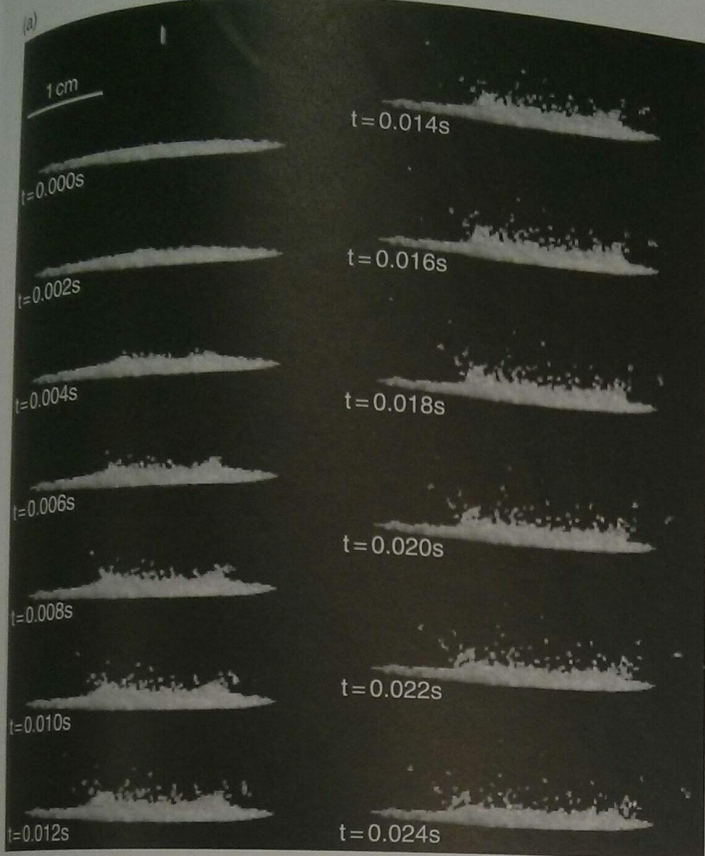


**Figure 10.10** Rainsplash experiments. Raindrops of known size impact clean sand of selected diameter, and the pattern of ejected grains is documented. (a) Sequence of photographs over 1/40th of a second showing one impact, and the grain-grain collisions that dominate the ejection pattern. (b) Definition sketch for the concentration factor, dictating the asymmetry of the ejection pattern, with downslope corresponding to  $\theta = 0$ . (c) Representative impact ejection patterns on increasingly sloped targets, ranging from 0–30°. Note increasing asymmetry to the ejection pattern (increasing concentration factor) with slope (after Furbish *et al.*, 2007, Figures 3, 6, and 11, with permission from the American Geophysical Union).

They further point out that this is a means by which the bush can command, or harvest, any nutrients in the surrounding soil, self-generating a resource island. Clever bush! Of course, upon death of the bush and decay of the canopy, the slope effects take over, and the form diffuses due to the dominance of downslope transport, as again shown in Figure 10.11.

One might wonder how to go about measuring rainsplash transport. The drop size distribution is clearly important to document when attempting to assess the role of rainsplash sediment transport. This is done using a remarkably simple contraption: a pan filled with flour. When exposed to the rain, the drops ball up and become coated in a monolayer of flour dust. This is then

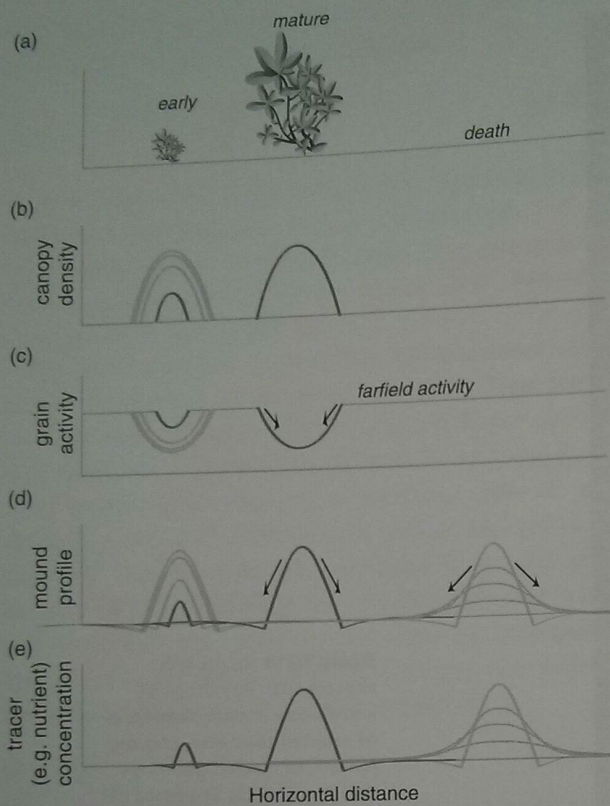


**Figure 10.11** Rainsplash induced growth of mounds beneath growing plant canopies (see Furbish et al., 2009). (a) Canopy evolution from early to mature stages. (b) Canopy density at early (left) and mature (right) stage. Temporal patterns are shaded on left of (b)–(d), showing asymptotic growth to mature stage. (c) Reduction in grain activity below far-field activity due to canopy growth. Arrows depict inward transport of grains due to gradients in grain activity. (d) Evolution of mound growth beneath the plant. Arrows depict slope-driven outward “drift” of particles. At steady state, outward slope-induced drift equals inward activity-gradient transport. After death of the plant, drift, uncompensated by activity gradient related transport results in topographic diffusion of the form. (e) Concentration of near-surface soil tracers, showing net loss of tracers from the moat around the plant, and enhancement of concentrations beneath the plant. Plants harvest nearby nutrients, becoming resource islands.

dried, and the resulting mixture is sifted. The size distribution of pellets can then be converted to the size distribution of raindrops knowing that the volume of the pellet corresponds to the surface area of the drop.

Measurement of the rates of sediment transport driven by raindrops, or the rainsplash transport rate, is commonly accomplished using a device called the Ellison splash board, developed by Ellison in the 1940s. This device, shown in Figure 10.12, separates that material being splashed uphill from that being splashed

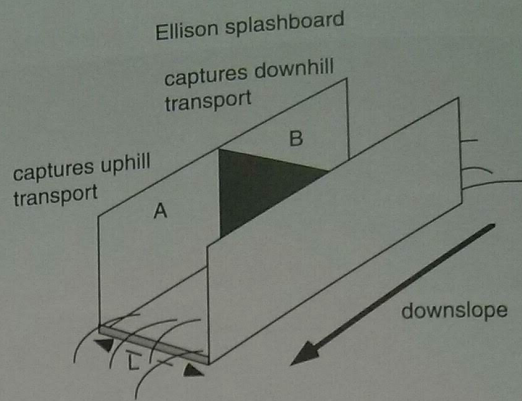


**Figure 10.12** An Ellison splashboard, shown here without its lid, allows documentation of net downslope rainsplash transport by differencing that mass of grains caught in trough A, representing uphill-splashed grains, from that in trough B, representing downhill-splashed grains. Division by the width of the trough,  $L$ , and the time interval,  $T$ , over which the measurement occurred results in a net transport rate:  $Q = (M_A - M_B)/LT$ . The lid prevents grains from being splashed or sluiced out of the trough.

downhill, using a small board to prevent cross-over between measurement cups. It is the difference between the mass collected on either side of the board that measures the net downhill transport of debris.

### Creep

Creep is the slow downslope transport of soil or regolith by bulk motion under the influence of gravity. This motion occurs in a variety of settings. The motion is usually so slow that it is difficult to measure except on long timescales (months to years). Recall that if it can be shown that this motion is linearly related to the local slope, then the resulting steady hillslope form will be convex up and parabolic. What we need in order to solve the problem is the discharge of regolith through the upslope and downslope sides of the box. What is the physics of this slow motion? And what might the velocity profile of such motion look like?

### Solifluction: frost creep and gelifluction

Slow downslope movement of soil is a significant process in periglacial areas, and is responsible for lobate steps or terraces on hillslopes called solifluction lobes. This slow downslope motion occurs in the short summers of Arctic and alpine areas, and results from

### Box 10.3 Analogy to micro-meteorite bombardment

On other terrestrial planets on which the hydrologic cycle is either dormant or non-existent, there is obviously no raindrop transport. Nonetheless, the surfaces are barren of vegetation and are therefore subject to bombardment from other projectiles. These come in the form of meteorites. On planets without significant atmospheres, micro-meteorites are capable of reaching the surface of the planet before burning up by drag-heating in passage through the atmospheric blanket. Surfaces of the Moon, Mercury and Mars are therefore bombarded with the full size spectrum of interplanetary debris, summarized in Figure 10.13. As this debris is dominated by small diameter particles, the surfaces are subject to micro-meteoritic and primary crustal debris many effects. First, a regolith cover consisting of a mixture of micro-meteoritic and primary crustal debris grows as these meteorites accumulate. Second, the regolith is continually being churned up by new impacts (a process cleverly termed "impact gardening"). Third, it will move material down slopes, for the same reasons that rainsplash accomplishes net downslope transport. Old surfaces that have not been subject to rejuvenation by a very large impact or by a volcanic event are therefore smoothed at the small scale by these impacts. One need only look at the beautiful medium format Apollo photographs of the Moon (e.g., the frontispiece for this chapter) to be impressed with the diffused nature of the landscapes we visited (see Light, 1999). The image of a typical view of the surface of Mars in Figure 10.14 reveals the competition between the roughening of the surface by impact of large debris, and the smoothing of the surface by the much more frequent small particles.

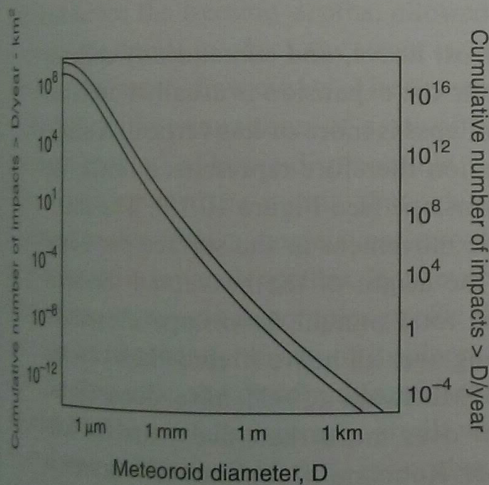


Figure 10.13 Present day impact rate at the top of Earth's atmosphere. The curve represents the cumulative number of impactors above that diameter to be expected in a given square km. The right axis is calculated by converting the impact rate to that over the entire surface area of the Earth (redrawn from Hartmann, 1999, Figure 6-4, with permission from Brooks-Cole).

the fact that these frozen soils attain excess water as they freeze through the growth of ice lenses. This excess water super-saturates the near-surface soil upon thawing from the surface downward. The saturated soil is weak when subjected to the shear stresses associated with the downslope component of the weight

of the material, allowing it to flow. Linc Washburn, in his extensive work in the Canadian Arctic and in Greenland, has documented carefully the velocities of solifluction lobes (see Figure 9.23). These can attain speeds of centimeters/day on even very shallow slopes. The velocity is clearly controlled by the thickness of the thawed layer, by the water content of the material, and by the slope. Let us consider a simple model of how the water content of the soil might affect the velocity profile. The latest soil to thaw is that immediately above the thaw front, at the base of the thawed layer. As soil thawed earlier will have had a chance to drain, and therefore to consolidate, it is likely that the soil is weakest immediately above the thaw front as well.

The most easily measurable quantity that might be used to test the relevance of this simple treatment is the surface velocity. Markers extending into the subsurface, however, will experience tilting due to the finite velocity difference between the base of the marker and the surface. This solifluction case is interesting in that the velocity profile ought to vary substantially through the season as the thaw proceeds. No motion will occur in the winter. The net motion over the course of a year ought to depend sensitively upon the maximum depth of thaw, and upon the duration of thaw, both of which will vary from year to year.



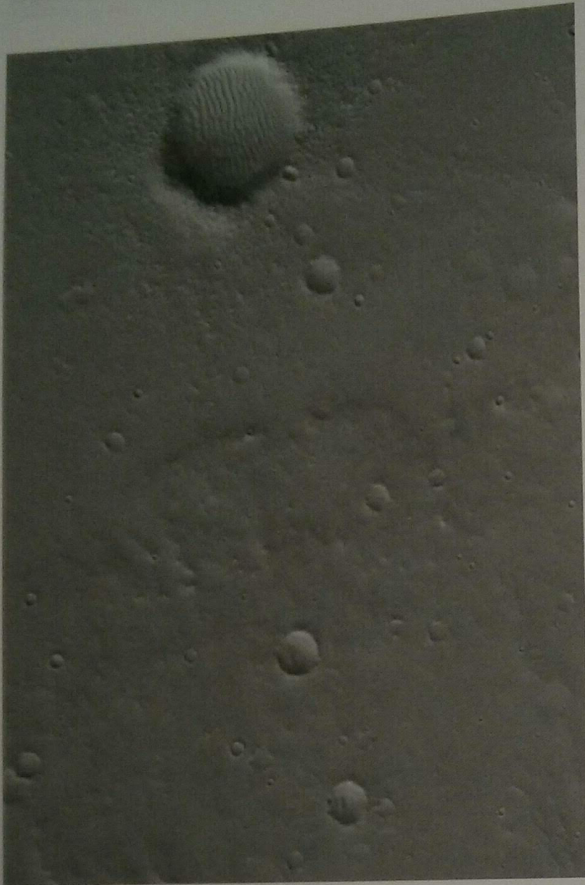


**Figure 10.14** Mars Global Surveyor (MGS) Mars Orbiter Camera (MOC) image showing a cratered surface in the Tempe Terra region. A wide range of crater sizes is clear. What is less clear is the dominance of small impact craters. These serve to blur the older craters through time. Large crater in the upper left has sand dunes on its floor. Location near: 31.0°N, 84.1°W. Image width: ~3 km (~1.9 mi). Illumination from: lower left. Season: Northern Winter (image taken by and available from NASA/JPL/Malin Space Science Systems. MGS MOC Release No. MOC2-1349, January 21, 2006, S1100389).

and even from place to place within a basin. If one desires a long-term soil transport rate on a particular slope, one must integrate the expected velocity profile over both depth (to obtain the transport rate at any instant), and over the thaw season. Finally, as not all seasons yield the same maximum thaw depth or duration, one should also integrate over a distribution of seasonal thaw cycles.

In regions prone to periodic freezing and thawing, regolith moves downslope by another means. We have already touched upon this in our discussion of periglacial processes in Chapter 9. Rather than flowing as a very viscous fluid, the soils periodically expand in a

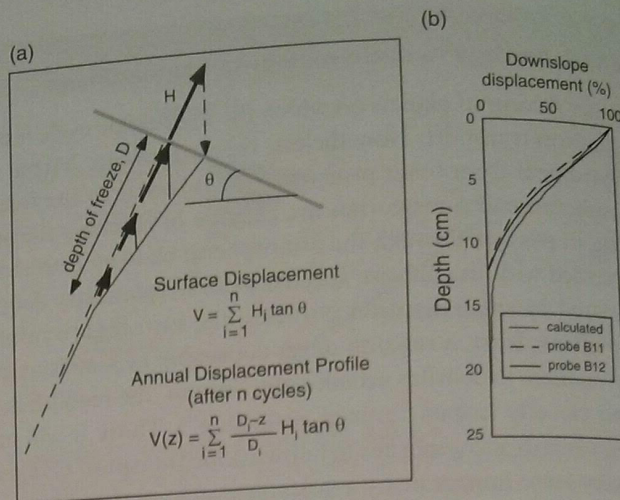


**Figure 10.15** Frost heave displacement profiles. While the displacement,  $V$ , from a single frost heave cycle of magnitude  $H$  is roughly linear with depth, the sum over  $n$  cycles results in a displacement profile that more smoothly asymptotes to zero with depth. In (b) two measured profiles are contrasted with the calculated profile based upon the summed linear profiles shown in (a) (after Matsuoka and Moriwaka, 1992, Figure 10, with permission from INSTAAR).

process called frost heave, and subsequently collapse upon thaw. While the expansion is usually normal to the slope, the collapse is more or less vertical. A single full cycle of motion therefore represents a ratcheting of material downslope (see Figure 10.15). The maximum downslope movement at the surface per heave cycle is set by the height of the heave and the local slope, while the total annual downslope movement requires summing over all heave (freeze-thaw) cycles. Matsuoka and Moriwaki (1992) have documented such movement over more than five years on hillslopes in the Sor Rondane Mountains of Antarctica using a clever device that allows real-time monitoring of the heave. Most previous studies used a set of dowel segments, or some other marker that is placed vertically in the soil, to be excavated at some later date, usually years after installation; the resulting pits are known as Young pits. This method yields information only about the total displacement profile, and yields no information about when within the period of the experiment the motion actually occurred. Previous workers had reported complex profiles, some of which were concave downslope, some concave upslope, some straight (see examples in Figure 10.16). Matsuoka and Moriwaki installed instead a flexible strip with a string of strain gages attached to it that

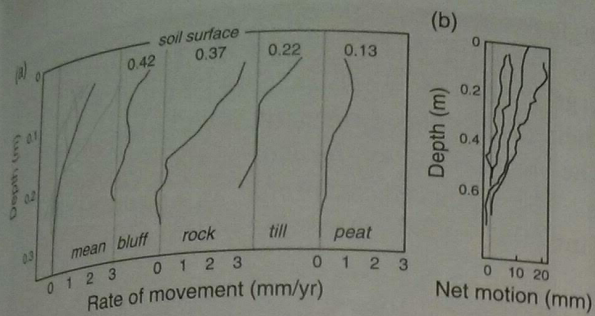


Figure 10.16 Displacement profiles from (a) Young pits as reported by Kirkby (1967, Figure 12, with permission to reproduce from the University of Chicago Press) and (b) segmented dowels as reported by Lehre (1987, Figure 4). Note slightly different vertical scales. Although the profiles vary in their detailed shape on various slopes (small numbers) and in different materials, the mean profile (left graph in (a)) demonstrates that the displacement declines monotonically to zero at depths of several tens of centimeters.

record the local curvature of the strip. By integrating the measurements of curvature, they can calculate the instantaneous displacement profiles of the strip. Simultaneous documentation of the temperature profiles, and hence the freezing depths, allowed them to determine the degree to which the strain events can be related to the freeze-thaw events. The agreement with simple theory (the summation of a set of linear displacement profiles) of heave displacement is striking. Their results support the notion that while the displacement profile from a single event may be linear, the addition of many such profiles, from events whose freeze depths vary, yields a complex profile that looks more like an exponential decay of displacement with depth. In their case, the distribution of freeze depths was such that the total displacement profile was convex up, as shown in Figure 10.15. This is another example of a process with both a deterministic element and a stochastic element. The deterministic aspect is the heave profile associated with a single event, while the stochastic one is the depth of a freeze-thaw event, which depends upon the vicissitudes of the weather.

Two recent sets of laboratory experiments shed more light on the process of downslope movement in the face of periodic freezing and thawing. Harris and Davies (2000) use a slab of soil 30 cm thick with a section 3 m long on a 12° slope. The apparatus and their results are shown in Figure 10.17. They combine the dowel-profile technique (here using stacks of unglazed tiles) with a pair of transducers that allow real-time recording of both slope-normal

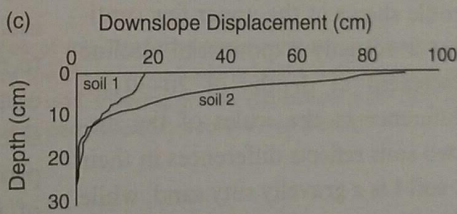
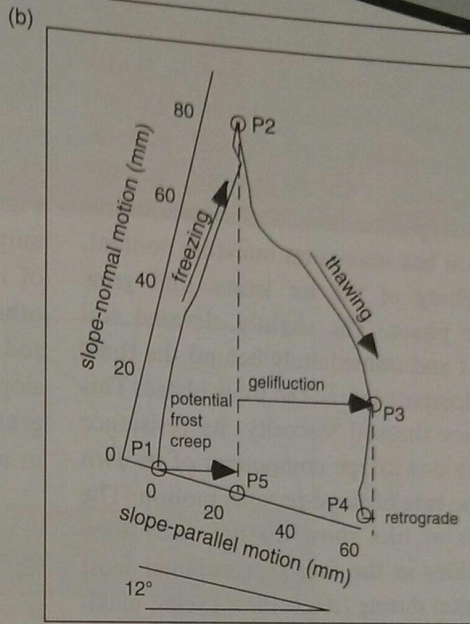
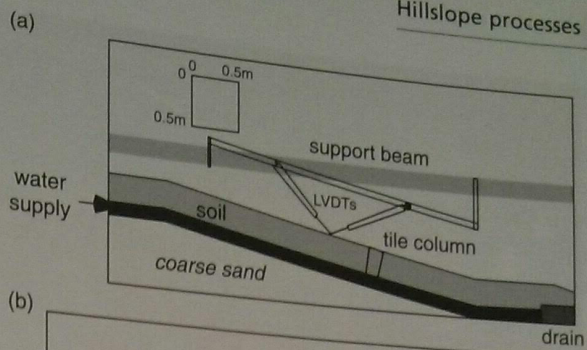


Figure 10.17 Gelifluction experiments. (a) Experimental set-up, with frost-susceptible soil on 12° slope, linear motion transducers attached to rigid beam above soil, and column of unglazed tiles embedded in soil. (b) Example of soil surface motion from LVDT records during a freeze-thaw cycle, showing contributions of frost creep and gelifluction (flow) to the downslope displacement of the soil. (c) Displacement profile after full four-cycle experiment, for two soil types, as deduced from tile column (after Harris and Davies, 2000, Figures 1, 3, and 6B, with permission from INSTAAR).

and slope-parallel motions of the surface to deduce the contributions of frost creep and of internal deformation to this downslope movement. The internal deformation component is called gelifluction. A typical freeze-thaw displacement record is shown in Figure 10.17. Heaving of the soil during freezing

results in only slope-normal motion, reflecting growth of ice lenses within the soil column. The maximum frost creep would be achieved if the soils were to experience purely vertical motion during thaw. What is seen in the experiments is that in the early and middle of the thaw phase the soil moves both downward and parallel to the surface. In other words, it flows. Late in the thaw, the motion returns to slope-normal, undoing a little bit of the downslope motion (this has been termed "retrograde motion" by Washburn). The physics involved during the thaw process entails the thaw consolidation of the soil, and the sensitivity of soil rheology to the moisture content and associated pore pressures. In the middle of the thaw event, the soil has maximum moisture content, derived from melting of the ice lenses that grew during the freeze phase. The slightly elevated soil water pressures at and immediately behind the thaw front eventually dissipate late in the thaw phase. This effectively increases the soil viscosity, its resistance to shear under the downslope component of its own weight, slowing the rate of slope-parallel motion. The exhumed columns of tiles show the net downslope displacement profiles in the face of combined frost creep and gelifluction during freeze-thaw cycles: maximum displacement occurs at the surface, a minor convexity of the profile shows in the upper few centimeters, followed by a roughly exponential decline toward zero displacement at depths of 20–30 cm. The several-fold difference in the scales of the displacements of the two soils reflects differences in their frost-susceptibility: soil 1 is a gravelly silty sand, while soil 2 is a fine sandy silt.

In a second set of experiments, done in a  $2 \times 1$  m box in which frost-susceptible soil was packed 0.3 m deep, Font *et al.* (2006) watched the displacements within the soil over 41 freeze-thaw cycles. The device and the final profiles are reproduced in Figure 10.18. They keep the room at a mean temperature below  $0^\circ\text{C}$ , which assures that a permafrost table develops, atop which an active layer freezes and thaws in each cycle. As water cannot drain downward through the permanently frozen substrate, the soil is more likely to remain saturated during thaw, promoting surface parallel motion.

We can cast more formally now the expected dependence of regolith discharge on slope and on the important features of the local climate. Given the theoretical displacement profiles shown to occur

in a single freeze-thaw cycle with a given freeze depth, we may integrate this to obtain the total regolith discharge in such an event, as indeed Font *et al.* did with their tile profiles. In general, we must integrate over the distribution of freezing events of varying depths. The displacement profile as a function of depth into the regolith,  $z$ , may be written

$$V_i = H_i \tan \theta \left[ \frac{\zeta_i - z}{\zeta_i} \right] \text{ for } z < \zeta_i \quad (10.39)$$

where the subscript  $i$  represents the  $i$ th freezing event,  $\zeta$  is the frost-penetration depth,  $H$  the height of the maximum heave, and  $\theta$  is the local slope. See Figure 10.19 for the definition sketch. The heave amplitude is set by the strain of the soil upon growth of ice lenses discussed in the periglacial chapter. In other words, we may say that  $H = \beta \zeta$ , where  $\beta$  is the soil strain upon freezing. Note also that the local slope may also be written  $\partial z / \partial x$ . We must now integrate this displacement profile with respect to depth in order to quantify the regolith discharge per event:

$$q_i = \int_0^{\zeta_i} \beta \zeta_i \rho_b \frac{\partial z}{\partial x} \left[ \frac{\zeta_i - z}{\zeta_i} \right] dz = \frac{\rho_b \beta}{2} \frac{\partial z}{\partial x} \zeta_i^2 \quad (10.40)$$

This is written as a mass discharge, and therefore includes the bulk density,  $\rho_b$ , converting from volume to mass. Note that the discharge varies as the square of the frost penetration depth. This is because both sides of the triangle representing the displacement profile have  $\zeta$  in them. The integral is simply the area of this triangle, which is half of the product of its depth,  $\zeta$ , with its width at the top. As the displacement at the ground surface is set by  $\beta \zeta_i (\partial z / \partial x)$ , the dependence is on the square of  $\zeta$ . This implies that deep frost events are more efficient at transporting regolith than shallow ones. In order to complete the analysis we must acknowledge that there exists a frequency of freezing events, or a number of events per year, and a range of frost penetration depths, both of which are set by the local climate.

In Figure 10.19 we show a plausible probability density function of frost depths, the most likely being shallow, and the likelihood falling off exponentially with depth (see Appendix B for this and other possible pdfs):

$$p(\zeta) = \frac{1}{\zeta_*} e^{-\zeta/\zeta_*} \quad (10.41)$$

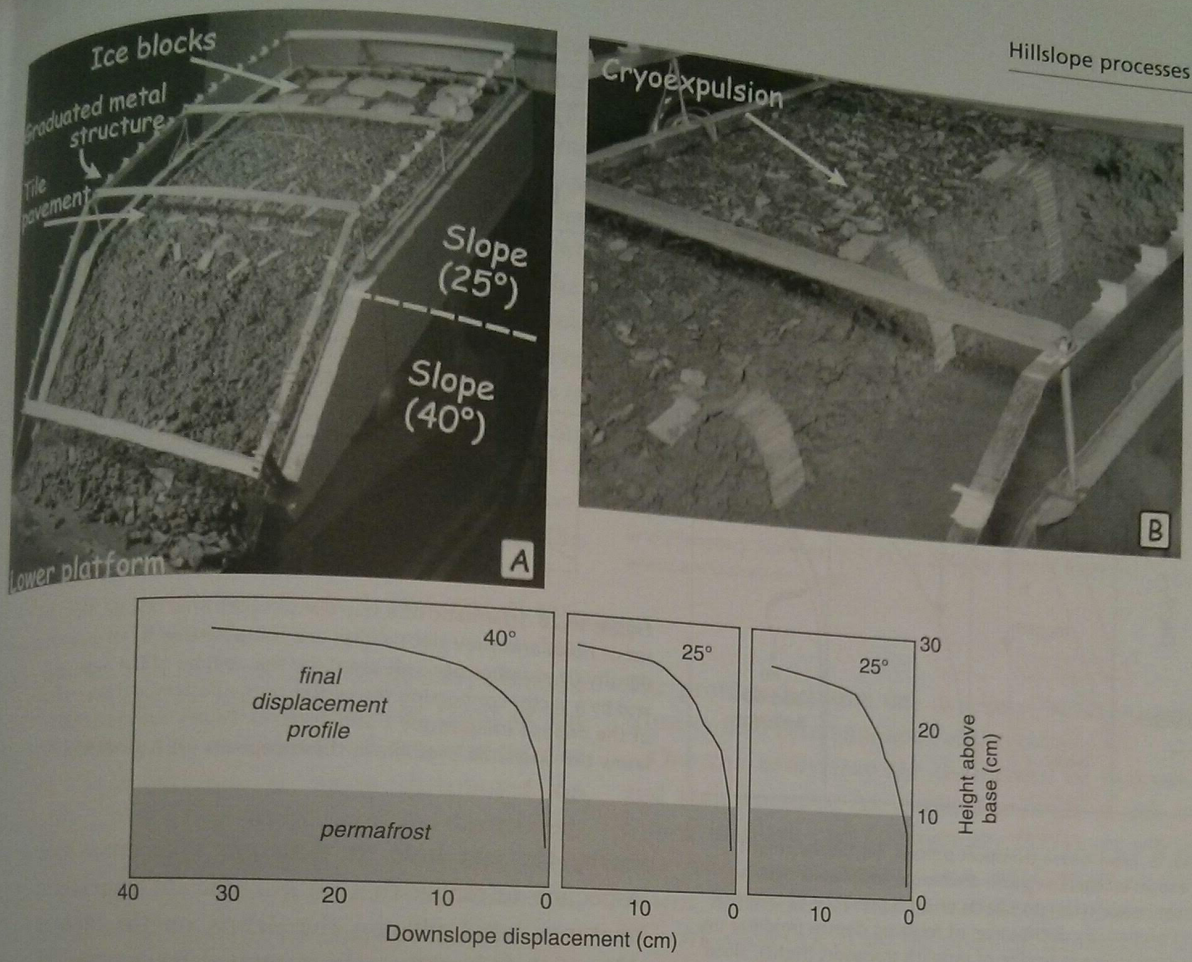


Figure 10.18 Experiments in periglacial activity on a sloping 2 × 1 m slab of soil. Top left: experimental set-up showing segments with 25 and 40° slopes. Top right: after 41 freeze–thaw cycles, exhumation of the tile columns tracking final soil displacement profiles. Bottom: tile displacement profiles shown after final cycle, as viewed through glass wall, showing greater displacement per cycle on the more steeply sloped site (leftmost) (after Font *et al.*, 2006, Figures 3 and 6, with permission from John Wiley & Sons).

where  $\zeta_*$  is the mean frost penetration depth. The total annual average regolith discharge is then

$$\begin{aligned}
 Q &= f \int_0^{\infty} q_p(\zeta) d\zeta \\
 &= f \frac{\rho_b \beta}{2} \frac{\partial z}{\partial x} \int_0^{\infty} \zeta^2 \frac{1}{\zeta_*} e^{-\zeta/\zeta_*} d\zeta \\
 &= f \frac{\rho_b \beta}{2} \zeta_*^2 \frac{\partial z}{\partial x}
 \end{aligned}
 \tag{10.42}$$

where  $f$  is the number of frost events per year. The flux of regolith is linearly dependent upon slope. Importantly, Equation 10.42 suggests how the flux might be governed by the climatic and by the material properties of the regolith. Note that the flux

increases as the square of the mean frost penetration depth,  $\zeta_*$ . This treatment is considerably more informative than the simpler but process-blind formula  $Q = -kS$ .

### Biogenic process examples

We have focused thus far on physical hillslope processes. In cases in which the landscape is entirely clothed in vegetation, surface processes such as rain-splash and even sheetwash are ineffective in moving particles from place to place. As can be seen in many such landscapes, however, the role of biological agents is clear. These roles can range from obvious to subtle, and can involve both animals and plants. Animal bioturbation includes the construction of mounds

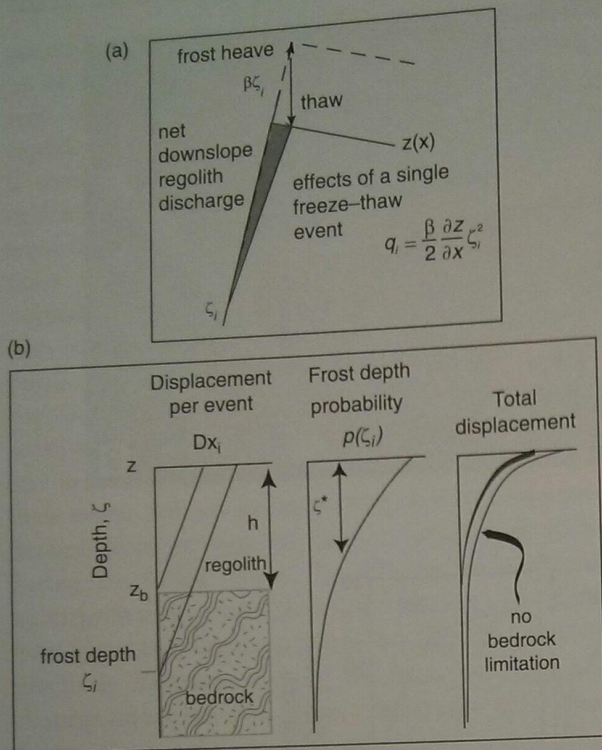


**Figure 10.19** Frost heave transport process. (a) Displacement profile and its integral, regolith discharge, associated with a single frost-heave cycle. (b) Effects of both presence of bedrock (left) and probability distribution of freezing depths (middle) on the long-term average profile of regolith transport (right). Note that the presence of bedrock limits the displacement profiles for all events in which the freezing depth is greater than the depth to the bedrock (after Anderson, 2002, Figure 8, with permission from Elsevier).

above ground, burrows below ground, lateral ploughing of the surface, particle ingestion and evacuation during foraging activities, food caching and prey excavation, wallowing and trampling, and the infilling of abandoned burrow structures (e.g., see review in Meysman *et al.*, 2006, and references therein). We can cast many of these processes into the same framework we have used to address the rainsplash and other processes, in that we can identify particular events, and must know something about the spatial intensity of these events.

### Rodents

Consider, for example, the case of fossorial (meaning burrowing) rodents. Burrowing creatures excavate tunnel systems within the soil, bringing some fraction of the soil mass to the surface. This mass is deposited

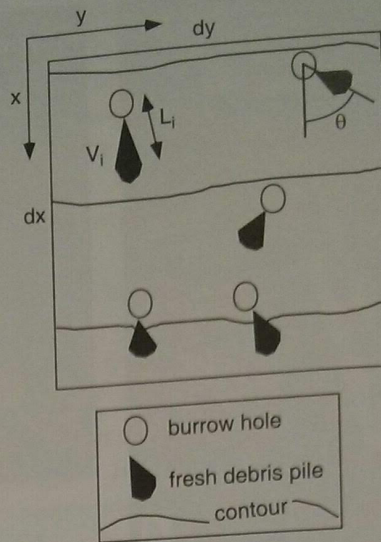


**Figure 10.20** Schematic of a burrow complex on a hillside. The set of holes and their debris piles are characterized by an areal density ( $N$ , number per unit area), by the volume of the deposit, and by a vector connecting the center of the burrow and the center of the deposit (magnitude  $L$  and angle  $\theta$ ). Finally, we must also know the timescale over which these deposits were generated,  $T$ .

nearly by the exit hole. It does not take much field inspection to realize that on a significant slope, these creatures avoid placing the debris on the upslope sides of their burrows. (In vegetated landscapes, this is the only debris that rainsplash and runoff can re-distribute, and it gets redistributed downhill ...) The problem of determining how to characterize this biological process as a geomorphic transport rule requires a characterization of both the individual soil-moving events, shown in Figure 10.20, and the number of such events per unit area per unit time (i.e., what we might call their "intensity"). In other words, we have a problem that is similar in structure to the rainsplash problem. Following our equation for flux in the rainsplash case (Equation 10.37), we have

$$Q_x = \frac{1}{T} \frac{dx dy}{dx dy} \sum_{i=1}^N \rho_b V_i L_i \cos \theta_i \quad (10.43)$$

where  $T$  is the period over which these events are summed,  $dx$  and  $dy$  are the lengths of the area in which  $N$  mounds were deposited, and  $\rho_b$  is the bulk density of the mound debris. This can be simplified to

$$Q_x = n \rho_b \frac{\bar{V}}{T} \bar{L} \int_0^{2\pi} \cos \theta p(\theta) d\theta \quad (10.44)$$

where we have defined the angle  $\theta$  to be the deviation from directly downslope (see Figure 10.20). Here  $n$  is the number of mounds per unit area of surface (e.g.,  $S \cdot m^{-2}$ ), and the overbars represent averages of volume and lengths. In this latter formulation, we have cast it in a way that is useful for field documentation. One must document the probability distribution of angles,  $p(\theta)$ , and have collected the volume and time together to indicate that one needs to document the volume removed from underground over a particular time interval. Notice that in each formulation the units of  $Q$  are  $M/LT$ . To reiterate, these odd units correspond to a particular mass passing across a unit length of slope in a unit time. If we want to know how much regolith passes a slope  $L$  wide, we must multiply this "lane discharge rate" by  $L$ .

What are the long-term effects of this sort of process and can we cast this as a simpler equation that will allow us to address the long-term shape-change of the landscape? All the constants in front of the integral relate to the *magnitude* of the process, the rate at which material is being distributed on the surface. On the other hand, all of the directionality of the process is embedded in the integral. If there is an even distribution of angles in each direction, i.e., if  $p(\theta)$  is a constant, then the integral will be zero (cosine has as much above 0 and below it), and there will be no net transport in the x-direction. Characterization of the propensity for critters to place their diggings downhill reduces to defining the function  $p(\theta)$ . This is perfectly analogous to the rainsplash problem, and what Furbish *et al.* (2007) termed the "concentration factor." It seems that the probability  $p(\theta)$  ought to depend upon the magnitude of the local slope. Say, for example, that

$$p(\theta) = \frac{1}{A} e^{-\left(\frac{\theta}{\sigma}\right)^2} \quad (10.45)$$

where the angle  $\sigma$  scales the sharpness of the propensity of an animal to place material downhill rather than uphill, and  $A$  is a constant that assures that the integral of  $p(\theta) = 1.0$  (all probability densities must have this property). The value of the integral in Equation 10.44 is a function of the angular scale,  $\sigma$ , which represents the sharpness of this angular discrimination. As  $\sigma$  increases, the probability distribution flattens out, the value of the integral declines, and the net downslope motion vanishes. We should expect that the discrimination depends upon the species.

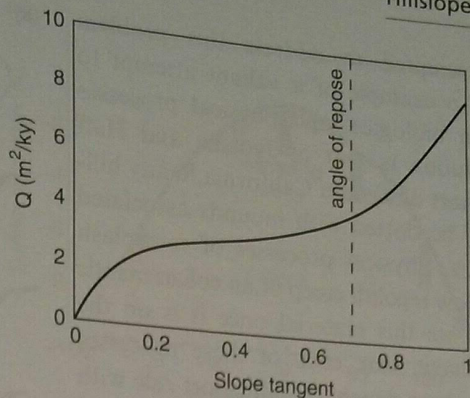


Figure 10.21 Theoretical dependence of regolith transport rate by gophers on slope (after Gabet *et al.*, 2003, Figure 8, reprinted, with permission, from the *Annual Review of Earth and Planetary Sciences*, Vol. 31, © 2003 by Annual Reviews, www.annualreviews.org).

The problem becomes one in animal behavior, and requires field determinations of the value of  $\sigma$ .

One can easily map the distribution of mounds, and their volumes. An excellent example of this is shown in Black and Montgomery (1991), in which they map gopher mounds in a small swale in the Marin headlands of northern California. This sort of work allows us to see the potential importance of critters in working the landscape.

Recent work on hillslopes in southern coastal California has added greatly to the data set on the biogeomorphological effects of rodents. Working in a landscape dominated by pocket gopher (*Thomomys bottae*) activity, Gabet (2000) provides us with quantitative information about the masses of the piles, the lengths from the exit portals, and the angles of the slopes on which the displacements occur. He proposes a nonlinear relation, illustrated in Figure 10.21, between the volumetric discharge of soil and the local slope in which discharge greatly increases with increasing slope.

Other complexities that must be addressed in this interesting arena of biogeomorphology include the need to assess to what degree creatures factor in other features of the environment as they choose where to live and to dig. For example, they likely avoid places where the regolith is less than some critical thickness (probably scaling with their own height). They may avoid slopes with a certain aspect, which would translate into an aspect asymmetry in their contributions to hillslope evolution. And so on.

Few have attempted to address this problem quantitatively. An example of a valiant attempt to incorporate both biological and physical processes in hillslope evolution is that of Jyotsna and Haff (1997). In the desert of eastern California, many hillslopes appear to be dotted with mounds associated with rodent holes. Physical processes of rainsplash and potentially slow regolith creep of an eolian mantle serve to redistribute this material once it is on the surface. As we have seen, each of these processes may be cast as a slope-dependent transport rule with coefficients reflecting the relative efficacy (efficiency) of the process. The roughness of the landscape will reflect the relative importance of the rodent-transport (mounding) process and the small-scale smoothing attributable to rainsplash and other processes.

Bioturbation has also been shown to be an important player at hazardous waste sites. At sites where contamination of soil is pervasive, and remediation activities focus on placing a non-eroding cap on the remaining contaminated soil, animal burrowing activities can lead to the much more rapid cycling of this material back up to the surface than anticipated (Smallwood *et al.*, 1998). Once brought to the surface, wind can re-suspend the finer material and transport it off site.

### Tree-throw

A theory for tree-throw can be composed in the same manner. Here the event is a tree falling over. The tree brings with it, embedded in its root structure, a mass of soil and at times rock, called a root wad. This wad is displaced from the hole from which it came by some fraction of a root wad diameter. This soil and rock mass is slowly released from the roots as the roots decay, generating a small mound to one side of the hollow illustrated in Figure 10.22. On relatively flat ground, this produces a characteristic mound and hollow micro-topography that can persist for centuries. The forests of the eastern United States are dotted with these features (see, for example, Schaetzel and Follmer, 1990; also Denny and Goodlett, 1956). Importantly, again we need directional information to assess whether tree-throw can be implicated in the net downslope movement of regolith. Schaetzel and Follmer suggest that the direction of tree fall has more to do with wind direction than with local slope. A tree-throw event locally roughens the landscape.

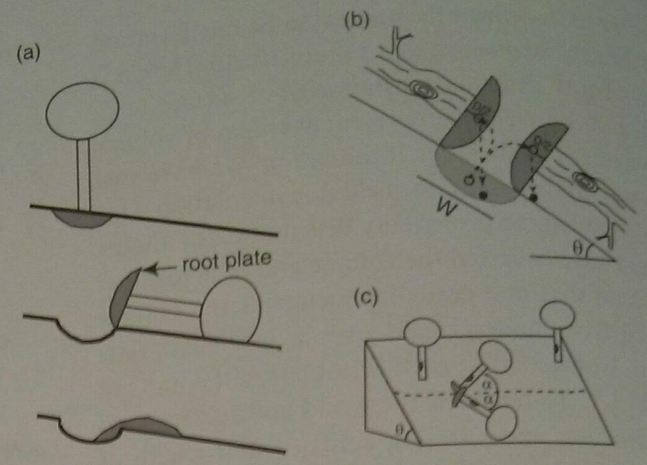


**Figure 10.22** Diagram of the tree-throw process, in which a root plate is tipped out of its original site, and ultimately decays, accomplishing net downslope transport. (a) Basic geometry, (b) details of the displacement of the center of mass of the root plate, and (c) definitions of angles used to calculate net downslope transport (after Gabet *et al.*, 2003, Figures 3–5, reprinted, with permission, from the *Annual Review of Earth and Planetary Sciences*, vol. 31, © 2003 by Annual Reviews, www.annualreviews.org).

Its degradation through decay of the root wad and subsequent small-scale surface processes serves to smooth the landscape. It is the competition between these roughening events and smoothing processes that gives the topography a particular roughness at the scale of meters in such forested landscapes.

We note that these are not the only processes that give rise to diffusion, and that importantly there are other processes, mostly associated with water running over the surface and within the shallow surface, that result in non-diffusive behavior. Without these processes, there would be no channels, and the world would indeed be much smoother than it is. We will cover these processes in later chapters, after briefly addressing the landslide problem.

### Pacing hillslopes

The rate of motion of regolith is in general very slow and difficult to document in many settings. We have turned to the use of cosmogenic radionuclides to establish long-term rates. Recall that if (and only if) a landscape is in steady state one may predict the spatial pattern of regolith discharge with distance from the divide. It must linearly increase with

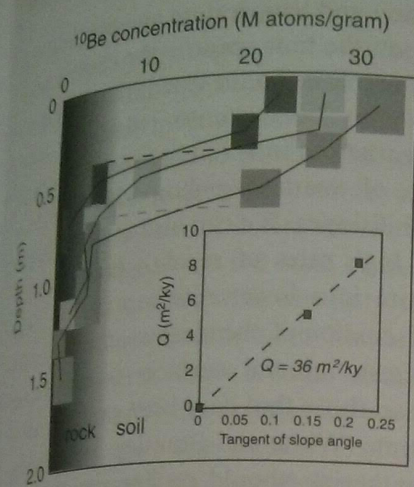


Figure 10.23 Profiles of  $^{10}\text{Be}$  in three test pits from the Black Diamond Mines Preserve Regional Park, California. Dashed lines depict base of soil in each profile. Boxes represent sample depth interval and  $1\sigma$   $^{10}\text{Be}$  values from two duplicate samples. Inset: relationship between slope and sediment discharge suggested by the  $^{10}\text{Be}$  data. The approximately linear relationship between slope and regolith discharge support Gilbert's view of convex hillslopes (after McKean *et al.*, 1993, Figures 2 and 3).

distance, at a rate governed by the rate of regolith production (Equation 10.6). As the regolith discharge is the product of regolith thickness with mean down-slope speed, the mean speed may be back-calculated using the measured regolith thickness:  $U = Q/h$ . And if the regolith is uniform in thickness, as it should be in steady state, then the mean speed must increase linearly from the divide.

Besides the instrumentation of hillslope profiles described above, there are two ways to estimate long-term speeds. We can use cosmogenic nuclides in two ways. McKean *et al.* (1993) used the inventories of atmospherically produced (so-called garden variety)  $^{10}\text{Be}$  in clay-rich soils of the coast ranges of California as a clock. These are nuclides produced within the atmosphere and swept out in precipitation, and subsequently tightly attached to clay particles in the soil. The integral of the profile, or the full inventory, should be proportional to time spent on the hillslope. They collected vertical profiles of  $^{10}\text{Be}$  at various distances from the divide. As reproduced in Figure 10.23, you can see that the inventory indeed increased with distance downslope at a rate that suggested the regolith discharge increased with slope. Their relationship suggested  $\kappa = 36 \text{ m}^2/\text{ka}$ , or  $0.036 \text{ m}^2/\text{yr}$ . Inspection of their plot in Figure 10.23 allows a quick calculation

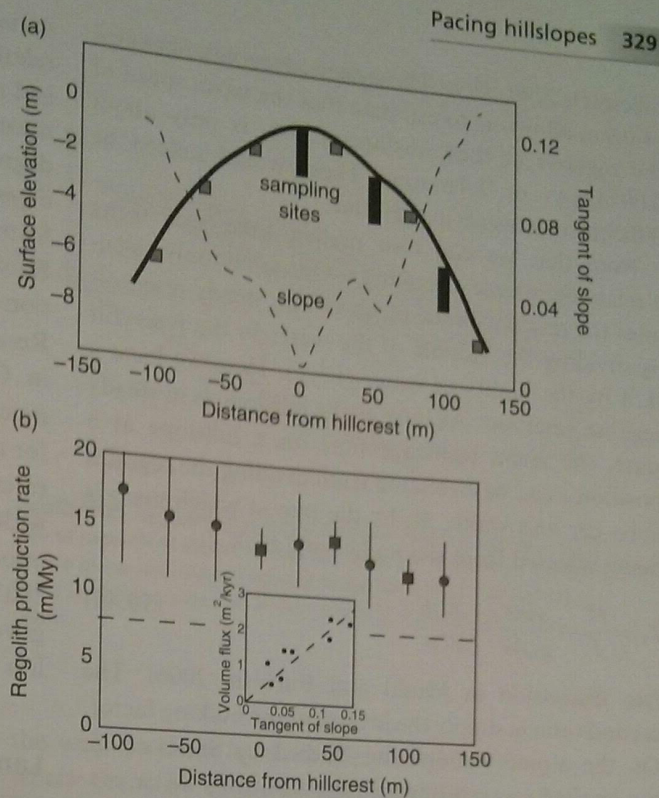


Figure 10.24 "Cosmo Hill" on Osborn Mountain, Wind River Range, Wyoming. (a) Topographic profile showing topography, slope, and locations of soil pits. Deep pits go to the bedrock interface at roughly 1 m. (b) Regolith production rates deduced from cosmogenic radionuclide concentrations in bedrock at base of pits; dashed line represents mean bedrock lowering rate on bare bedrock in this and other nearby ranges. Inset: volume flux of regolith deduced from cosmogenic radionuclide results, plotted against local slope. Linear fits indicate  $Q = -kS$  flux law (after Small *et al.*, 1999, Figures 5, 8, and 10, with permission from Elsevier).

of the mean speed. At a point on the landscape with slope = 0.15, the  $^{10}\text{Be}$ -implied soil discharge is  $5.2 \text{ m}^2/\text{kyr}$ . Dividing by the measured soil thickness of about 0.6 m, we can estimate the mean speed to be about  $9 \text{ m/kyr}$  or  $9 \text{ mm/yr}$ .

Using instead *in situ*-produced  $^{10}\text{Be}$ , Small *et al.* (1999) documented the evolution of profiles with distance from the divide in an alpine landscape in Wyoming. Their profiles showed that  $^{10}\text{Be}$  decreased slightly with depth into the regolith, likely reflecting persistent turbation over much of the profile. The inventory of  $^{10}\text{Be}$  in the regolith suggested that regolith production rates, shown in Figure 10.24(b), were roughly  $15 \text{ microns/yr}$ , and that the topographic diffusivity was  $\kappa = 18 \text{ m}^2/\text{ka}$ . The implied volumetric discharge of regolith at a distance of 125 m from the



hillcrest is 2200 m<sup>2</sup>/yr. The measured regolith thickness of 0.9 m allows us to estimate that the mean speed of the regolith at these distances,  $Q/h$ , is only about 0.0024 m/yr or 2.4 mm/yr. These would indeed be difficult to measure in real time.

Note that we can also predict timescales using a relatively simple calculation. One commonly calculates the residence time of water in a steady reservoir by dividing the volume of the water in the reservoir ( $L^3$ ) by the inputs of water ( $L^3/T$ ). Here we have a regolith reservoir. As long as the hillslope is in steady state, the mean residence time on a hillslope at a position  $x$  can be estimated from dividing the regolith mass per unit width,  $M$ , by the rate at which mass is being released from the underlying rock,  $I$ :

$$T_r = \frac{M}{I} = \frac{\rho_s hx}{\rho_r x \dot{W}} = \frac{h \rho_s}{\dot{W} \rho_r} \quad (10.46)$$

(see discussion in Mudd and Furbish, 2006). The second ratio is simply the inverse of the bulking factor. On the alpine Osborn site studied by Small *et al.*, the implied mean residence time is roughly 40 ka.

It is somewhat counterintuitive that the mean residence time of the soil remains constant over the entire slope; Equation 10.46 is independent of  $x$ . How can that be? It seems that regolith ought to age with distance from the divide. But we must remember both that fresh, zero-age regolith is being supplied uniformly to the base of the regolith, and that regolith speeds up with distance downslope. Recall that mean regolith speed must increase with distance from the divide:  $U = \dot{W}x/h$ . These factors of distance traveled and speed of travel balance out. We can see this by redoing the calculation above based upon not the inputs but on the outputs from the regolith reservoir. At steady state, the mean residence time may equivalently be calculated by dividing the mass per unit width in the box by the rate at which it is being lost at any chosen distance from the divide,  $x$ :

$$T_r = \frac{M}{Q} = \frac{\rho_s hx}{\rho_r U h} = \frac{\rho_s x}{\rho_r U} \quad (10.47)$$

In order for this expression to be equivalent to that in Equation 10.46, and in particular for the timescale not to depend on  $x$ , the mean velocity  $U$  must vary with  $x$ . And indeed it does, linearly so. The timescales described here have strong implications for the chemical evolution of regolith. The chemical weathering in soil will depend upon not only the intrinsic climatic

variables of precipitation and temperature and plant-related acidity, but upon the time spent in the chemical reactor that is the regolith. To the extent that the mean residence time may be taken to reflect the degree of chemical weathering in a soil, we ought to expect that any index of weathering should be uniform on steady-state hillslopes. We can also see from Equation 10.46 that high rates of regolith production ought to translate into lower residence times. Recalling from our discussion of chemical weathering in Chapter 7 that fresh mineral surfaces weather much more rapidly than those that have been exposed for a long period of time (White and Brantley, 1995), rates of chemical weathering should decline rapidly with mean residence time. This is likely the explanation of the common observation (e.g., Riebe *et al.*, 2001a–c) that chemical weathering rates are strongly governed by (or slaved to) physical weathering (regolith production) rates.

## Landslides

We have dealt a fair bit with hillslope processes that lead to the rounding of hilltops. Diffusive processes, those that result in regolith discharge that varies solely and linearly with the local slope, are indeed common. Rainsplash, frost heave, solifluction, all of these accomplish the rounding of the landscape. But on yet steeper slopes, further from the hillcrest, it is equally common to see more or less straight slopes on which the primary means of passing material from one place to another is not by slow creep of material, but by catastrophic landslide events. Landslide scars dot the hillslopes, showing as either bare rock or non-vegetated regolith patches amongst the trees and bushes. We will see that landslides play an important role in setting the locations of channel heads, the tips of the channel network, in some landscapes. Clearly, they can also pose some of the most lethal natural hazards a landscape can offer up.

The landslide problem is a classic case in geomorphology, involving a system in which there is a distinct threshold. Below this threshold, essentially nothing happens. Above it, a lot happens. In addition, landsliding is an inherently stochastic process. One cannot simply look at the landscape and expect to be able to deduce what it will look like ten years later. This is one of the things that makes

geomorphology both interesting and difficult. We have only recently begun to recognize the complexity (richness) of this type of problem. Let us be explicit in what we mean by stochastic, as the term comes up time and time again in geomorphic circles. It can be explained best in distinction to its antonym, deterministic. If a system is deterministic, then with sufficient knowledge about the state of the system at one time, we can predict with certainty the state of the system at some future instant. This is not the case in stochastic systems. There is some randomizing element in the problem. We can describe its future state in only a probabilistic way. The trajectory of a cannonball is essentially deterministic (which is why there were look-up charts for gunners), while that of a dust mote is stochastic.

But back to landslides . . . There are several parts to the problem. We must first assess the requirements for generation of a failure – in other words, we must come up with an equation that spells out the conditions that define this failure threshold. Even the simple analysis we will present should reveal the salient, or important, parts of the problem: the dependence upon the slope, the materials, the degree of saturation, whether there are trees on the slope or not, and so on. Then we must worry about what happens in the aftermath of the failure. What sort of mixture of rock and water is going to race down the hill? Does it behave like an intact block, or does it pulverize into fist-sized blocks that travel as a granular flow, or does it transform into an intimate mixture of debris and water that we call a debris flow? Each of these event types has its own mechanics. We are frankly only beginning to be able to deal with the complexity of this post-failure physics.

### The force balance at failure

Consider first the diagram of a segment of a planar hillslope shown in Figure 10.25. We wish to develop an expression that reflects the forces acting on this block of material at the time of failure. The plane at depth could be the interface between the regolith and the bedrock, or it could be a joint plane or plane of weakness within the bedrock. For now, you might want to think of it as a brick on a sloping plank of wood. Presumably right at the time of failure the forces are exactly balanced; it is not yet accelerating. The forces acting in the problem are all generated by

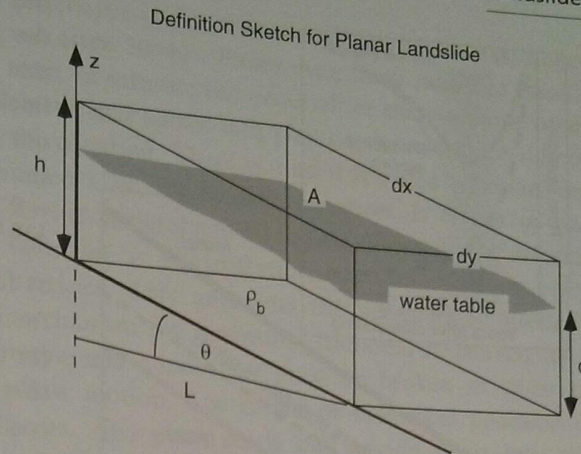


Figure 10.25 Segment of a planar hillslope showing geometry of a slab of regolith of area  $A = dx dy$  and thickness  $h$  above a potential failure plane with slope  $\theta$  relative to the horizontal. Also shown (bold line) is the water table with a height  $d$  above the failure plane.

the weight of the material. The weight is  $F = mg$ , where the mass of the block  $m = \rho_b h dx dy$ ,  $\rho_b$  being the bulk density of the material. Of course, the weight acts vertically. The component of this weight acting to try to shear the block from the underlying material, what we will call the driving force, is therefore  $F \sin \theta$ . Given that the block of soil is on a slope, the volume that comes into calculation of the mass involves a parallelogram of width  $L$  and height  $h$ . Noting that the cross-sectional area of the parallelogram is  $Lh$ , and that  $L = dx \cos \theta$ , the driving force becomes:

$$F_d = \rho_b (h dy dx \cos \theta) g \sin \theta \quad (10.48)$$

The resisting forces are essentially frictional, arising from the micro-roughness of the surfaces in contact. The greater the interlocking of grains, the higher is the force necessary to break or fail the contacts. The frictional resistance is the product of the force normal to the contact times the friction coefficient that is a measure of the interlocking of roughness. The normal force is  $F \cos \theta$ , while the friction coefficient has been given the odd designation of “ $\tan \phi$ ” in the soils engineering literature.

$$F_r = [\rho_b (h dy dx \cos \theta) g \cos \theta] \tan \phi \quad (10.49)$$

Because we are dealing with arbitrary blocks of soil rather than discrete blocks, like the brick on the plank, it is more appropriate to cast the balance in terms of stresses rather than forces. A stress is simply

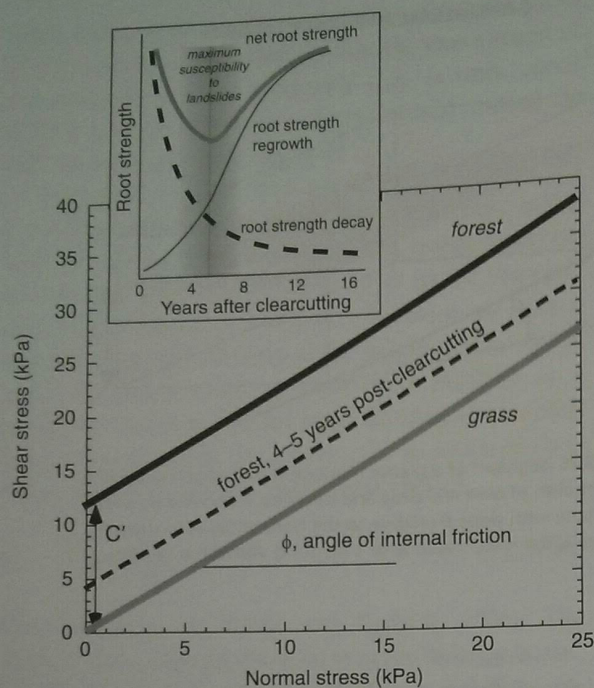


**Figure 10.26** Coulomb rheology plot of shear stress vs. normal stress at failure for three soils, a grass soil with little to no cohesion,  $C'$ , a forest soil with significant cohesion, and the same forest soil 4–5 years after clearcutting. This last case demonstrates the significant reduction of root-related cohesion as the fine roots decay. Inset: evolution of root strength after clearcutting, showing that the cross-over between root decay and root regrowth governs the timing of greatest susceptibility to landsliding (after Sidle *et al.*, 2006, Figure 2, with permission from Elsevier).

a force per unit area, which we can obtain by dividing through our expressions for force by the expression for the area of the base of the block, or  $dx \, dy$ . Note here that we use the along-slope distance  $dx$ , rather than the horizontal length  $L$ . The balance of stresses at failure then becomes:

$$\begin{aligned} \text{driving stresses} &= \text{resisting stresses} \\ \rho_b g h \sin \theta \cos \theta &= \rho_b g h \cos \theta \tan(\phi) \\ \text{or} & \\ \rho_b g h \sin \theta &= \rho_b g h \cos \theta \tan(\phi) \end{aligned} \quad (10.50)$$

You can see from the plot in Figure 10.26 that the origin of the name  $\tan \phi$  is simply that it is the slope on the plot of shear stress vs. normal stresses upon failure. So far, what we have described is the “dry, cohesion-less” case: the brick on a dry wood plank, or a dry pile of sand. The pile will fail when the angle anywhere is great enough that the left-hand side of

the equation, the driving stresses, is greater than the right-hand side, or the resisting stresses. Note that in this case (and this case only) the density, the thickness and the acceleration due to gravity cancel out from both sides of the equation. Recalling that  $\sin/\cos = \tan$ , the equation becomes simply

$$\tan \theta = \tan \phi \quad (10.51)$$

at failure. This equation has a couple of important ramifications. First, one can use the angle of repose (or the angle at which the material fails as it is tipped to greater and greater angles) as a measure of the coefficient of friction. Because this failure takes place internal to the material, this angle  $\tan \phi$  is also called the “internal angle of friction” or more simply the “friction angle.” Second, note what will happen to the angle of repose as one goes from Earth to Mars, say – nothing! The angle of repose of dry material should be independent of the acceleration due to gravity. The lee slopes of sand dunes on Mars should be exactly the same as those on Earth, i.e., about  $31^\circ$ .

Unfortunately, this simple equation does not capture the most general case. We have to introduce three elements of reality: water, cohesion in the form of mineral cohesion, and cohesion in the form of roots. Let us start by adding water to the problem. Water enters in several ways. First, by filling the pores, it changes the bulk density of the material. The expression for the bulk density of a saturated porous medium is  $\rho_b = \rho_g(1 - \eta) + \rho_w \eta$ , where  $w$  denotes water,  $b$  bulk, and  $g$  grains, and  $\eta$  is the porosity of the medium. In general, we wish to know the mean density of the column of material over the potential failure plane. This is

$$\bar{\rho}_b = \frac{\rho_{\text{sat}}^d + \rho_{\text{dry}}(h - d)}{h} \quad (10.52)$$

where here  $d$  denotes the water table height above the failure plane. You can check this by noting that when  $d = h$ , i.e., the water table is all the way up to the surface and the entire soil mass is saturated, the mean density becomes the saturated density. Similarly, when it is all dry,  $d = 0$ , and the density is that of the dry material. Now if this were the only role that water played, i.e., making the material heavier, the effects would come in equally on both sides of the stress balance equation. They would cancel out. Merely changing the density of the brick does not change the slope on which it begins the slide. But that is not

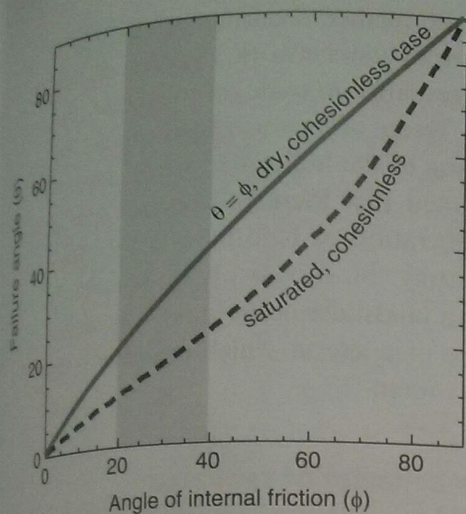


Figure 10.27 Failure angle as a function of the angle of internal friction,  $\phi$ . For dry conditions, the relationship is 1:1, meaning that the angle of internal friction can be read from the angle of repose. Such experiments show that typical values of the angle of internal friction are between 20 and 40° (shaded region). In wet (fully saturated) conditions, the failure angle is reduced significantly, by roughly a factor of two in the region of typical angles of internal friction.

the only effect water has on the system. In a crude way, we can think of the water as producing a water pressure (again, a force per unit area) at the potential failure plane, that supports some portion of the normal stress of the material. This will promote failure, as the normal stress comes into the frictional resistance. Formally, we define an “effective stress” as the normal stress less the water pressure:

$$\bar{\sigma}' = \bar{\rho}_b g h - \rho_w g d \quad (10.53)$$

Once this effect is incorporated, the symmetry of the force balance is broken. No longer can the density simply be canceled out. The graph of the failure angle,  $\theta$ , as a function of the coefficient of internal friction now has to include the degree of saturation ( $d/h$ ) of the material. We show in Figure 10.27 the dry and fully saturated ( $d = h$ ) cases. Over a reasonable range of angles of internal friction, the slope at which failure occurs is roughly half of that at which a dry slope will fail. Typical values of the angle of internal friction are 20–40° (for pure sand we have already shown it to be 31°), meaning that slopes above about half of this angle should not be expected to be stable if they are ever saturated.

This is not what we observe in nature. In the coast ranges of Oregon, for instance, where it rains several

meters per year, sometimes at very high rates, slopes are often 30–40°. Either even these rains are insufficient to saturate the material, or there is some other factor that comes into play on the resistance side of the equation. There is, and it is called cohesion, denoted  $C$  in the balance equation. It comes in two flavors, mineral and biological. The origin of mineral cohesion is electrostatic attraction between platy particles. This augments the geometrical interlock mechanism for generating frictional resistance, as it represents bonds that must be broken in order to allow motion. The origin of biological cohesion is roots. Any plant sends out myriad roots into the subsurface, each one of which has a tensile strength that must be exceeded before it fails. Obviously, the larger ones provide more resistance – taking more stress either to sever them or to pull them out of the soil – but there are many more of the smaller ones than large ones. The resistance to failure on any plane in the subsurface therefore depends upon the plant type and its age. While this problem has not been worked out in any very formal way, we do have evidence from the field that is pertinent to deciphering the relative roles of different sizes of roots. It has been documented that freshly logged landscapes in the Pacific Northwest of the USA will generate the largest number of landslides about 4–5 years after the clearcutting. This is clearly visible by the offset of the pre- and post-cutting failure curves in Figure 10.26. This is about the time it takes for roots of the 1-mm diameter scale to rot, losing their binding strength.

To recap, the final equation for the stress balance at failure for a planar landslide, humbly called the Master equation, is

$$\bar{\rho}_b g h \sin \theta \cos \theta = [\bar{\rho}_b g h \cos \theta \cos \theta - \rho_w g d] \times \tan(\phi) + C' \quad (10.54)$$

where  $C'$  denotes the sum of the mineral and root contributions to cohesion at the failure interface. In geological engineering circles, it is common to take the ratio of the resisting stresses to driving stresses, which we would always want to be greater than 1. This ratio is called the “factor of safety,”  $F_s$ . To be complete, the factor of safety is therefore:

$$F_s = \frac{[\bar{\rho}_b g h \cos \theta \cos \theta - \rho_w g d] \tan(\phi) + C'}{\bar{\rho}_b g h \sin \theta \cos \theta} \quad (10.55)$$

When this quantity is well above 1.0, the slope should be stable even in the worst-case scenario ( $d = h$ ), while if it drops below 1.0, the driving stress exceeds the resistance and the slope is likely to fail.

Plants do two more things that we ought not to ignore. First, all geologists know that plants suck. In particular, they suck water out of the soil and up into their stems as a necessary ingredient in the photosynthesis of new plant matter. This net transport of water out of the soil, in what is called the evapotranspiration process, reduces the likelihood of soil saturation, thereby reducing the likelihood of failure. In terms of the Master equation (Equation 10.54), this lowers the water table,  $d$ . Anyone who has cut down a tree or hauled firewood a long way knows that trees are also heavy. By felling a tree, and removing it from the hillslope altogether, the weight of the tree and hence both the contributed normal and shear stresses it represented, vanish from the stress balance. It turns out that the net effect of removing the weight of the trees is one of stabilization on relatively shallow slopes, and destabilization of slopes steeper than the internal angle of friction. Can you prove this to yourself?

We conclude with one last note on the failure mechanics. The above analysis is quite simplistic in many ways. First, while we assessed the role of water by addressing the position of the water table, in reality the relevant quantity is the pore water pressure (e.g., Iverson, 1997). In addition, we have treated the problem as one with planar hillslopes. This is never the case. Hillslopes are always crenulated in the cross-slope direction, giving rise to noses or ridges separated by troughs or hollows. The subsurface water we have been talking about is actually in motion (it is after all on a slope; even though it is in the subsurface, this causes flow). It will travel down the fall line, converging in the troughs and diverging on the noses, increasing the likelihood of saturation, and of the generation of high pore pressures, in the hollows while reducing these quantities on the intervening noses. As you might suspect, landscapes such as the coast ranges of Oregon show the largest number of failures in the troughs. In fact, this has huge implications for the whole landscape. These failures gouge out the troughs yet further, maintaining them as points of convergence for groundwater in the landscape. The failures race down the troughs, mix thoroughly, and generate very mobile debris flows, which

in turn accomplish further scouring of the upper portions of the drainage network. Studies of this landscape have revealed a cycle of filling of the hollows by slow creep of material, punctuated by the periodic sluicing of the hollows by landslides.

It should be noted that there is a distinct spatial pattern to the generation of landslides in the aftermath of clearcutting in forests. It is commonly observed that most landslides occur in hollows immediately downslope of a site at which drainage from a logging road is routed.

### A primer on the behavior of saturated granular materials

In recent experimental and theoretical work, researchers have carefully documented the behavior of saturated granular materials (e.g. Iverson 1997; Iverson *et al.*, 1997; 2000). While many models for the rheology of granular materials under these conditions have been proposed, recent work suggests that much of the behavior during deformation may be understood using the classical Coulomb description. As has been advocated for decades, this is best summarized in the Coulomb–Terzaghi equation,

$$\tau = \sigma' \tan \phi \quad (10.56)$$

where  $\tau$  and  $\sigma'$  are the local shear and the effective normal stresses acting on a plane and  $\phi$  is a friction angle characterizing the material. This can also be written as

$$\tau = (\sigma - P_w) \tan \phi \quad (10.57)$$

where  $P_w$  is the water pressure. We have already seen this in our analysis of landslide failures. Note in particular the role played by water pressure. The shear stress necessary to cause motion is reduced as the water pressure increases. In order to understand the behavior of the granular material we therefore must have a clear picture of the water pressure field.

The feedback between water pressure and displacement is well illustrated in a recent set of lab experiments. In the ring shear device shown in Figure 10.28(a), designed to allow large strains in the material, a saturated sandy loam was placed in the annulus along with several miniature pressure transducers and a bead column that would allow tracking of both local water pressure fluctuations and total displacement. The normal force and the shear force were carefully monitored.

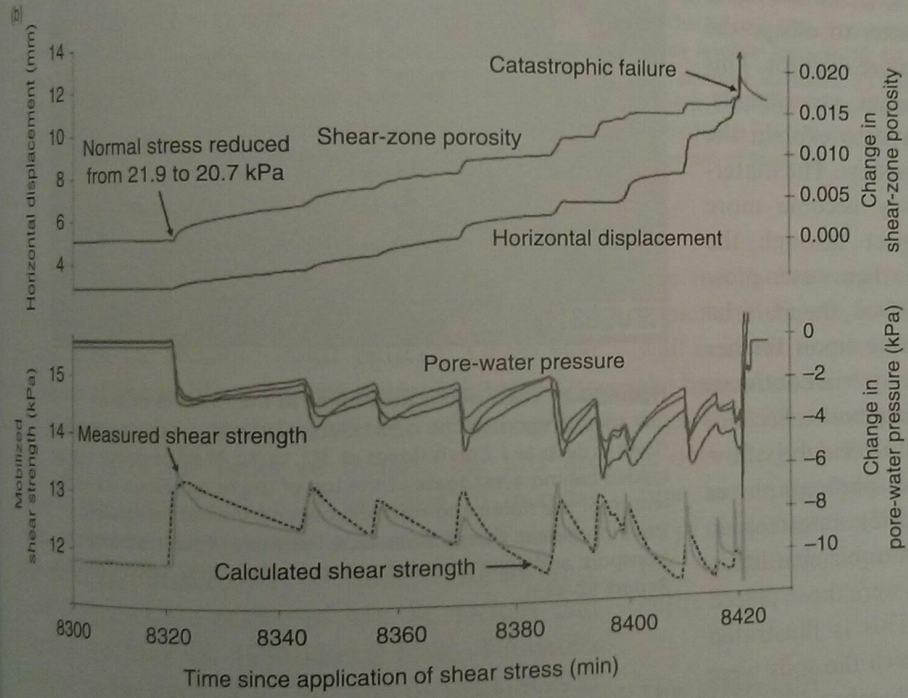
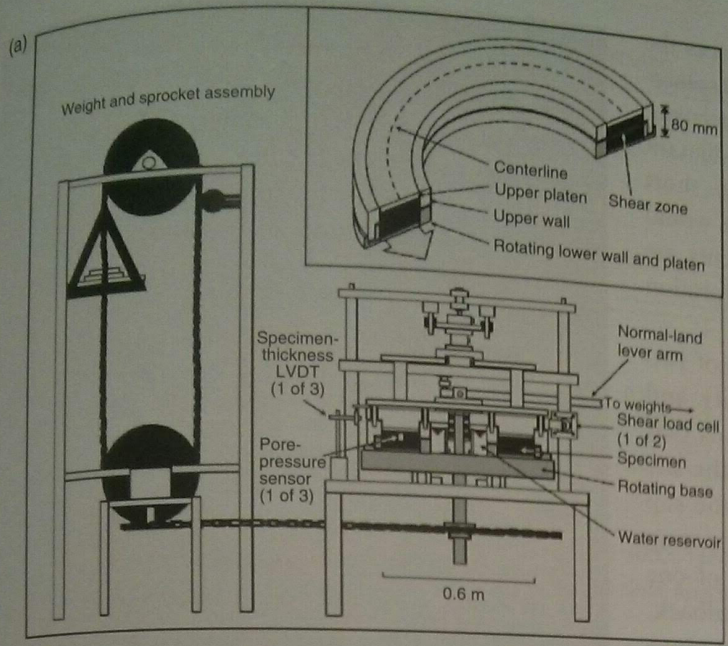


**Figure 10.28** Ring shear device for exploring the roles of pore pressure on the shear straining of granular materials. (a) Ring shear device showing in top right the cross section of the annulus in which the granular material is placed. (b) Histories of horizontal displacement (top) and measured pore pressure (bottom) (after Moore and Iverson, 2002, Figures 1 and 2).

and the displacement of the top platen with respect to the bottom was measured using a set of linear motion transducers (devices that report micron-scale displacements). The resulting histories of displacement and water pressure are shown in Figure 10.28(b). Water pressure builds up until some threshold is crossed, at which time displacement begins to occur. The water pressure immediately drops, stalling the motion event. This series of events repeats itself quasi-periodically.

Interestingly, the experiment ends with an event of a different sort: the displacement is unchecked and the water pressure remains high. This is a catastrophic failure from which the system cannot recover. This and other similar experiments have been interpreted to reflect a strong feedback system that is inevitable in granular materials under shear. When a granular material is forced to shear, grains in one layer must rise to move out of their pockets. This dilation enlarges

pores into which water can be pulled. This reduces the high water pressure that was promoting the displacement in the first place, and hence stalls the displacement event. This feedback has been dubbed "dilatant strengthening." The shearing occurs, then, in short displacement events; it is not continuous, as it would be in a viscous material. Only when these events are averaged over times large compared to their duration does the motion appear to be smooth.

These experiments point to the importance of two material properties: the hydraulic conductivity and the degree of compaction. It should be obvious that the efficiency with which water is drawn to the site of dilation should influence the duration of the slip event. Also, the more dilatant the material, meaning the more pore space is generated by motion of one grain layer over another, the stronger the feedback. More compact materials, in which grains must move a significant fraction of their diameter to escape the pockets with others grains, will be more dilatant. This is illustrated on two scales in recent experiments. First, it is this effect that is invoked to explain the final failure of the ring shear experiments. The material between the platens has slowly become more porous, more dilated, less compact through the course of the experiment. Finally, when water pressure is high enough to promote an event, the material has no more pore space to generate upon further shear, and the feedback is lost. The system continues to move with no dilatant strengthening brake. Second, in large-scale experiments in the USGS debris flow flume in Oregon (shown in the photograph in Figure 10.29; see Iverson *et al.*, 1992), catastrophic failure of saturated soils was shown to be most likely for the least compacted soils, which were those placed most gently into the apparatus. This is illustrated in Figure 10.30. Experiments in which the soils were tamped upon emplacement in the chamber displayed instead the sets of displacement events that result from the dilatant-strengthening feedback.

This material behavior is pertinent to several geomorphic and geological systems. The relevance to landsliding and to subsequent deformation of the landslide mass is obvious. The shear of fault gouge, a saturated granular material caught between two rock walls that are moving with respect to one another, should sound a lot like the ring shear experiments with a linear rather than annular symmetry. Similarly, till at the base of large glaciers is caught in

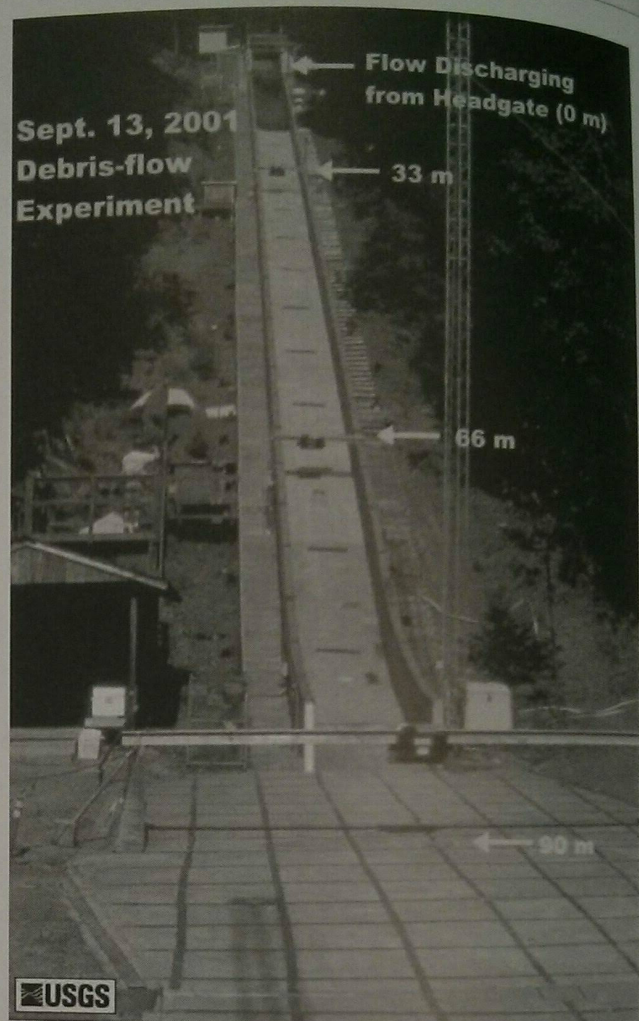


**Figure 10.29** USGS Debris flow flume in the foothills of the Cascades, Oregon. Flume is 95 m long, 2 m wide, and can contain flows as deep as 1.2 m. It slopes at 31°. Up to 20 m<sup>3</sup> of debris can be loaded behind a headgate at the top of the flume. Flows travel the length of the flume and form deposits on the flat foreground. Experiments can therefore include the study of flow initiation, transport, and deposition (after Iverson *et al.*, 1992, USGS Open-File Report 92-483).

an analogous situation. The walls enclosing the natural experiment are instead ice above and rock below, and again it is very likely to be saturated.

### What oversteepens the slopes?

One might reasonably ask what processes are involved in the generation of a slope that is too steep. It must have become too steep via some process that somehow increased its slope. The mechanisms are several, although there are a couple primary culprits. One mechanism is tectonic or volcanic tilting.

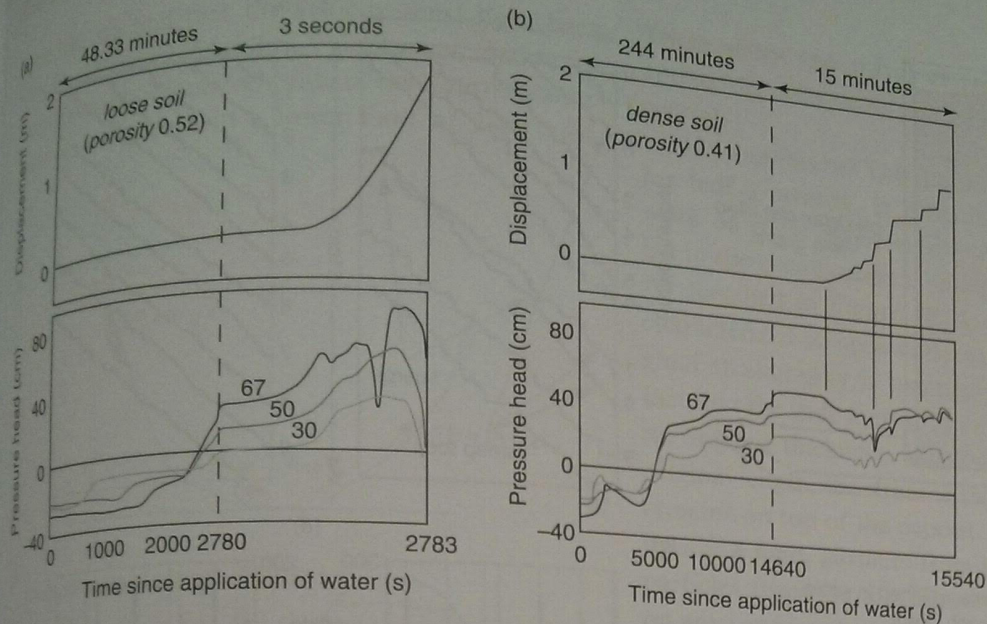


Figure 10.30 Experimental investigation of the role of soil compaction on landslide initiation. Experimental apparatus is the USGS debris flow laboratory in Oregon. The same sandy soil is used at densities that differ by only 10%. Top plots show the displacement history over two timescales. Bottom plots show corresponding pressure histories that differ by only 10%. (a) The loosely packed low-porosity soil fails catastrophically over 3 seconds, associated with pore pressure increases at three levels in the soil (30, 50, and 67 cm). (b) The dense soil deforms only slowly in incremental steps, taking 15 minutes to accomplish a comparable displacement. Each displacement event is clearly associated with a drop in pore pressure, shown by vertical lines connecting events in the two plots (redrawn from R. Iverson *et al.*, 2000, parts of Figures 3 and 4, reprinted with permission from the American Association for the Advancement of Science).

Tectonic tilting can be large in areal scale, but is typically small in amplitude. Tectonic tilt is the spatial derivative of the tectonic uplift pattern. Given that the scales of the uplift belts are many kilometers to tens of kilometers, and the amplitude of the surface deflections is of the order of meters, the tilts are typically less than 1 m/km. If we need to increase slopes by several degrees, this will not do. Volcanic mechanisms are occasionally to blame, as for instance in the failure of the edifice of Mt. St. Helens that triggered the May 18, 1980 lateral blast. Tiltmeters deployed on the flank of the volcano by the USGS at that time documented changes in tilt of several degrees as the magma neared the surface. And indeed the ensuing debris avalanche is one of the ten largest yet documented (e.g., the catalog of Costa and Schuster, 1988).

Yet by far the principal means of steepening a slope is not through tilting of any kind, but rather by removing mass from the toe of the slope. This can easily be accomplished by either a river or a glacier (or, for that matter, humans). Removal of the toe locally oversteepens the slope, which is therefore where the majority of landslides nucleate. One can simulate

this mechanism very well with a simple apparatus, depicted in Figure 10.31. The lowering of the sliding wall is meant to mimic the lowering of the channel at the base of the hillslope. One can see in the profiles of Figure 10.32 several characteristics of real hillslopes in both the geometry of the slope at any snapshot in time, and in the dynamics of the process. The majority of the failures involve small numbers of grains, but the occasional slope-clearing landslide resets the entire slope.

### The aftermath

Now that our piece of hillslope has failed, what happens to the mass of material in the failure? The result depends upon several factors, including the height of the drop once it fails, the degree of saturation of the rock and soil mass, and so on. An extensive nomenclature has sprung up around the classification of mass movements, the chief parameters being whether the mass is wet or dry, and whether it travels fast or slow. For now let us just consider the fast ones. When these also happen to be wet, they have a high likelihood of transforming into



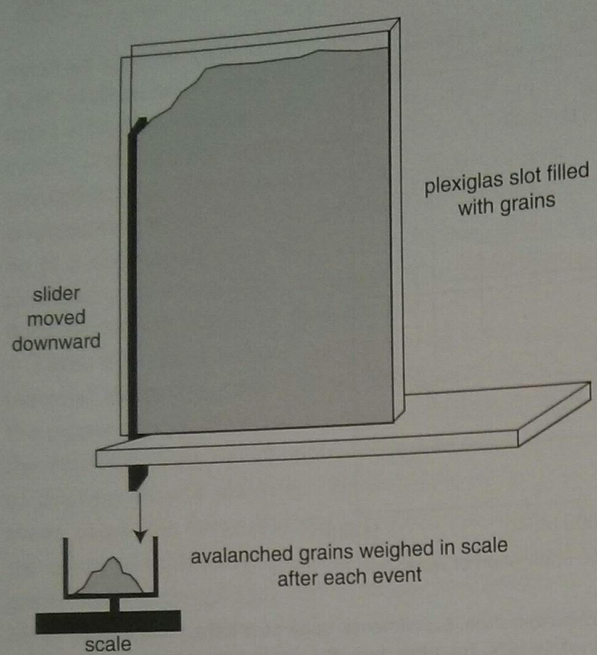


**Figure 10.31** Sketch of grain-avalanche apparatus. Plexiglas-walled slot filled with grains (e.g., dry beans) is made to avalanche through downward motion of a slider on its margin. The weight of each resulting avalanche is recorded, producing a time series of landslides and a distribution of landslide volumes.

debris flows, which can travel huge distances away from the source.

First, consider a few examples. It is commonly found that the landslide mass ends up well away from its source. There are numerous examples of a landslide traveling all the way down a valley wall and well up onto the opposite side of the valley (wiping out everything in the path). In other words, they appear to travel with very little friction. These "long runout" slides have been characterized by the ratio of the length of the runout to the vertical height of the drop:  $R = L/H$ . These ratios can be very high. To develop some sense of what these numbers mean, we will use some simple scaling to assess the expected runouts, and the expected velocities of the emplacement of these landslide masses.

A landslide has fallen from its niche in a hillside shown in Figure 10.33, and has come to a screeching halt at an altitude of  $z'$  on the other side of the valley. We can use the values of  $z$  and  $z'$  to constrain the velocity history of the slide mass, or at the very least to constrain the speeds at which the landslide mass crossed the valley floor. If all the potential energy of

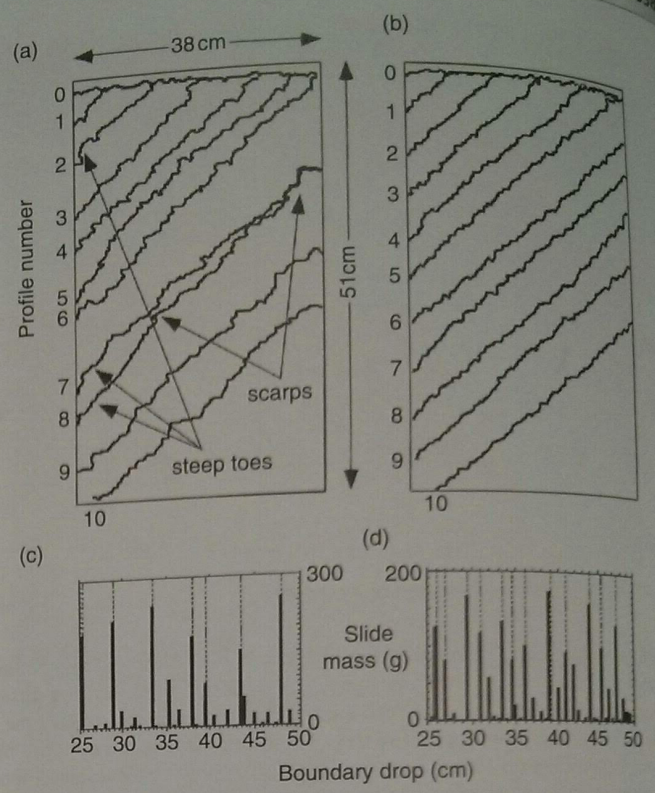


**Figure 10.32** Hillslopes of beans. As shown in profiles of (a) and (b), beanslides occur sporadically as the boundary on the left-hand side of the box is dropped smoothly and slowly. The recorded slide masses shown in (c) and (d) result in a probability distribution of slides in which 70% of the slide mass occurs in 10% of the events. Large slope-clearing events reset the slope angle. Intermediate size events clear the lower slopes, steepening the toes of the slope, giving the appearance of an oversteepened "inner gorge" (after Densmore *et al.*, 1997, Figure 1, with permission from the American Association for the Advancement of Science).

the slide mass (relative to that it would have at the valley bottom) were to be converted to kinetic energy, it would be traveling at a speed calculated from

$$mgz = \frac{1}{2}mv^2$$

or

$$v = \sqrt{2gz} \tag{10.58}$$

as it crossed the valley floor. On the other hand, we know that it had to have been going at least  $v = \sqrt{2gz'}$  in order to have had enough kinetic energy to reconvert back to its potential energy at the site of deposition. Therefore, we know that the real velocity must have been  $\sqrt{2gz} > v > \sqrt{2gz'}$ , as it wiped out the village. In the case of the 1717 Troilet slide in the Italian Alps, which wiped out a town and many

livesrock, we find that the velocity must have been between 320 and 125 km/hr. A similar calculation for the prehistoric Saidmarreh slide in the Zagros Mountains of Iran results in a lower limit of 240 km/hr.

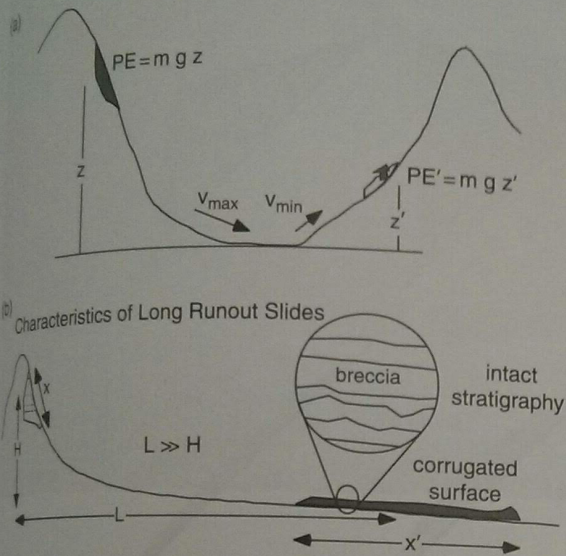


Figure 10.33 (a) Landslide source on left valley wall and deposit on right valley wall showing means of estimated maximum and minimum speeds at which the landslide crossed the valley floor. (b) Portrait of a long runout landslide, one in which  $L > H$ , including the failure zone, the runout path, and the brecciated deposit.

These slides can travel at remarkable speeds, and apparently experience very low frictional losses of energy.

How can this be? This has been a topic of hot debate for half a century. It has stimulated much detailed work on these major landslides in the field, and has led to the construction of complex numerical models. As sketched in Figure 10.33, these slide masses are characterized as openwork breccias in which the original stratigraphy is surprisingly intact. Despite the fact that the slide mass may be ten times thinner than its original thickness, and ten times longer than its original length, the strata in the top of the failed mass remains on top of the deposit. It has not been stirred up like a fluid, particles from the bottom mixed with particles from the top. These are strong constraints on any working theory of such events.

The hypotheses to explain long runout slides have been both varied and interesting. One of the most intriguing was that proposed by Ron Shreve, who in 1960 published his PhD research on the huge prehistoric Blackhawk slide (Shreve, 1968a,b). An aerial photo of this magnificent slide is shown in Figure 10.34. This 4 km-wide rockslide came down off the east side of the San Gabriel Mountains and flowed many kilometers out into the Mojave Desert. In order to explain the long runout of the Blackhawk slide, he called upon its traveling upon a cushion of compressed air. In careful



Figure 10.34 Blackhawk landslide. Roughly 17 000 years old, this slide was emplaced in only a couple minutes from its failure site in the San Gabriel Mountains (photograph by Kerry Sieh, with permission to reproduce).

mapping of the slide, he noted that it must have passed over a lip in the topography. Upon landing, the mass trapped the air, which formed a hydroplane-like low-viscosity fluid that could rapidly shear, transporting the mass until the air managed to escape (Shreve, 1968a).

Later arguments have tended to favor another mechanism involving simply the interactions of grains within the slide mass. One of the chief problems with the air cushion hypothesis is that slides with similar geometries have been seen in images of the Moon, which of course lacks an atmosphere. The most likely model at present is one in which the particles of the finely comminuted (meaning broken up) mass all bounce off one another in a hectic manner, one on one, those near the base of the slide bouncing forcefully off the bed over which the slide is moving. This "granular flow" behaves in some ways as if the grains are like atoms in a gas, the transfer of momentum and energy from place to place within the flow occurring through the binary collisions of the grains. Supercomputer simulations of a flow with up to  $10^7$  grains (Campbell *et al.*, 1995) have reproduced many of the salient features of the real world slides, in particular their long runout and the lack of disruption of the stratigraphy. This is shown in Figure 10.35 both in different times during the simulation, and at different sites in the final deposit.

Initiation of landslides is more likely when the ground is accelerated during an earthquake. The huge and numerous landslides that were triggered by the 2002 strike-slip Denali earthquake, as exemplified by Figure 10.36, are particularly well delineated by having traveled across glaciers occupying the valley floors. In tectonically active landscapes such as New Zealand, landslides are clearly a dominant geomorphic agent. Careful mapping of almost 5000 landslides across the Southern Alps that have occurred within the last 60 years has revealed an inverse power-law relationship between frequency of landslides and their size (here their mapped area). As can be seen in Figure 10.37, landslides that are 10 times larger in area occur roughly 20 times less frequently.

### Debris flows

Another possible outcome of a landslide is the transformation of that mass into a debris flow. As landslides are often saturated upon failure, the intimate

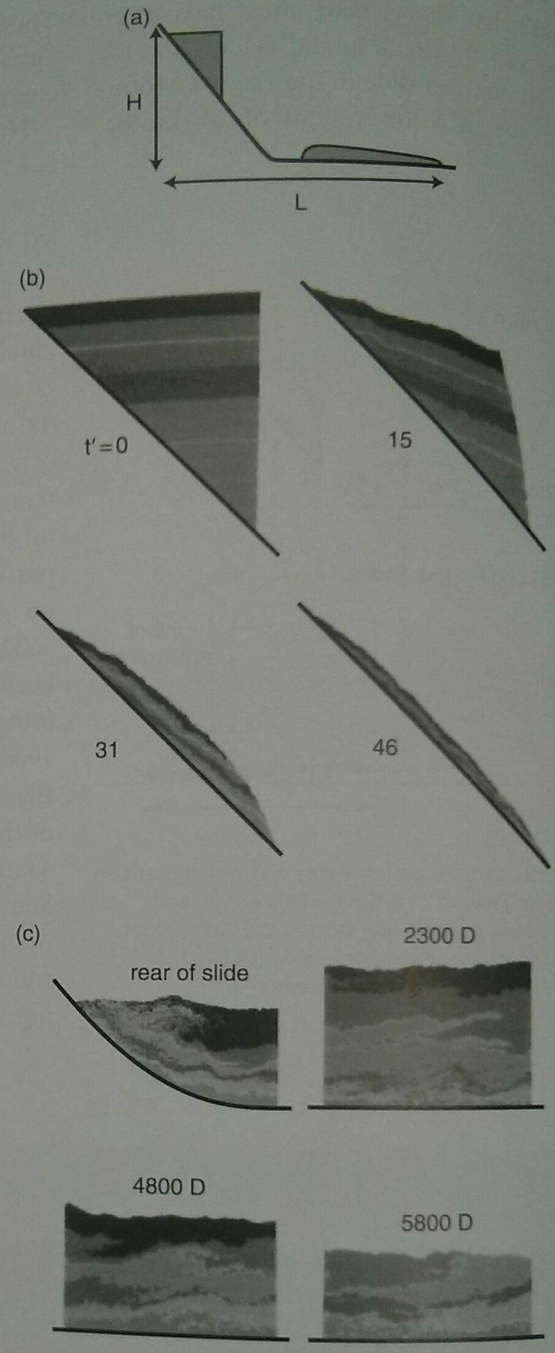


**Figure 10.35** Results of numerical simulations of long-runout landslides using one million colored particles with initial horizontally layered stratigraphy. (a) Geometry for the simulations, with steep slope leading to a flat surface through a rounded corner. (b) Frames from several times in the simulation as the triangular stack of one million particles is released. Time displayed in non-dimensional form  $t' = t\sqrt{g/D}$ . (c) Final deposit shown at four positions (denoted by numbers of particles of width  $D$ ). Note that the stratigraphy displayed by differently colored particles remains intact through the event, and in the final deposits shown in the bottom plots (from Campbell *et al.*, 1995, Figure 1 and Plates 1 and 3, with permission from the American Geophysical Union).

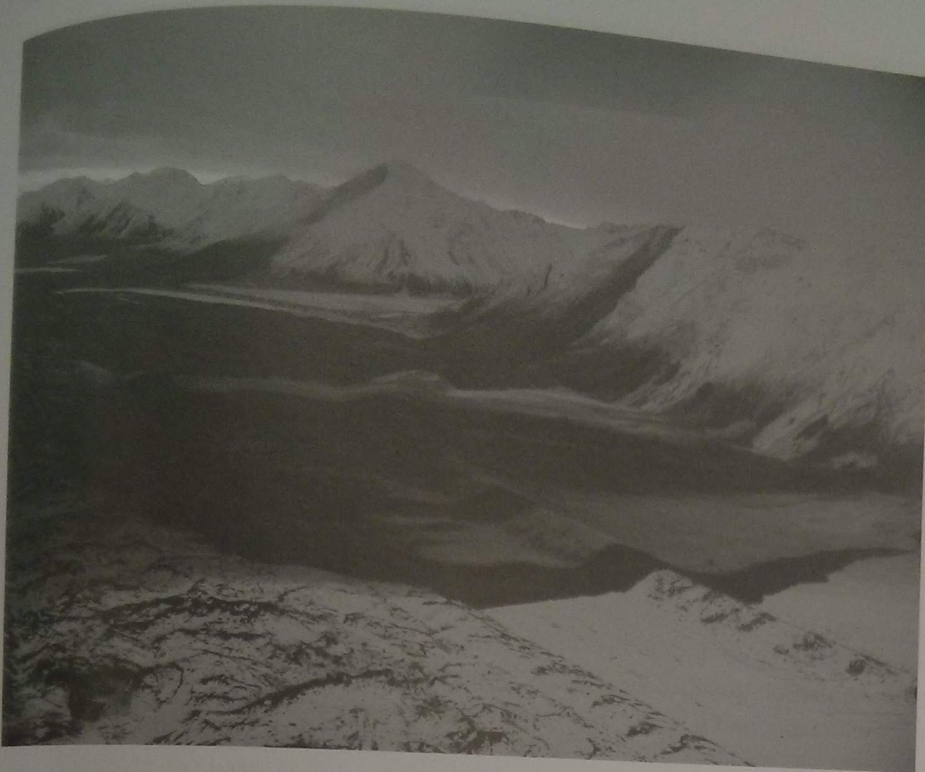


**Figure 10.36** Long runout landslides triggered by the M7.9 Denali earthquake of November 2002. Several landslides flowed across the Black Rapids Glacier (photograph taken by Peter Haeussler, USGS Alaska Volcano Observatory, on November 4, 2002).

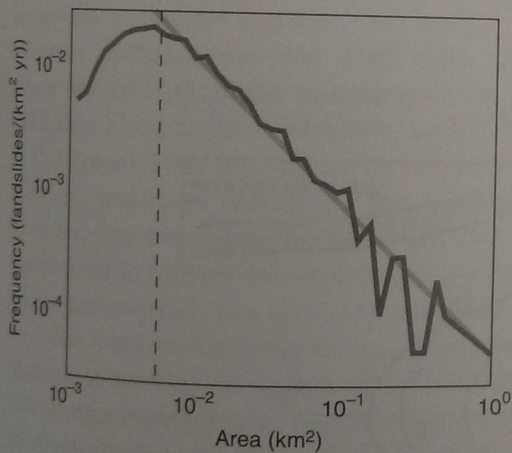


**Figure 10.37** Probability distribution of landslides in New Zealand's Southern Alps. Landslides with areas below the dashed line are either not detected, given the mapping method, or are in fact absent. Straight line fit to landslides above this size indicates a power-law area distribution (after Hovius *et al.*, 1997, Figure 2).

mixing of water and rock particles during the initial failure can promote this transformation into a fluid, well-mixed mass. Many images of these debris flows are well captured in a USGS open file report (Costa and Williams, 1984), in which we see how varied the

behavior of these flows can be. Their speeds vary from less than 1 m/s to more than 10 m/s. Their high densities (roughly  $2000 \text{ kg/m}^3$ ) allow transportation of large blocks and debris. These are a major means by which volcanoes extend their hazard well away from the volcanic cones themselves, as debris flows can travel tens of kilometers on low slopes. In Japan, the engineers charged with the duty of designing structures that will allow common debris flows to pass through major towns on the flanks of the volcanoes are highly revered. They are called "sabo engineers," and they have constructed concrete trapezoidal channels tens of meters across that serve to pass the flows safely by. The possibility that large-scale failures of these volcanic edifices can occur has only recently been established. A classic example of such a flow is the Osceola flow on which a portion of the city of Tacoma is built, in the shadow of Mt. Rainier. These pose a considerable hazard to surrounding civilization. (An excellent reference for this is the USGS film titled *Perilous Beauty, the Hidden Dangers of Mt Rainier*.)

But it is not only volcanic terrain that debris flows impact. They are common in arid regions, including the Los Angeles basin, and the eastern Sierras, for example. The alluvial fans of the eastern Sierras owe

### Box 10.4 Estimation of flow speeds and debris flow discharge from paleo-flood evidence

There are two steps to the analysis. We wish to calculate mean velocities first, from which discharges can be calculated. We will use a technique that does not require knowledge of the material behavior in order to calculate the velocities. We employ the "super-elevation" of the flow as it rounds a corner to calculate the mean velocity of the flow. This may be measured from a survey of mudlines left on the banks of the channel. Once again, we call upon a balance of accelerations acting on the fluid, this time as it comes around a bend. In Figure 10.38, we show that the accelerations are: (1) centripetal acceleration, which may be written  $\langle u \rangle^2/R$ , where  $\langle u \rangle$  is the mean velocity of the fluid in the channel cross section, and  $R$  is the radius of curvature of the bend; and (2) the component of gravity acting inward down the surface slope, written  $g \sin(\beta)$ , where  $g$  is the acceleration due to gravity ( $9.81 \text{ m/s}^2$ ), and  $\beta$  is the cross-channel slope of the debris flow surface as it rounds the bend. Setting these expressions equal to each other and solving for the mean velocity yields  $\langle u \rangle = \sqrt{Rg \sin \beta}$ . Note that all we need to measure in the field is the radius of curvature of the channel, and the surface slope of the slope. Now that we have constrained the mean velocity of the debris flow, it is simple to calculate the discharge through this section of the channel: the discharge is the mean velocity times the cross-sectional area (which gives a volume per unit time):  $Q = \langle u \rangle A$ , where  $A$  is the cross-sectional area of the channel. To get the mass discharge (mass per unit time) we need to multiply the volume discharge by the bulk density of the fluid,  $\rho_b$ , which is given by  $\rho_b = \rho_g(1 - v) + s\rho_w v$ , where  $\rho_g$  is the grain density,  $\rho_w$  is the density of water,  $v$  is the porosity of the matrix, usually roughly 0.35, and  $s$  is the degree of saturation. This is 1.0 if all pores are filled (i.e., saturated), and 0 if dry. The transformation of a landslide to a debris flow suggests a high degree of saturation, i.e.,  $s = 1$ .

their shape to repeated deposition of debris flows with highly variable mobility (e.g., Whipple and Dunne, 1992). Those debris flows of low mobility tend to come to a halt in the channel, and serve to plug the channel so that subsequent flows are diverted. The channels and channel-plugging snouts on two adjacent debris fans are easily visible in the airborne laser swath mapping image of Figure 10.39.

Debris flows and long runout landslides belong to a class of flows that we could call granular mass flows. These include the pyroclastic flows that pose such hazards associated with volcanoes. All are concentrated mixtures of dense grains in a less dense liquid or gas driven downslope by gravity. In a recent summary, Iverson and Vallance (2001) emphasize that these flows are neither steady nor uniform, and that the state of the material mixture varies greatly both temporally and spatially from the time of initiation through its transit downslope to the final site of deposition. It is therefore not appropriate to assign such a flow a rheology in the sense we have described for a fluid, say, with a viscosity or a yield stress. These mixtures can exist in at least two states,

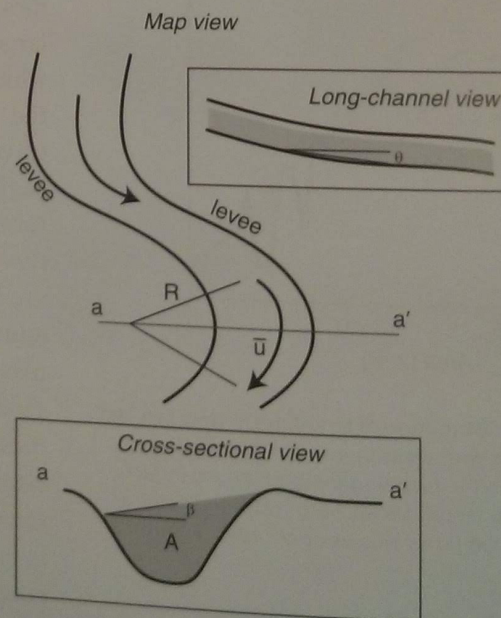


**Figure 10.38** Sketch of a debris flow channel showing how one may deduce the mean velocity,  $u$ , in the channel from deposits and scour marks left in the aftermath of a debris flow. The radius of curvature of the channel bend,  $R$ , is documented from map view geometry. The super-elevation angle is documented from depositional and scour marks in the channel cross section,  $a$ - $a'$ .

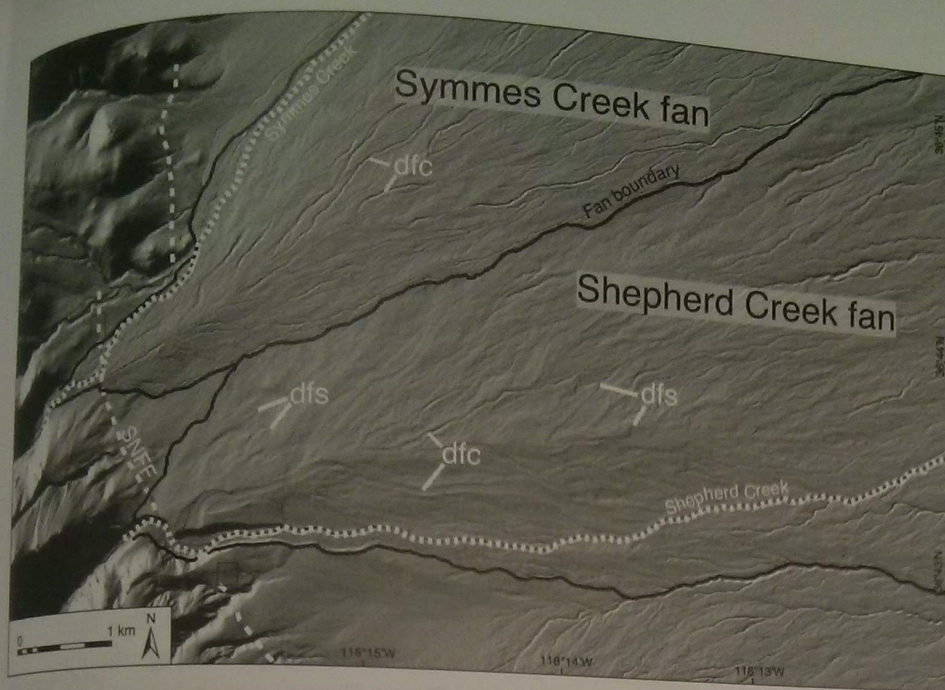


**Figure 10.39** Shaded-relief map of Shepherd and Symmes Creek fans, bounding the eastern Sierras. Topography is derived from airborne laser swath mapping (ALSM) topographic data with resolution of 1 m/pixel. The fan boundaries are outlined by solid black lines; the active channels are shown by dotted white lines. SNFF, Sierra Nevada frontal fault. Examples of former debris flow channels and snouts are labeled as *dfc* and *dfs*, respectively. It is the plugging of the channel by a low-mobility debris flow that diverts subsequent flows, promoting the formation of a fan-like form (after Duhnforth *et al.*, 2007, Figure 2, with permission from the American Geophysical Union).

ranging from essentially a rigid solid to a fluid. The variables that control the state of the mixture are somewhat analogous to those that control the state of other materials we have dealt with (recall the phase plot of  $H_2O$ , which can change from liquid to solid (ice) along a phase boundary defined by a line in  $P$ - $T$  space). Here the pressure involved is the fluid pressure, and more specifically the non-equilibrium pressure, that over or below that fluid pressure that would exist in hydrostatic equilibrium at some depth within the material. The temperature is more difficult to define, but represents the degree of agitation of the mixture; it involves the speeds of the particles just as true temperature involves the distribution of speeds of the molecules in a fluid. That the fluid pressures and the degree of agitation in the flow vary in both space and time as it travels from its source to its site of deposition dictates that even its state will vary in a complex way.

To a good approximation, the mixture behaves as a Coulomb material, in which the shear stresses are related to the normal stress as in Equation 10.56. And as in the landslide initiation problem, fluid pressures play a key role. We may write the equation for the normal stresses as

$$\sigma = (\rho_s - \rho_f)v_s gh \cos \theta - P_w \quad (10.59)$$

where  $\rho_s$  and  $\rho_f$  are densities of the solid and fluid phases. Here the volumetric grain concentration,  $v_s$ , shows up explicitly, and again we see the role of fluid pressures in  $P_w$ . It turns out that the grain concentration varies only slightly in most flows, meaning that the dominant determinant of the normal stresses (and hence the shear stresses) is the fluid pressure. The essence of the problem of describing the flow, or of predicting the flow behavior, therefore lies in the spatial and temporal evolution of the fluid pressures within the material. Fluid pressures can diffuse within a mixture, moving from sites of high pressure toward sites of low pressure.

The problem gets even more complex (and interesting) when we acknowledge that the diffusivity that governs the redistribution of these pressures may involve the grainsize distribution, and that grains can become segregated within these mixtures while in motion. In particular, coarse grains come to the top (just as the hazelnuts come to the top in an agitated jar), and because the flow speed is fastest at the top, these coarse grains move to the fronts and sides of flows, where they exert high flow resistance. This can lead to an instability in which the flow fronts break up into fingers that characterize the leading edges of pyroclastic flows (e.g., Pouliquen *et al.*, 1997).

### Hillslope models

We are now in a position to link models of hillslope transport with those of regolith production to generate animations of landscapes. We show in Figure 10.40 an example of modeled hillslopes in the face of both regolith production and regolith transport. They are meant to mimic the parabolic hilltops depicted in Figure 10.4 in the Wind River Mountains, although many alpine summits display similar smooth convex profiles. The regolith production rule used is that in which rates are slow on bare bedrock, increase to a maximum, and then decline with further regolith thickness. Initial conditions (in this case flat) are rapidly “forgotten” in the landscape as the form evolves toward a steady parabolic form with uniform regolith thickness. The steady curvature of the hilltop is dependent upon the efficiency of the transport process, all else being equal. The transport process being

mimicked is that of frost heave. By reducing the mean frost penetration depth by a factor of two, the transport rate on a given slope declines, and the curvature needed to accommodate the regolith being produced increases.

In a much more complex situation, Densmore *et al.* (1998) attempt to simulate the evolution of a landscape driven by normal faulting. There the channel incision rates through the rock of the rising footwall block steepen the adjacent slopes so that they become bedrock landslide-dominated. The triangular facets that signify a normal faulted landscape are evident (e.g., frontispiece to Chapter 4). Koons (1989) addressed the rapidly evolving landscape of New Zealand, and was among the first to quantitatively address the role of orographic precipitation.

In another tectonically active landscape, this time dominated by thrust and strike-slip faulting, the uplifted staircase of the Santa Cruz marine terraces decay topographically as they age. While these terraces saw

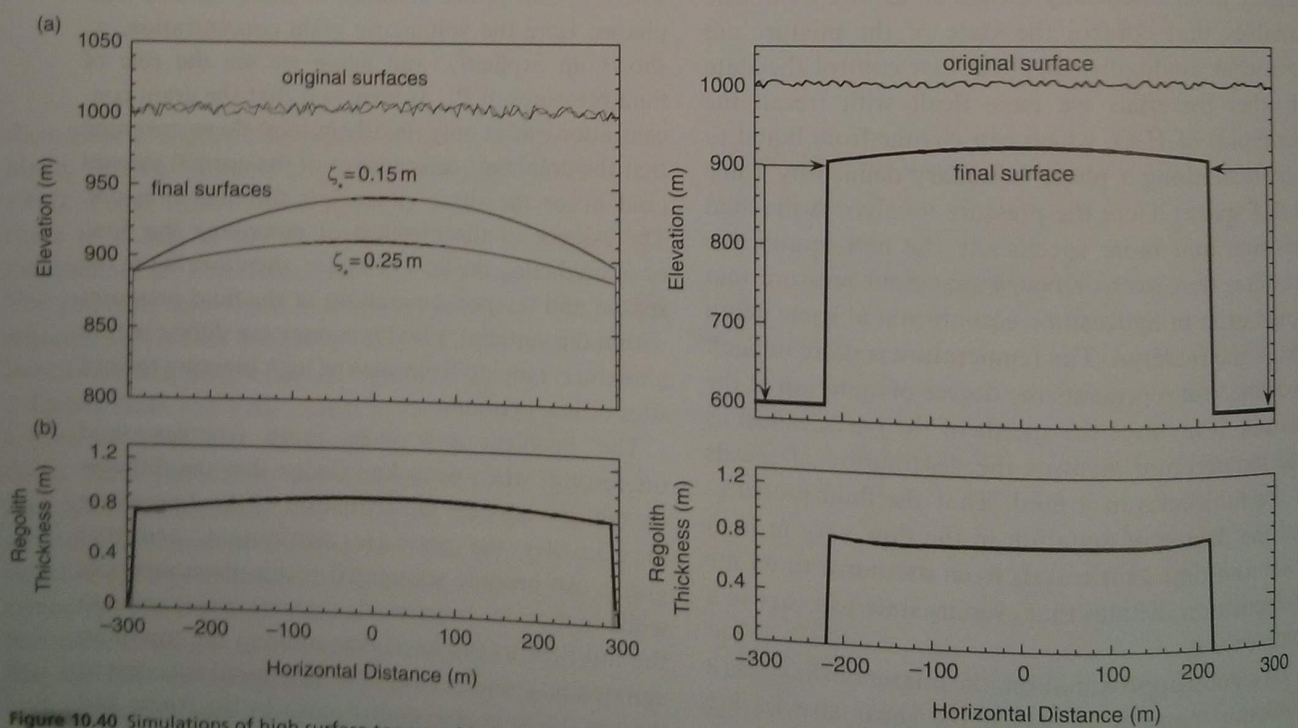


**Figure 10.40** Simulations of high surface topographic and regolith cover evolution, and their dependence on boundary conditions and hillslope transport efficiency. Top panels: original and final profiles of topography, and their dependence on boundary conditions and down-wearing of adjacent valleys. Bottom panels: final profiles of regolith thickness. Left simulation: boundary conditions include only glacial lateral migration of glacial valley wall. Final profiles are nearly parabolic, and have uniform but thin (~0.8 m) regolith. Some simulations show bare bedrock at the crest of the hill, others do not, depending upon the particulars of the initial conditions (after Anderson, 2002, Figures 15 and 20, with permission from Elsevier).

early work based on the diffusion equation, later research addresses not only the transport of terrace sands but the generation of regolith from the underlying sandstones. Only then can the asymmetry of the decaying cliffs be understood (see discussion in Chapter 18, Figure 18.6).

We have discussed diffusive processes that tend to round hillcrests. As we will see in Chapter 11 in our discussion of water in the landscape, the overland flow of water down a hillslope is not expected to produce convex hilltops. However, as discussed in Chapter 11, Dunne (1990) has shown that the wide convex tops that bound long hillslopes in Kenya

cannot be attributed to the motion of grains by rainsplash. Rainsplash is simply not efficient enough to accomplish this in the allotted time. Instead, his models, reproduced in Figure 11.18, demonstrate that the overland flow and associated sheetwash process can act as a diffusive process. Surface grains are indeed entrained in the overland flow, but the typical storm doesn't last long enough to transport them all the way down the slope. So they are dropped, and far from their initial positions, as if they had taken long leaps instead of the small hops associated with rainsplash. The result is a more efficient diffusive process, resulting in broad convex hilltops.

## Summary

We formally address the question of hillslope form by casting the problem as one of conservation of mass, here of regolith. This approach is one we take at the start of many geomorphology problems, whether it be the conservation of mass of ice on a glacier, the mass of sediment on a channel bed, the volume of water in a channel segment or a lake, and so on. In this case the exercise serves to focus the need for knowledge of what sets both the rate of regolith production (Chapter 7), and the rate of regolith transport down a slope.

Many hillslopes have convex tops, which can be attributed to the dominance of diffusive transport processes at least near the hillcrests. The diffusion equation describing the evolution of convex hilltops and of the smoothing of microtopography arises when this expression for conservation of regolith mass is combined with an expression for regolith transport in which the transport rate is linearly related to the local hillslope angle.

We have explored several specific processes that can be characterized by a linear dependence on local slope, including rainsplash, the burrowing of fossorial rodents, tree-throw, frost heave, and solifluction. In each of these cases, we must describe the geomorphic result of individual events, and then sum over these events. In most cases the events themselves could be described as deterministic (once the initial conditions are known, the outcome is certain), while the summation takes place over a distribution of events that has a stochastic character and must therefore be described statistically.

The random nature of particle motion in the regolith when subjected to several of these mechanical processes has inspired some to embrace the statistical mechanical treatment of the problem. At present this work is on the leading edge, treating either the vertical motion (bioturbation) of sediment, or rainsplash. But the approach appears to be extendable to other processes, and may guide the collection of relevant field information.

Hillslopes are strongly slaved to the local conditions at their base, which are in general set by the fluvial or glacial systems. Rapid incision can trigger steepening of lower slopes and can lead to landslides. We have summarized the simplest calculation of hillslope stability in the "infinite slope" case, and have illustrated the role of slope, regolith thickness, and groundwater pressures. The latter guides an assessment of the climatic conditions under which failure is favored, and allows us to deduce the role of hillslope convergence or divergence in governing the likelihood of failure.

The post-failure fate of landslide material varies greatly with local conditions, but includes in long runout landslides some of the most remarkable events in geomorphology. These are likely governed by particle collisions in the granular material that become increasingly efficient as the grains are further crushed into very elastic cores of the original blocks. Debris flows are one end-member result of a landslide. They too are very mobile, and can transport debris from sources in mountainous terrain onto debris-flow fans that bound especially arid mountains.



## Problems

1. On a hillslope with regolith 1.2 m thick, and a regolith production rate of  $8 \mu\text{m}/\text{yr}$ , what would be the mean residence time of regolith in the regolith column?

You then note that this slope is 100 m long and that the regolith is uniform in thickness. Calculate the residence time another way, this time by addressing the entire regolith "reservoir" on the hillslope, and the volumetric regolith discharge rate at the base of the slope. Are the calculated residence times equivalent?

2. Plot the expected steady-state pattern (as a function of distance from the crest) of discharge of regolith on a convex hillslope in a climate in which the production rate of regolith is  $20 \mu\text{m}/\text{yr}$ . Report your answer in  $\text{m}^2/\text{year}$ .

If the regolith was 0.8 m thick, what would be the spatial pattern of the mean downslope velocity of the regolith?

How would these numbers change if 25% of the mass loss occurred in solution?

3. How much strain does a soil sustain from the growth of tree roots? Assume that the tree roots are 10 cm in diameter, are simple vertical tap-roots, and are spaced at 1.5 m spacing. (Obviously this is a very simple model of roots!)

How much ought the soil to inflate vertically due merely to this taproot growth if the soil is 1 m thick? Do the experiment in a small beaker to illustrate this effect.

4. On a hillslope with a weathering rate of  $20 \mu\text{m}/\text{yr}$  and an effective hillslope diffusivity of  $0.02 \text{ m}^2/\text{yr}$ , what would be the expected curvature of the hillslope? Plot the full topographic profile if the summit of the hillslope, at  $x = 0$ , is 1000 m. The channels at the edge of the hillslope are 200 m from the hillcrest.

5. *Steady regolith discharge.* On a 150 m long hillslope, regolith is being generated at a uniform

rate of 40 microns/yr. Calculate and plot the distribution of downslope regolith discharge with distance from the crest.

6. *Slope stability.* Consider a long linear hillslope with a slope angle of  $25^\circ$ . It has soil that is 1 m thick, and a shear test on the soil reveals that its internal angle of friction is  $31^\circ$ , with a cohesion (including roots) of 5000 Pa and a porosity of 35%. Perform a stability analysis on this slope for the worst-case scenario of full saturation. If you find that it is indeed unstable under full saturation, assess the water table height that is required to cause failure.


7. *Runout of a large landslide.* Consider a landslide mass that fails from an elevation of 2500 m. The valley floor onto which the rockmass tumbles lies at 1700 m. The mass comes to a screeching halt on the opposite valley wall at an elevation of 1950 m. Calculate the maximum and minimum speed at which the mass is traveling as it crosses the valley floor. Given these estimates, estimate how much time a citizen of the valley floor would have to get out of the path of the slide if they were fortunate enough to have witnessed its initiation.

8. Consider the plot of landslide areas in Figure 10.38. Assess the slope of the straight line required to fit the data, and report the resulting probability density function for landslide area.

9. *Thought question.* Explain as simply as you can why a compacted granular material is less likely to fail catastrophically on a slope than is a loosely packed material.

10. *Thought question.* How might the odd spiky landscape illustrated in the photograph at the start of the chapter, from the Tsingy Park in Madagascar, form? It certainly violates our expectation of convex hilltops. What rule set might explain this cusp-like appearance?

## Further reading



Butler, D., 1995, *Zoogeomorphology*, Cambridge: Cambridge University Press, 239 pp.  
*This is one of only a few summary treatments of the role of biology in geomorphic systems.*

Carson, M. A. and M. J. Kirkby, 1972, *Hillslope Form and Process*, New York: Cambridge University Press, 475 pp.  
*A classic book on hillslopes by two of Britain's most prominent geomorphologists, this summary of the state of our*

*understanding in the early 1970s is still a useful reference on the topic.*

Selby, M. J., 1993, *Hillslope Materials and Processes*, 2nd edition, Oxford: Oxford University Press, 451 pp.  
*This encyclopedic treatment of the hillslope literature in the early 1990s remains a reference book. Much of this material was also included in Selby's geomorphology text *The Earth's Changing Surface* (1985).*